The Role of Leak Channels in Regulating Endocrine Pituitary Cell Excitability

Submitted by Marziyeh Belal to the University of Exeter as a thesis for the degree of Doctor of Philosophy in medical studies in December 2020.

I certify that all material in this thesis which is not my own work has been identified and that no material has previously been submitted and approved for the award of a degree by this or any other University.

Signature: Marziyeh Belal

Abstract

The pituitary gland produces a variety of hormones that regulate other glands and organs throughout the body to control critical bodily functions including growth, metabolism and the stress response. Endocrine pituitary cells are electrically excitable: they generate action potentials to regulate their intracellular calcium level ($[Ca^{2+}]_i$) and eventually hormone secretion. The interplay between hypothalamic neurohormones and feedback signals coming from peripheral endocrine glands controls hormone secretion from pituitary cells by regulating the properties of ion channels and in turn the pattern of electrical activity. Therefore, elucidating the mechanisms underlying hormone secretion involves characterisation of ionic conductances which govern pituitary cell excitability.

This PhD thesis explores how sodium and potassium leak channels regulate pituitary cell excitability. Leak channels play an important role in tuning the resting membrane potential, appropriately maintaining it close to the threshold for generating action potentials in all pituitary cells. The dynamic clamp electrophysiology technique was used to virtually vary the conductance of the leak channels, and evaluate their effect on the pattern of electrical activity and intracellular calcium concentration in the GH4 lacto-somatotroph cell line as well as in murine primary pituitary cells. It was found that very small alterations in the conductance of sodium and potassium leak channels result in substantial changes in the patterns of electrical activity and intracellular calcium oscillations in both GH4 and primary pituitary cells. Increasing the conductance of sodium leak channels by only a few fractions of a nanosiemen (nS) enhanced the excitability of pituitary cells significantly. In contrast, increasing the conductance of potassium leak channels by comparable values reduced the excitability and intracellular calcium concentration of the cells.

Despite the crucial role of sodium leak conductance in tuning the resting mem-

brane potential at depolarised levels away from the potassium equilibrium potential, the molecular identity of this channel in pituitary cells has remained unknown. One candidate protein channel is the sodium leak channel, non-selective (NALCN). The NALCN channel is widely expressed in the central nervous system, and has been characterised as a key modulator of cell excitability in several neuronal populations. Hence, in the second stage of my PhD, I constructed a lentiviral vector to knock down the NALCN channel in murine primary anterior pituitary cells in culture, and evaluate NALCN's role in regulating cell excitability and intracellular calcium concentration using electrophysiology and calcium imaging techniques. I discovered that: (1) NALCN encodes for sodium leak channel to acutely adjust the resting membrane potential and sustain intrinsically-regulated spontaneous firing in endocrine pituitary cells; (2) the NALCN channel is crucial for maintaining spontaneous $[Ca^{2+}]_i$ oscillations; (3) NALCN mediates the major depolarising inward leak current in pituitary cells; and (4) as in neurons, extracellular calcium inhibits NALCN activity in pituitary cells. These discoveries advance our understanding of how cell excitability and consequently hormone secretion is regulated in endocrine pituitary cells.

Acknowledgements

I would like to express my sincerest gratitude to Professor Paul Winyard for all of his continous support, integrity and encouragement throughout my Ph.D., and for giving me many valuable advice and suggestions, and keeping everything at the right pace.

I would also like to thank Dr Joel Tabak for giving me the opportunity to do a Ph.D. and for providing me the tools that I needed to conduct and complete my research. Also, to Dr Jamie Walker for his insightful comments on my work and my scientific writings. And to Dr Mariusz Mucha who patiently taught me various aspects of the molecular biology. Also, to Dr Arnaud Monteil for his valuable collaboration and inputs to my project, which took my Ph.D. to another level. Thank you very much Arnaud for always replying to my emails swiftly and comprehensively, and communicating your knowledge and guidance with me from a distance.

My deep gratitude to Dr Mino Belle for his personal and professional support throughout my Ph.D., and for raising all the thoughtful questions and discussions, and for communicating his meticulousness and rigor in the experimental procedures and data analysis with me which inspired me a lot.

Special thanks to my Ph.D. friends Maria and Judith, for being very supportive, caring and genuine friends, for many insightful conversations as well as laughter during lunch and coffee breaks, for countless game nights, outdoor activities and travelling. I am very grateful for the strong friendship bond we made together.

To my parents for always supporting me and helping me to accomplish my goals, and for raising me with so much love and respect. Without you, my journey would have been very difficult.

Lastly, to the most precious person of my life my partner Conor, for always believing in me and supporting me, and for all the amazing surprises that made

my Ph.D. life very exciting. Also, for helping me with coding and providing your valuable insight for my data analysis. You have been my rock in times of difficulties. From the bottom of my heart: words cannot describe how much I love you and I am very proud of you.

I dedicate my PhD thesis to the innocent victims of flight PS752 many of whom were scientists pursuing their life passion. The plane was shot down accidentally by the Islamic regime of Iran killing all passengers and crew in January 2020 after being misidentified by an air defense unit as a "hostile target." Their memory will never be forgotten.

Table of Contents

List of Tables

List of Figures

Abbreviations

4-AP, 4-aminopyridine.

ACTH, adrenocorticotropic hormone

α-MSH, α-melanocyte stimulating hormone

ATP, adenosine triphosphate

AVP, arginine vasopressin

BK channel, big-conductance voltage- and calcium-activated potassium channel

BSA, bovine serum albumin

Cav channel, voltage-gated calcium channel

$[Ca^{2+}]_i$, cytosolic free Ca^{2+} concentration

$[Ca^{2+}]_o$, extracellular free Ca^{2+} concentration

cAMP, cyclic adenosine 3', 5'-cyclic monophosphate

cDNA, complementary DNA

CMV, cytomegalovirus

CRF, corticotropin releasing factor

CRH, corticotropin releasing hormone

DMEM, Dulbecco's Modified Eagles Medium

DMSO, dimethyl sulfoxide

DNAse I, deoxyribonuclease I

ER, endoplasmic reticulum

FBS, foetal bovine serum

FFA, flufenamic acid

FSH, follicle-stimulating hormone

GABA, gamma-aminobutyric acid

GFP, green fluorescent protein

GH, growth hormone

GHRH, growth hormone releasing hormone

GnRH, gonadotropin-releasing hormone

GΩ, gigaohm

GPCRs, G protein-coupled receptors

HCN, hyperpolarisation-activated and cyclic nucleotide-dependent Na^+ channels

HEK, human embryonic Kidney

HEPES, 4-(2-hydroxyethyl)-1-piperazineethanesulfonic acid

HIV, human immunodeficiency virus

IGF-1, insulin-like growth factor-1

ITS, insulin-transferrin-sodium

$[\mathbf{K}^+]_o$, extracellular free K^+ concentration

Kca, calcium-activated potassium channel

Kir, inwardly rectifying potassium channel

K2P, two-pore domain K^+ channels

Kv, voltage-gated potassium channel

LB, lysogeny broth

LH, luteinizing hormone

MES, methane sulfonate

$[\mathbf{Na}^+]_o$, extracellular free Na^+ concentration

$\mathbf{Na}_b$, background sodium channel

$\mathbf{Na}_v$, voltage-gated sodium channel

NALCN, Na^+ leak channel/nonselective

NALCN KD, NALCN knockdown

NLf-1, NALCN localization factor-1

$NMDG^+$, N-Methyl-D-glucamine

NSCC, non-selective cationic channels

pA, pico amperes

PBS, phosphate buffered saline

PBST, phosphate buffered saline + 0.01% triton x

PCR, polymerase chain reaction

PKA, protein kinase A

PRL, prolactin

PVN, hypothalamic paraventricular nucleus

q-RT-PCR, quantitative reverse transcription PCR

RMP, resting membrane potential

RRE, reverse response element

SCN, suprachiasmatic nucleus

SCR, scramble

SFK, Src family of tyrosine kinase

SP, substance P

TEA, tetraethylammonium chloride

TM, transmembrane

TRH, thyrotropin-releasing hormone

TRPC, canonical transient receptor potential

TRPML, transient receptor potential cation channel, mucolipin subfamily

TTX, tetrodotoxin

VGCC, voltage-gated calcium channel

VSV, vesicular stomatitis virus

VSV-G, vesicular stomatitis virus glycoprotein

WT, wild type

Chapter 1

Introduction

1.1 Introduction to the pituitary gland and its hormones

The pituitary gland, also known as a "master gland", is composed of three distinct parts: (1) the neurohypophysis or posterior pituitary where the axonal terminals originating from hypothalamic nuclei (paraventricular nucleus and supraoptic nucleus) are located; These neurons synthesise vasopressin and oxytocin, and transport them to the posterior pituitary where they are released into the general circulation; (2) the intermediate lobe which consists of melanotrophs where the α-melanocyte stimulating hormone (α-MSH) is synthesised and released; and (3) the adenohypophysis or anterior pituitary which is a heterogeneous population of cells comprising the major portion of the entire pituitary gland. The anterior pituitary is populated with several secretory cell types each of which synthesises and releases essential hormones that regulate other glands and organs throughout the body to control critical bodily functions such as growth, metabolism, reproduction and the stress response (Musumeci et al, 2015). Table 1.1 summarises the main functions of anterior pituitary cell types and their targets.

1.1.1 Regulation of pituitary hormone secretion

In vivo measurement of pituitary hormone levels across several time points from numerous animals (e.g. mouse, rat, rhesus monkey, sheep and human) has revealed an episodic or pulsatile rhythm in the pattern of the hormone secretion (Belchetz et al, 1978; Clark, 2002; Plotsky and Vale, 1985; Henley et al, 2009; Clarke, 2019). The observed oscillatory rhythms in the concentration of pituitary hormones *in vivo*

imply that there are regulatory interactions between different types of molecules, which give rise to these naturally occurring oscillations. This is because an isolated hormone or receptor will never generate any oscillations (Goldbeter, 1996). A series of studies from the 1950s onwards demonstrated that a key player in driving these ultradian oscillations in pituitary hormones is the pulsatile secretion of stimulatory and inhibitory factors from neurons of the hypothalamic paraventricular nucleus (PVN) (Guillemin, 1967; Belchetz et al, 1978; Plotsky and Vale, 1985).

Cell types	**Hormones produced**	**Main targets of these hormones**	**Function**
Corticotroph	ACTH	Adrenal glands (Adrenal cortex)	Regulating the glucocorticoid & mineralocorticoid secretion
Thyrotroph	TSH	Thyroid gland	Regulating T_3 and T_4 secretion (Controlling metabolism)
Somatotroph	GH	Liver, muscle, bone	Promoting growth and metabolism
Lactotroph	PRL	Ovaries, mammary glands, uterus	Controls lactation and the secretion of milk, oestrogen and progesterone
Gonadotroph	LH, FSH	Gonads (testes, ovaries)	Controlling the secretion of androgens (testosterone, dihydrotestosterone), progesterone and oestrogen

Table 1.1: The list of endocrine anterior pituitary cell types, their hormones, targets and main functions in mammals.

1.1.2 Hypothalamic regulation of hormone secretion

In 1955, Guillemin and Rosenberg reported that isolated dog and rat anterior pituitary cells in culture stop secreting adrenocorticotropic hormone (ACTH) 8 days after their isolation, however the addition of hypothalamic fragments to the culture restored ACTH secretion (Guillemin and Rosenberg, 1955). During the same period, Saffran and Schally confirmed that hypothalamic fragments contain a factor that controls the secretion of ACTH by the pituitary gland (Saffran and Schally, 1955). These studies led to the discovery of a new peptide molecule initially termed corticotropin releasing factor (CRF, later known as corticotropin releasing hormone) originating from the hypothalamus, which controls ACTH secretion from the anterior pituitary gland (Guillemin and Rosenberg, 1955). Further studies showed that the hypothalamic PVN also produces a number of other stimulatory factors such as growth-hormone releasing hormone (GHRH), gonadotropin-releasing hormone (GnRH) and thyrotropin-releasing hormone (TRH), as well as inhibitory factors including dopamine and somatostatin to regulate hormone release from the anterior pituitary (Guillemin, 1967). Further investigations showed that the episodic secretion of the hypothalamic factors into the hypophyseal portal vessels drives the physiological pulsatile secretion from pituitary gland (Belchetz et al, 1978; Clark 2002; Plotsky and Vale, 1985). For instance, in rhesus monkeys bearing hypothalamic lesions it was demonstrated that a constant administration of exogenous GnRH failed to rescue the normal pulsatile pattern of gonadotropin secretion including luteinizing hormone (LH) and follicle-stimulating hormone (FSH) (Belchetz et al, 1978). In contrast, the intermittent delivery of a synthetic GnRH once per hour (which is the physiological frequency of LH/FSH secretion in the rhesus monkey) restored the normal pattern of gonadotropin (FSH and LH) release (Belchetz et al, 1978).

1.1.3 Feedback signals from periphery

Follow-up studies reported that the FSH secretion *per se* is not reliant on episodic GnRH input to the pituitary gland. Rather, FSH secretion is dependent on the negative feedback loop arising from elevated steroid hormones in the periphery (re-

viewed in Clark, 2002). Other studies also confirmed that the observed pulsatile secretion of growth hormone by the pituitary gland is modulated by both the interaction between the feedforward action of GHRH and somatostatin as well as negative feedback from peripheral peptides (e.g. IGF-1) (Plotsky and Vale, 1985; Anderson et al, 2004; Barinaga et al, 1983; Bilezikjian and Vale, 1983; Clark et al, 1988). Similarly, negative feedback by elevated glucocorticoid levels in the periphery inhibits the expression and secretion of corticotropin releasing hormone (CRH) in the hypothalamus (Tasker and Herman, 2011), and supresses ACTH release and transcription in pituitary cells (Deng et al, 2015). Further studies also reported the autocrine and paracrine feedback regulation of hormone secretion in the pituitary gland (Stojilkovic et al, 2010). Overall, the network of different hormones interacting *via* positive and negative feedback loops originating from the central nervous system and periphery leads to the episodic pattern of hormone secretion from pituitary gland. Figure 1.1 illustrates the key points described in sections 1.1.2 and 1.1.3.

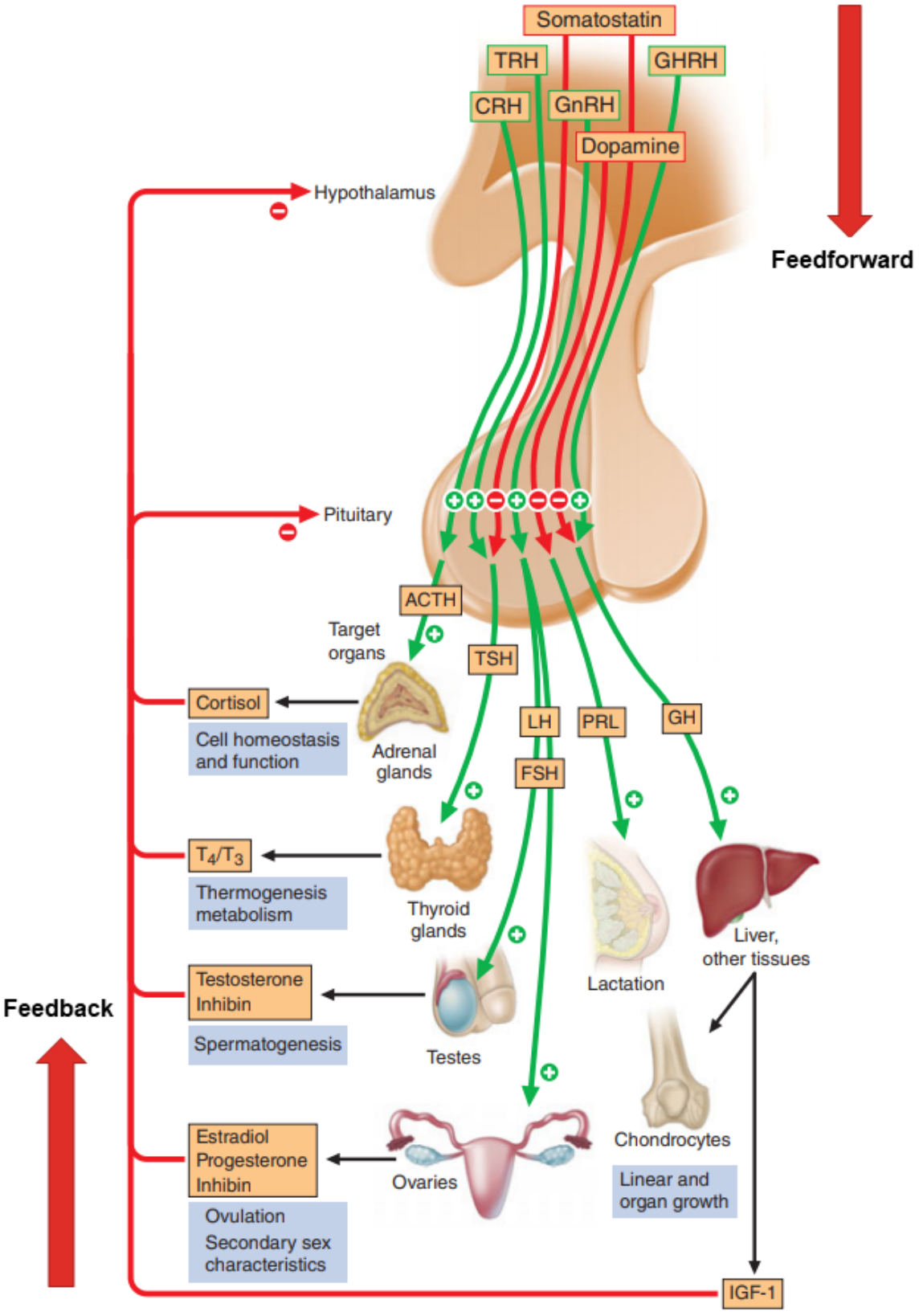

Figure 1.1: Feedforward and feedback signals originating from brain and periphery to regulate hormone secretion from pituitary gland.
Episodic secretion of the hypothalamic neurohormones into the hypophyseal portal vessels drives the physiological pulsatile secretion from pituitary gland. Following that, the negative feedback induced by elevated peripheral hormone levels inhibits the expression and secretion of pituitary hormones and the hypothalamic neurohormones. Overall, the network of different hormones interacting *via* positive and negative feedback loops originating from the central nervous system and periphery leads to the episodic pattern of hormone secretion from pituitary gland (the diagram is adapted from Harrisons Manual of Medicine, 18th Ed, p.1126).

1.1.4 The importance of pulsatile secretion

The fluctuation in hormone levels is a key aspect of normal physiology (Lightman et al, 2008; Leng and Brown, 1997). The constant exposure of cells to hormones results in desensitization of receptors and down regulation of processes essential for secretion, and eventually an inability of cells to respond to hormone signals (Lightman et al, 2008, Leng and Brown, 1997). In fact, interruption in the pulsatility of pituitary hormones (and other hormones such as insulin) can cause a number of psychiatric and metabolic disorders (Young et al, 2007 and 2004; Lightman et al, 2008).

1.2 Cell excitability and hormone secretion

Neurons were the first cells to be found capable of generating electrical activity. It was then quickly discovered that the most important role of electrical activity in neurons is signal transmission which happens *via* the flow of ionic currents. The ionic charges are spread on the inner and outer surface of the cell membrane thus making it function as a capacitor. The voltage difference between the intracellular and extracellular space established by the ionic charges is called the membrane potential, with the extracellular space acting as the reference point. In neurons, the application of an electrical signal at any location on the cell membrane can alter the membrane potential locally and that could be used to conduct the signal. However, the current flow and signal propagation over extensive distances will decay due to the gradual loss of currents through the cell membrane unless a driving force is used to amplify the signal. Although for short distance signalling the current decay may not be problematic, for long distance signalling, a passive signalling machinery is not sufficient and an active signalling pathway is required. Thus, neurons employ complex and interacting voltage-dependent ion channels that can trigger the explosion of ion influx and efflux, defined as an "action potential", once the membrane voltage reaches a certain threshold (initially discovered by Emil du Bois-Reymond, 1848). Using this machinery, the electrical signalling can carry a message and travel at 100 m/s or more without any decay (Hodgkin, 1937a, Hodgkin 1937b).

In 1975, it was discovered for the first time that endocrine pituitary cells are also excitable and can generate action potentials in a similar way to neurons (Kidokoro, 1975). This excitability of small spherical endocrine cells which secrete hormones at a significantly lower rate than neurons releasing neurotransmitters appeared as an exotic behaviour at first sight and raised questions concerning its physiological purpose. Before this discovery, Douglas and colleagues were using electrophysiology techniques to unravel the molecular cascades of hormone secretion from the endocrine medullary chromaffin cells in the adrenal gland (Douglas, 1968). They followed the thought lines of muscle physiologists studying the role of membrane potential and Ca^{2+} in muscle contraction who had previously introduced the concept of excitation-contraction coupling. This inspired the idea of stimulation-secretion coupling in endocrinology with Ca^{2+} playing the central role (Douglas, 1968). These discoveries paved the way for researchers studying the role of excitability in endocrine pituitary cells. Collectively, their work indicated that the stimulation of secretion is associated with alterations in membrane potential and that endocrine anterior pituitary cells generate rapid, coordinated movements of ions across the cell membrane which leads to reversible changes in the membrane potential called action potentials (reviewed in Mollard and Schlegel, 1996). Of note, although endocrine pituitary cells are not perfectly spherical *in situ* and can emanate some cytoplasmic processes, these cells approximate this phenotype when isolated *in vitro*.

Over the past decades, the use of the patch clamp electrophysiology technique combined with calcium imaging has provided solid evidence for the modulation of action potentials by stimulatory and inhibitory factors, which results in the regulation of $[Ca^{2+}]_i$ transients in endocrine pituitary cells (reviewed in Mollard and Schlegel, 1996). Temporal and spatial $[Ca^{2+}]_i$ changes control numerous cellular functions including secretion, protein synthesis and gene expression over a wide time scale (milliseconds to hours) in endocrine pituitary cells (reviewed in Mollard and Schlegel, 1996). For example, spatial distribution of cytosolic Ca^{2+} oscillations and its distance from large dense-core hormone vesicles regulate the rate of hormone secretion in pituitary cells (reviewed in Zorec 1996). Further, the amplitude of the cytosolic calcium oscillations and consequently hormone secretion is regulated by

the Ca^{2+} localisation, gating mode of voltage-gated calcium channels as well as the driving force during the channel opening, which determines the amount of Ca^{2+} influx (Parsons et al, 1995). For modulating the activity of various intracellular calcium-sensitive enzymes such as adenylyl cyclase (Cooper et al, 1995) and for modification of structural proteins such as depolymerisation of actin (Vitale et al, 1995), global Ca^{2+} alterations over a timescale of seconds is required. Other crucial cellular activities such as the induction of immediate early gene expression requires a long (minutes to hours) and constant exposure to cytosolic Ca^{2+}, which is tightly regulated by the pattern of electrical activity produced by endocrine pituitary cells (Li et al, 1994 and 1996). The pattern of electrical activity and consequently the associated cytosolic Ca^{2+} oscillations differs among and within different pituitary cell types which impacts the pattern of secretion. Many experimental and theoretical works have shown that both basal and receptor-controlled hormone secretion by the pituitary gland depends on the excitability of pituitary cells (Leng and Brown, 1997; Stojilkovic et al, 2010; Fletcher et al, 2018).

1.2.1 Pacemaking mechanism

Endocrine pituitary cells express various voltage-gated channels including voltage-gated calcium, potassium, sodium and chloride channels, and generate action potentials autonomously associated with transients of intracellular Ca^{2+} (Kwiecien and Hammond, 1998). In the absence of external stimuli, 50 to 75% of pituitary cells (depending on the preparation) fire action potentials resulting in rhythmic Ca^{2+} entry through L-type voltage-gated Ca^{2+} channels (Stojilkovic et al, 2010). Initially, it was speculated that the spontaneous firing in pituitary cells is a consequence of isolating and dissociating pituitary cells. However, Bonnefont and Mollard (2003) recorded the electrical activity from acute pituitary slices (in situ) and confirmed the existence of spontaneous firing in intact pituitary cells (approximately 70% of cells were spontaneously active). Therefore, the term “pacemaker” has been used to describe this spontaneous oscillating mode, meaning that pituitary cells have the ability to produce repetitive membrane electrical activity in the absence of any external stimuli. This characteristic of pituitary cells implies that their membrane

potential is sustained close to the activation threshold of the voltage-gated Ca^{2+} channel (L-type) which is responsible for the initiation of action potentials. In fact, in the absence of hypothalamic factors, it is the balance between hyperpolarising and depolarising leak currents which determines the pattern of electrical activity: in some pituitary cell types the membrane potential is maintained below the threshold and thus cells are silent, whereas in other cells the membrane potential reaches the threshold which leads to the generation of action potentials (Fletcher et al, 2018). In some pituitary cell types such as lactotrophs and somatotrophs and their clonal cell lines (e.g. GH3 and GH4 cells), it has been repeatedly demonstrated that the spontaneous firing is sufficient to drive the cytosolic Ca^{2+} level above the threshold required for stimulus-secretion as well as stimulus-transcription coupling (reviewed in Kwiecien and Hammond, 1998; Stojilkovic et al, 2010; Fletcher et al, 2018). Interestingly these cells (lactotrophs and somatotrophs) with a relatively high level of basal hormone secretion are the ones which are under tonic inhibition by hypothalamic factors dopamine and somatostatin respectively. However, in other pituitary cell types such as gonadotrophs, the spontaneous generation of electrical activity is not sufficient to drive the intracellular Ca^{2+} level to the threshold required for basal hormone secretion (Iida et al, 1991). Instead, it maintains the intracellular Ca^{2+} concentration near but below the threshold level; additionally, it is suggested that the spontaneous firing in gonadotrophs refills the Ca^{2+} stores (e.g. endoplasmic reticulum) in between peaks of FSH and LH release *in vivo* (Stojilkovic et al, 2005). Gonadotrophs are activated in an episodic manner by pulsatile GnRH secretion into the portal vessels, and thus the capability to replenish cytoplasmic Ca^{2+} stores in the absence of GnRH enables these cells to maintain a responsive state. A responsive state or set point is a state that enables the cells to be readily regulated either positively or negatively.

1.2.2 Spiking and bursting

In pituitary cells, electrical events or action potentials are generated by the interaction between calcium and potassium channels. During the upstroke of an electrical event, Ca^{2+} enters the cell and thus depolarizes the membrane potential. Subse-

quently, the potassium channels with slower activation kinetics mediate the flow of K^+ out of the cells reducing the membrane potential and terminating an electrical event. Under basal conditions, there are two categories of action potentials (or electrical events) observed in anterior pituitary cells, for which the pattern is determined by duration and amplitude of the electrical events (Figure 1.2). Some pituitary cells such as gonadotrophs generate high amplitude action potentials with a short duration (a few tens of milliseconds, Figure 1.2) (Stojilkovic et al, 2005). Although other types of pituitary cells including lactotrophs, somatotrophs and corticotrophs can generate spikes, more often, they generate bursts or a combination of bursts and spikes (Van Goor et al, 2001; Tsaneva-Atanasova et al, 2007; Liang et al, 2011). Bursts in pituitary cells (termed as "pseudo-plateau bursts") are lower amplitude electrical events with longer durations than spikes, in which the membrane potential oscillates over the action potential peak, and repolarises after hundreds of milliseconds (Figure 1.2).

1.2.3 The ionic composition underlying bursts and spikes

In neurons, tetrodotoxin (TTX)-sensitive voltage-gated Na^+ channels are crucial for the rise of action potentials (Hille, 2001). Although all endocrine pituitary cells express TTX-sensitive voltage-gated Na^+ channels, the blockade of these ion channels impact neither the pattern of spontaneous firing nor the resting membrane potential in the majority of anterior pituitary cells (Van Goor et al, 2001; Tsaneva-Atanasova et al, 2007; Kucka et al, 2012). However, inhibiting the L-type Ca^{2+} channels stops the spontaneous firing without influencing the resting membrane potential in pituitary cells (Van Goor et al, 2001; Tsaneva-Atanasova et al, 2007; Kucka et al, 2012). This signifies the key role of the L-type Ca^{2+} channels in the depolarisation phase of action potentials. It has been suggested that the lack of contribution of TTX-sensitive Na^+ channels in regulating membrane excitability and hormone release is most probably due to the inactivation of a high percentage (above 90%) of these channels at the resting membrane potential (-60 to -45 mV) in the majority of pituitary cells *in vitro* (Van Goor et al, 2001). However, this does not explain why some cells mainly produce spikes and some produce bursts.

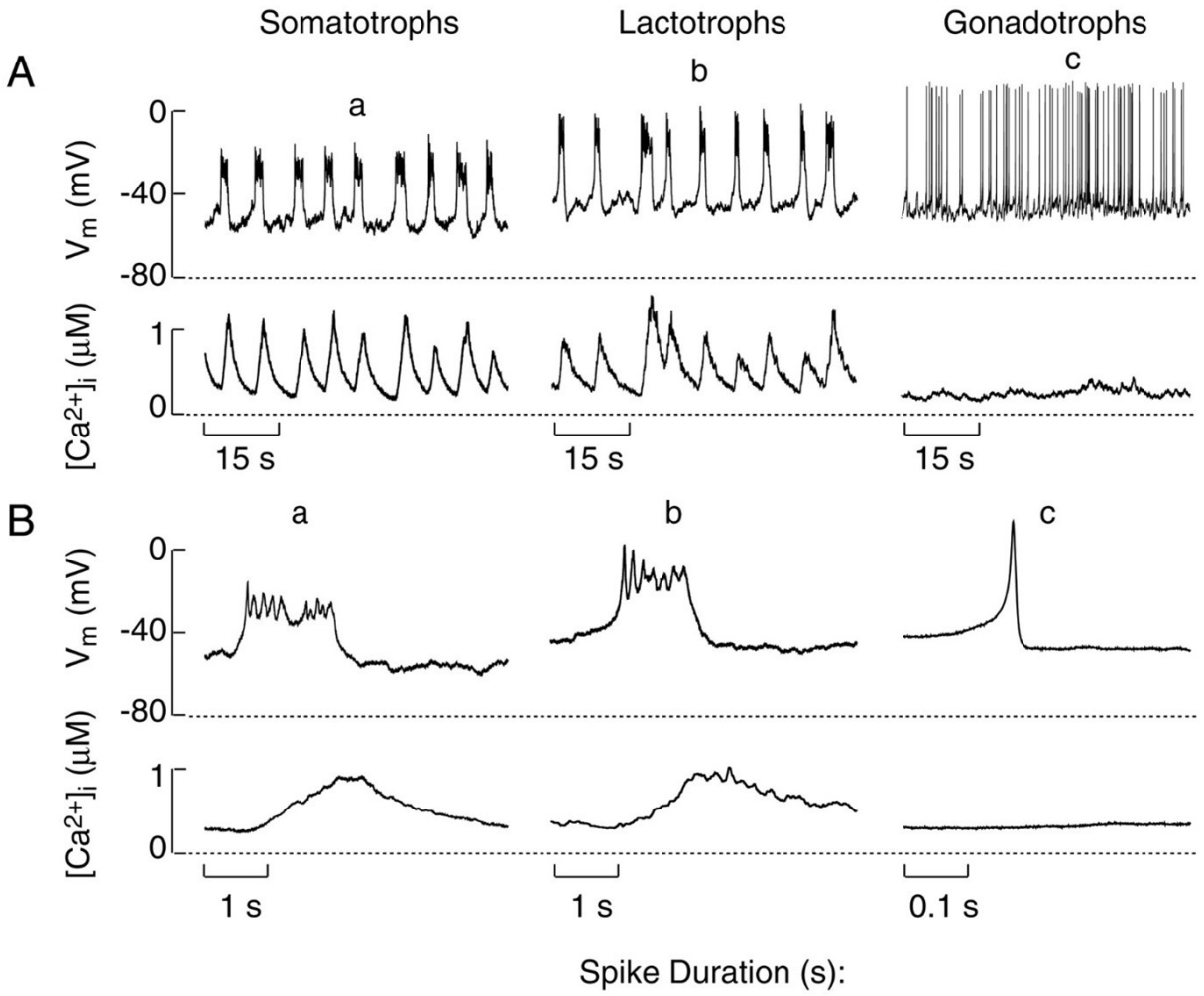

Figure 1.2: Parallel measurement of membrane potential (Vm) and intracellular calcium concentration in three pituitary cell types.
A) Longer duration action potentials facilitate larger calcium influx. **B)** Selected electrical events (corresponding to a, b and c in panel A) and their corresponding calcium transients which are illustrated on an expanded timescale (notice the difference in the time domain for gonadotrophs), (Reproduced from Van Goor et al, 2001).

The large conductance voltage-gated and Ca^{2+}-dependent potassium channel (BK) has been found to be expressed more, and consequently produce larger currents, in somatotrophs and lactotrophs than in gonadotrophs (Van Goor et al, 2001a; Van Goor et al, 2001b). BK channels become activated during the depolarisation phase of the action potential and act in conjunction with the delayed rectifier K^+ channels to repolarize the action potential (Miranda et al, 2003). Both pharmacological studies and mathematical modelling have shown that BK channels have a paradoxical role in regulating the pattern of firing in endocrine pituitary cells, and are a key component of bursting behaviour (Van Goor et al, 2001b; Tabak et al, 2011, Duncan et al, 2016). These studies have demonstrated that first, the addition of the membrane-permeable Ca^{2+} chelator BAPTA-AM converts the bursting pattern in somatotrophs into high amplitude spikes (Van Goor et al, 2001b). This is because BK channels are Ca^{2+}-dependent, and BAPTA-AM rapidly chelates the cytosolic Ca^{2+} resulting in the reduction of the Ca^{2+} nanodomain and thus attenuates the BK channels activation. Second, the blockade of BK channels by either iberiotoxin or paxilline converts bursts into high amplitude spikes in somatotrophs, whereas inhibiting SK channels using apamin has negligible impact on the firing pattern of the cells (Van Goor et al, 2001b). In contrast, increasing cytosolic Ca^{2+} in somatotrophs by adding GHRH or by increasing extracellular KCl does not change the bursting pattern to spiking, and only depolarized the resting membrane potential and enhanced the bursting frequency (Van Goor et al, 2001b).

How can an inhibitory current (BK) promote longer duration action potentials and play a stimulatory role by changing the spiking pattern to bursting in pituitary cells? It has been illustrated that the addition of BK-like current with faster activation (using dynamic clamp) into a spiking gonadotroph can convert the spikes into bursts (Tabak et al, 2011). However, the addition of BK-like current with slower activation reduces the burst frequency. The implication is that the fast activation BK channels become active quickly during the depolarisation phase of the action potentials, and since it is conducting a hyperpolarising current, it reduces the amplitude of the action potentials and consequently prevents from the full activation of delayed rectifier K^+ conductance responsible for repolarization. Although the fast

activation BK channels conduct a hyperpolarising current, the overall magnitude of the current is too small to fully repolarise the action potentials (Tabak et al, 2011). This is why its activation only slightly hyperpolarises the membrane potential below the activation threshold of delayed rectifier K^+ channels. This enables the membrane potential to oscillate around the depolarised level for hundreds of milliseconds during which a large amount of Ca^{2+} enters the cell leading to a global Ca^{2+} change (Schlegel et al, 1987). This global Ca^{2+} change is sufficient to activate the BK channels that are distant from the L-type Ca^{2+} channels (slow activation BK channels) to repolarise the action potentials. This type of burst is named "pseudo-plateau bursting".

1.2.4 Electrical activity-driven Ca^{2+}

It has been repeatedly demonstrated that the removal of extracellular Ca^{2+} or applying L-type Ca^{2+} blockers (e.g. verapamil or nifedipine) abolishes cytosolic Ca^{2+} transients in pituitary cells (reviewed in Fletcher et al, 2018). This indicates that the L-type Ca^{2+} channel is not only responsible for the rise of action potentials in pituitary cells but also facilitates the rhythmic entry of Ca^{2+} during the upstroke of each action potential. Ca^{2+} plays the role of second messenger and regulates the activity of a plethora of cellular signalling pathways (Clapham, 2007). The various patterns of spontaneous firing exhibited by different pituitary cell types have a significant impact on the cytosolic Ca^{2+} dynamics and overall Ca^{2+} levels. Simultaneous recording of membrane potential and intracellular Ca^{2+} concentration has shown that the average Ca^{2+} level is low in autonomously spiking gonadotrophs (20-70 nM), however it is much higher (300-1200 nM) in autonomously bursting lactotrophs, somatotrophs, corticotrophs, and GH3, GH4 and AtT-20 cell lines (Van Goor et al, 2001; Tsaneva-Atanasova et al, 2007; Holl et al, 1988; Lewis et al, 1988; Guerineau et al, 1991; Wagner et al, 1993). Recording from acute pituitary slices has also shown oscillatory bursts of cytosolic Ca^{2+} (Bonnefont et al, 2000). The pattern of cytosolic Ca^{2+} oscillations is not only varied among different pituitary cell types but also among cells of the same cell type population. For instance, a fraction of lactotrophs exhibit greater basal PRL secretion which is associated with

spontaneous cytosolic Ca^{2+} transients and a depolarized resting membrane potential (Lledo et al, 1991). On the other hand, the larger fraction of lactotrophs do not show oscillatory cytosolic Ca^{2+} transients, and these cells are silent with hyperpolarized membrane and low cytosolic Ca^{2+} level (Lledo et al, 1991). It has been suggested that the heterogeneity in the pattern of electrical activity and $[Ca^{2+}]_i$ transients observed in a clonal cell population can be due to the noisy transcription and translation of ion channels (Richards et al, 2020). Moreover, the stochastic opening and closing of ion channels can have a significant impact on the pattern of electrical activity in 1) small cells or 2) cases where only a handful of copies of certain ion channels are expressed (Richards et al, 2020). For instance, there are a small number of BK channels (each channel with 100 pS conductance) expressed in lactotrophs, somatotrophs and corticotrophs, and thus the random opening of a BK channel can have a large effect on the pattern of electrical activity (Richards et al, 2020).

The discrepancy observed in the patterns of cytosolic Ca^{2+} oscillations between cells spiking and those displaying pseudo-plateau bursting is because of the gating dynamics of Ca^{2+} channel activation, which leads to a distinct spatial distribution of cytosolic Ca^{2+} in each cell (Stojilkovic et al, 2005). In both spikes and bursts, the membrane potential depolarises sufficiently and reaches the activation threshold of L-type Ca^{2+} channels expressed in pituitary cells (Van Goor et al, 2001; Kuryshev et al, 1995). However, high voltage-gated Ca^{2+} channels are open for a short period of time in spikes (several tens of milliseconds) and consequently the elevated intracellular Ca^{2+} level is localized to nanodomains at the inner pore of open Ca^{2+} channels. Whereas in bursts, the channels remain open for a significantly longer time (several hundreds of milliseconds) and thus a significant amount of Ca^{2+} enters the cells leading to a global Ca^{2+} signal (Stojilkovic et al, 2005). This is because the nanodomains Ca^{2+} overlay resulting in a global Ca^{2+} signal which is easily detected by fluorescent Ca^{2+} dyes as demonstrated by confocal imaging of pituitary cells (Tomić et al, 1999). As a result, the total intracellular Ca^{2+} over time is much higher in "bursters" than that in spikers under basal conditions (Stojilkovic et al, 2005).

1.2.5 The role of extracellular Ca^{2+} in cell excitability

Ca^{2+} is an essential trigger of hormone secretion; extracellular Ca^{2+} is needed for both basal and receptor-regulated exocytosis in endocrine pituitary cells (Kwiecien and Hammond, 1998). When pituitary cells are incubated in Ca^{2+} deficient medium, hormone secretion drops and eventually disappears (Stojilkovic et al, 2010). Alterations in the extracellular Ca^{2+} concentration, within a physiological range, cause remarkable changes in both basal and receptor-regulated hormone secretion in murine and human anterior pituitary cells (Zivadinovic et al, 2002; Ferry et al, 1997; Emanuel et al, 1996; Naor et al, 1980). Overall, any procedure that leads to an increase in cytosolic Ca^{2+} level consequently results in an increase in hormone release. It is well established that Ca^{2+} plays a central role in hormone release, irrespective of the nature of stimulatory or inhibitory factors (Stojilkovic et al, 2010).

Under basal conditions (or at resting state) the physiological concentration of extracellular Ca^{2+} of excitable cells is in the range of mM, thousands of times higher than the intracellular Ca^{2+} level which is in the range of approximately 10-100 nM (Baker and Reuter, 1975). As previously mentioned, excitable cells such as endocrine pituitary cells express voltage-gated Ca^{2+} channels (VGCCs) in their membrane, which allows them to significantly enhance the cytosolic Ca^{2+} level (by several fold) in response to depolarisation from resting membrane potential (RMP) (Stojilkovic and Catt, 1992; Mollard and Schlegel, 1996). While the cytosolic calcium level increases drastically when cells are triggered by stimulatory factors for a long period of time, extracellular Ca^{2+} level may drop noticeably too. This can be due to the Ca^{2+} flowing from outside to inside the cells through VGCCs. In neurons, in places where the extracellular space is very small and limited, repetitive stimulatory signals can cause extracellular Ca^{2+} to drop from about 1.3 to 0.1 mM (Lu et al, 2010). The alteration of Ca^{2+} levels in extracellular fluid can be more erratic outside the blood brain barrier (Brown and MacLeod, 2001), where the pituitary gland is located. It has been demonstrated that extracellular Ca^{2+} negatively regulates the excitability of pituitary cells: a reduction in extracellular Ca^{2+} within a physiological range results in membrane depolarisation and consequently increases cytosolic Ca^{2+} level (Stojilkovic, 2006; Zivadinovic et al, 2002). The same scenario occurs in neurons:

extracellular Ca^{2+} negatively regulates neuronal excitability (Burgo et al, 2003; Chu et al, 2003; Frankenhaeuser and Hodgkin, 1957; Xiong et al, 1997; Yaari et al, 1983). Frankenhaeuser reported that tissues that usually do not give anode break response (fast spiking right after the termination of hyperpolarizing current) can do so if Ca^{2+} is removed from the external medium (Frankenhaeuser, 1957). Together, these findings indicate the crucial role of extracellular Ca^{2+} in regulating membrane excitability. However, the effect of extracellular Ca^{2+} on membrane excitability contrasts the effects of extracellular Na^+ and K^+, where a reduction in $[Na^+]_o$ or in $[K^+]_o$ normally oppresses cell excitability (through their contribution to leak current which will be discussed in Section 1.6).

As an ion with positive charges and much higher extracellular concentration, Ca^{2+} flux into the cell should depolarize the membrane potential in a similar manner to the effect of Na^+ and K^+. Thus, a drop in extracellular Ca^{2+} should reduce the concentration gradient of Ca^{2+} and consequently decrease Ca^{2+} movement into the cell. Intuitively therefore, the expected outcome of a $[Ca^{2+}]_o$ drop would be less Ca^{2+} influx leading to the oppression of cell excitability, which is the opposite of what has been observed. Hence, the observed excitatory effect of $[Ca^{2+}]_o$ reduction must involve pathways other than the alterations in Ca^{2+} flux across the cell membrane *per se*. It is worth noting that many experiments have been done between the 1950's and 1970's using the giant axon of squid and large muscle-fibres of the spider crab, demonstrating that there is a very low concentration of cytosolic free ionized Ca^{2+} (in nano Molar range) (Baker and Reuter, 1975). Interestingly, the radioactive Ca^{2+} injected into the axoplasm, very quickly was chelated and disappeared (Baker and Reuter, 1975). Taking these points together, the effect of Ca^{2+} on membrane excitability is more than simply creating chemical and electrical gradient across the membrane. In fact, there is another level of complexity which is the enormous number of chemical interactions that Ca^{2+} has with many proteins and enzymes inside cells leading to the regulation of many fundamental cellular processes (Nicholls and Kuffler, 2012). Therefore, its temporal and spatial distribution in the cytoplasm needs to be extremely carefully tuned, and only limited concentrations of Ca^{2+} can be free and ionized at specific locations and times in the cell. For this purpose, cells

have evolved proteins such as calmodulin which behaves as a Ca^{2+} chelator (Nicholls and Kuffler, 2012).

So what is the mechanism underlying the excitatory effect of $[Ca^{2+}]_o$ reduction? Frankenhaeuser and Hodgkin investigated this problem by evaluating the voltage dependency and activation of voltage-gated Na^+ and K^+ channels in varying concentrations of extracellular Ca^{2+} in the medium using the voltage clamp method (Frankenhaeuser and Hodgkin, 1957). They reported that reducing $[Ca^{2+}]_o$ shifted the activation and inactivation curve of voltage-gated Na^+ channels in a more hyperpolarized direction. As a result, less depolarisation (due to the lower activation threshold) was required for the channels to become active and fire action potentials, leading to an increase in cell excitability. Frankenhaeuser and Hodgkin (1957) proposed that this outcome could be due to the charge screening effect of Ca^{2+}. Ca^{2+} as a positively charged ion interacts with negative charges arising from proteins on the membrane surface and neutralises them (Nicholls and Kuffler, 2012). The cell membrane itself is composed of phospholipids and proteins which contain negative charges; these negative charges on the outer surface of the membrane are compensated by the extracellular positive charges and thus attract the uncompensated negative charges of the inner surface of the membrane (Figure 1.3) (Nicholls and Kuffler, 2012). The charge difference between the two surfaces of the membrane can create an alternative local transmembrane potential, which can directly influence the activity of voltage-gated transmembrane proteins such as ion channels (Nicholls and Kuffler, 2012). This is the reason that Frankenhaeuser and Hodgkin (1957) suggested that upon the reduction of $[Ca^{2+}]_o$, many negative charges on the outer membrane surface remain unscreened, and that decreases the effective potential gradient across the membrane whilst the electrical potential between cell interior and exterior stays the same (Figure 1.3). Therefore, when the $[Ca^{2+}]_o$ decreases, less depolarisation is required to increase the membrane potential to the activation threshold of voltage-gated sodium channels. However, one problem with this theory is that decreasing the local transmembrane potential upon the reduction of $[Ca^{2+}]_o$ could also move the voltage dependence of the activation of voltage-gated potassium channels and the inactivation of voltage-gated sodium channel in the same direc-

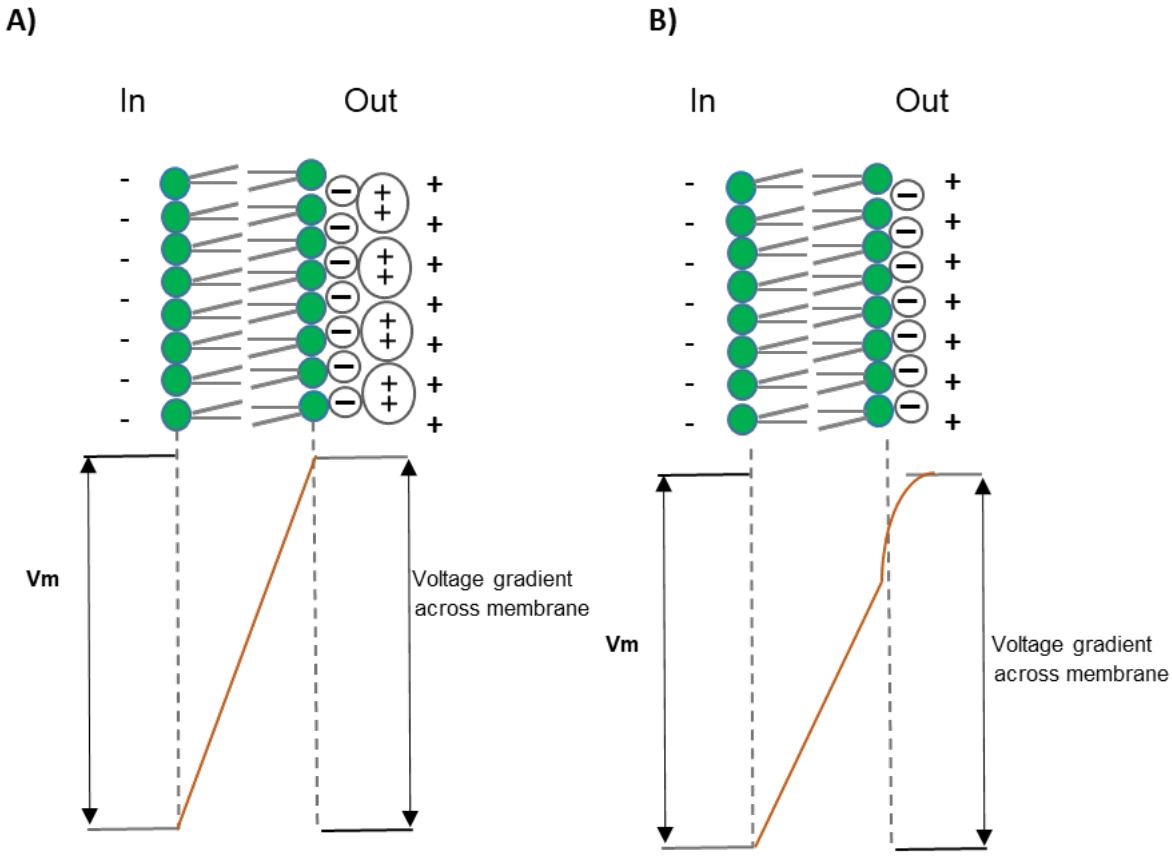

Figure 1.3: The charge screening effect of cations across the cell membrane.
A) The separation of anions and cations across the membrane during resting state leads to an electrochemical potential (Vm or resting membrane potential) the value of which is determined by the ionic composition of the intracellular and extracellular solutions. The negative charges located on the outer membrane surface are neutralized by divalent cations and thus the voltage difference between the extracellular and intracellular medium is the same as Vm. **B)** if the divalent cations such as Ca^{2+} are eliminated from the extracellular fluid, resulting in unneutralized negative charges on the outer membrane surface, the local transmembrane potential decreases (the red line). This can affect the activity of voltage-dependant proteins such as ion channels located in the membrane. (The figure is modified from Nicholls and Kuffler, 2012).

tion. This would result in the reduction of cell excitability. Moreover, Stojilkovic and colleagues performed an experiment in which they maintained the ionic strength of extracellular solution by adding an equal amount of divalent cation Mg^{2+} upon reduction of $[Ca^{2+}]_o$ to compensate the screening effect of Ca^{2+} (Zivadinovic et al, 2002). Interestingly, even after maintaining the ionic strength, the membrane potential of pituitary cells still depolarized upon the reduction of $[Ca^{2+}]_o$ (Zivadinovic et al, 2002). Moreover, this depolarisation and therefore excitation induced by the reduction of extracellular Ca^{2+} can happen through other mechanisms too. In fact, it has been reported that in various neuron types, a reduction of $[Ca^{2+}]_o$ activates inward nonselective cationic current in somas and nerve endplates (Formenti et al, 2001; Hablitz et al, 1986; Smith et al, 2004; Xiong et al, 1997). In pituitary cells, however, it has not been shown yet whether a drop in extracellular Ca^{2+} activates inward leak current. Further, the molecular identity of the ion channel mediating the inward leak current in response to a drop in $[Ca^{2+}]_o$ in pituitary cells has not been yet discovered. In Chapter 4, these questions will be addressed.

1.3 Ion channels and transporters involved in firing activity in pituitary cells

The role of ions in the excitation of muscle cells and neurons has been studied for more than a century. Sidney Ringer in the 1880s demonstrated that the external solution infusing a frog heart must comprise of potassium, sodium and calcium salts in a certain ratio for the heart to sustain beating for a significant period of time (Moore, 1911; Cordell, 1995). Shortly after in 1888, Walther Nernst showed that the diffusion of electrolytes across a semi permeable membrane creates an electrical potential; this work inspired the idea of ions determining the bioelectric potential (Nernst, 2015). In the early 1900s, Julius Bernstein accurately suggested that excitable membranes are mainly permeable to K^+ ions during the resting state and that the membrane permeability to other ions enhances during excitation (Bernstein, 1902). His theory was greatly supported by the illustration of a transient reduction in membrane resistance during excitation, which indicates the increase in membrane conductance to other ions (Cole and Curtis, 1941). Over the twentieth

century, the primary roles of each of the ions in Ringer's solution (Na^+, K^+, Ca^{2+}) were discovered.

Throughout evolution, excitable membranes have developed sophisticated molecular instruments to maintain and use the concentration gradient of various ions across the cell membrane. The cell membrane is composed of a phospholipid bilayer with a hydrophobic middle part which functions as a barrier against the passage of ions. This barrier enables the cell to keep a specific concentration of electrolytes in its cytosol which is different from the ones in the extracellular solution as well as in cytoplasmic membrane-enclosed organelles. However, in order to modulate intracellular ionic concentration as well as creating different membrane potentials, cells have had to develop various ways of transporting ions across the cell membrane. Early studies on the ionic transportation system across the membrane were primarily focused on ionic flux: changing the concentration of Na^+, K^+ and Ca^{2+} and replacing them with other cations to measure the ionic influx and efflux and their kinetics. These studies indicated two distinct transportation machineries: transporters and channels. The initial view of a transporter was a ferryboat which carries ions and translocates them backwards and forwards across the cell membrane (Laprade et al, 1975). This idea was amended since several studies purified and cloned the transporter proteins from membranes and revealed that they are too large to translocate or go through significant conformational changes at the speed required for the ionic fluxes (Benz and Läuger, 1976). The use of crystallography techniques and structural investigations provided clearer evidence about the transporter mechanism; the latest view is that transporters are transmembrane proteins composed of several interacting helical structures in which subtle conformational alterations result in the exposure of ion binding sites alternating between the cell interior and exterior (Gadsby, 2007). As a result, the binding sites of transporters either face out or in, but not to both sides simultaneously. This allows the transporters to move ions against their concentration gradient using ATP (Gadsby, 2007).

The other transportation machinery is ion channels, which unlike transporters, form aqueous pores that can be open to both the extracellular and intracellular space simultaneously, enabling the ions to pass continuously without interruption. The

porous system is supported by the results from single channel electrophysiological recordings showing that the rate of ion passage *via* a single open channel can be more than one million *per se*cond (Neher and Sakmann, 1976). This speed is much too high for any transporter system other than a continuous pore. Moreover, Doyle and colleagues provided a direct proof of the pore mechanism by the use of X-ray and structural analysis of the K^+ ion channel (Doyle et al, 1998). They showed that the ion channel is an integral transmembrane protein with a continuous aqueous pore through which the ions pass (Doyle et al, 1998).

Transporters and ion channels are both essential for the proper operation of excitable membranes. Transporters are utilized to maintain the concentration gradient of the primary ions across the plasma membrane in animal cells (Therien and Blostein, 2000). For instance, ATP-mediated transporters use the chemical energy of phosphate bonds in ATPs to pump Na^+, K^+ and Ca^{2+} against their concentration gradient to sustain relatively low Na^+ and Ca^{2+} levels as well as high K^+ level inside the cell (Therien and Blostein, 2000). As a result, the cytosolic K^+ concentration is around 20 times higher than in extracellular solution, whereas the intracellular Na^+ level is at least ten times less than the extracellular level (Steinbach and Spiegelman, 1943; Steinbach, 1940, 1941). Thus, transporters convert the chemical energy of ATPs into the electrical potential to produce action potentials during excitation. However, because each action potential occurs on the millisecond time scale and thus requires a very fast ion exchange across the cell membrane, transporters do not play a major role during the excitation process. Instead, ion channels drive the movement of ions throughout excitation in excitable cells such as endocrine anterior pituitary cells.

Neher, Sakmann and colleagues published a series of papers in the 1970s about the function of a single ion channel in the cell membrane, and their conclusions provided foundational principles of ion channel function. Several predictions they made regarding the operation of ion channels were exact and opened the doors for future research in the channelosome. According to their work: (1) the opening and closing of individual ion channels is statistically independent and happens randomly, the probability of which is impacted by the concentration, exposure time

and the type of stimulus; (2) there is a distinction between factors affecting the properties of single channels and factors producing or modifying different groups of channels. The latter conclusion led to extensive research characterizing ionotropic and metabotropic channels (Neher and Sakmann, 1976; Hille, 2001). Later works indicated that every ion channel can be considered as an excitable entity which exclusively responds to a particular stimulus, including: an alteration in membrane voltage (voltage-dependent ion channels); a neurohormone (or neurotransmitter in neurons, which activates either ligand-gated or receptor-gated ion channels); mechanical pressure; pH change; or a change in temperature for mechanosensitive, pH-sensitive and temperature-sensitive ion channels respectively (Hille, 2001). The response is either opening or closing of the channel pore. The opening of the ion-selective pore enables specific ions to move passively along their electrochemical gradient, whereas closing of the pore stops the flow (Hille, 2001). The orchestrated opening and closing of a particular type of ion channel leads to the generation of action potentials which can be in the form of either spike or burst or a combination of both.

1.4 Leak channels and their contribution in tuning membrane excitability

As discussed in previous sections, one way of controlling the cell excitability is through its resting membrane potential which is determined by the ion flux across the membrane during the resting state (Hille, 2001). Across a semipermeable membrane, for each ion, the reversal or equilibrium potential is defined as the membrane potential at which the chemical gradients and electrical forces are in balance and thus the net flow of the ion *via* any open channel is zero (Nernst, 2015). In the case of biological systems, there are several types of ions in the extracellular and intracellular solution and thus each ion tends to drive the membrane voltage towards its own reversal potential (also called Nernst potential). The Nernst potential can be quantified by the following equation which is the logical implication of thermodynamic laws:

$$E = \frac{RT}{zF} \ln \left(\frac{[ion]_{out}}{[ion]_{in}} \right) \tag{1.1}$$

Where

E: Nernst potential (between inside and outside of the cell) in volts

R: Ideal gas constant in Joul/mol.Kelvin

T: Temperature in Kelvin

F: Faraday's constant in coulombs per mol

z: Ion valence

$[ion]_{out}$: The extracellular ion concentration

$[ion]_{in}$: The intracellular ion concentration

Thus, various types of ions tend to drag the membrane potential towards their own Nernst potential. However, in this competition, the comparative contribution of each ion in determining the membrane potential depends on the ion permeability and membrane conductance for each ion which can be calculated by Goldman-Hodgkin-Katz (GHK) equation (ion permeability is the capability of an ion to pass through the ion channel regardless of whether it is moving across the membrane, and thus is an intrinsic feature of the ion, whereas membrane conductance is the measure of the ion movement across the membrane). The equation is:

$$V_{rest} = \frac{RT}{F} \ln \frac{P_K[K^+]_{out} + P_{Na}[Na^+]_{out} + P_{Cl}[Cl^-]_{in}}{P_K[K^+]_{in} + P_{Na}[Na^+]_{in} + P_{Cl}[Cl^-]_{out}} \tag{1.2}$$

where P is the ion permeability. Deriving this formula from the Nernst potential equation, Goldman, Hodgkin and Katz could demonstrate that the conduction and excitation in excitable cells can be described quantitatively (Hodgkin and Huxley, 1952). More importantly, they could show that each biological cell can be described as an electrical circuit with the membrane as capacitor, ion channels and transporters as resistors and the extracellular and intracellular solutions as the conductive medium (Figure 1.4) (Hodgkin and Huxley, 1952). In the central nervous system and the pituitary gland, the membrane potential is primarily set by K^+, Na^+ and Cl^- because of prevailing concentrations of these ions in extracellular and intracellular fluids as well as their high permeability *via* the cell membrane (Hille, 2001). When pituitary cells (as well as neurons) are at the resting condition, the majority of the voltage-gated and time-dependent ion channels are closed. Therefore, the voltage- and time-independent "background leak conductances" that are constitutively open have the major contribution in determining the resting mem-

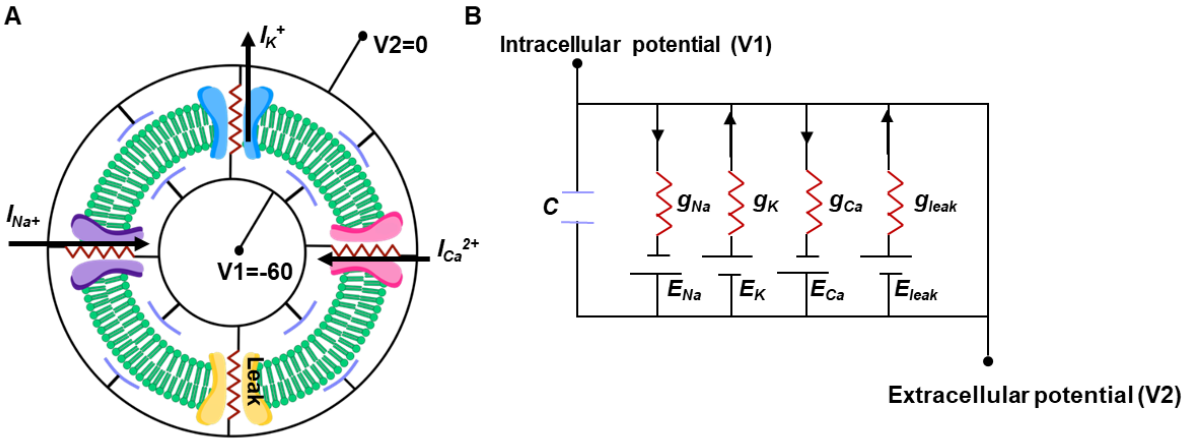

Figure 1.4: The electrical circuit model of a spherical cell.
A) The cell membrane (green) is composed of a lipid bilayer which is hydrophobic and non-conductive. The phospholipid structure and the proteins located in the membrane contains negative charges. The negative charges on the outer membrane attract positive charges (cation) and thus are neutralized. This leads to the positive charges lining up on the outer membrane surface, which attract the inner membrane negative charges that are left uncompensated. As a result, the negative charges line up on the inner part of the membrane and create a local transmembrane potential. This set up in the biological membrane turns it into a capacitor. The transmembrane proteins specialized for conducting the ions behave like a conductor or a resistor ($R = 1/g$). While they are open, the conductance for ion passage increases. The higher the conductance, the lower the resistance and vice versa. The black arrows show the direction of the ion flow down their concentration gradients. The intracellular and extracellular solution containing electrolytes act like a conductive medium. The difference between the intracellular and extracellular potentials creates the membrane potential. The cell membrane (capacitor) is in parallel with the ion channels (resistors). **B)** By removing the biological elements, we are left with a physical electrical circuit whose function follows Ohm's law. E represents the equilibrium potential for each type of ion channel, and C represents the capacitor. This circuit model reduces the complexity of a biological membrane down to its basic components which makes it easier to evaluate its function.

brane potential (RMP) (Hodgkin and Huxley, 1952). The background K^+ leak conductance is mediated through many potassium leak channels such as K2P family (2 pore-domain potassium) channels (Goldstein et al, 2005). The background K^+ leak current tends to set the resting membrane potential at its reversal potential which is about -85 mV in pituitary cells under physiological conditions. However, the recorded resting membrane potential in anterior pituitary cells is in the range of -65 to -45 mV (Stojilkovic, 2012), which is significantly depolarized relative to the K^+ equilibrium potential. This can be explained by the presence of Na^+ leak conductance detected in recordings of endocrine anterior pituitary cells (Fletcher et al, 2018). Na^+ concentration in extracellular medium is about 10-13 times higher than in intracellular space (which is established by Na^+/K^+ pump) and thus Na^+ leak current drives the membrane potential towards its reversal potential which is +60 mV. However, Na^+ leak conductance is only a fraction ($\approx$4% in the giant axon of squid) of the K^+ leak conductance under resting condition (Hodgkin and Katz, 1949). Thus, the resting membrane potential is much closer to the reversal potential of K^+ than to that of Na^+. Moreover, as the Na^+ reversal potential is far away from the RMP, resulting in a high depolarizing driving force for Na^+, sodium leak conductance has the capability to significantly adjust the resting membrane potential and regulate cell excitability. Excitability relies on the resting membrane potential, since action potentials fire once the membrane potential reaches a threshold where voltage-sensitive ion channels open and successively go into inactivation mode. To regenerate action potentials, the voltage-sensitive ion channels must recover from inactivation *via* reaching a negative voltage below the activation threshold corresponding to the resting membrane potential. In Chapter 3, the relative contribution of Na^+ leak conductance over K^+ leak conductance in regulating the resting membrane potential will be explored in pituitary cells.

1.4.1 Potassium leak channels

Leak conductance regulates cell excitability by influencing the duration, frequency and amplitude of action potentials *via* their contribution to the resting membrane potential (Golestein et al, 2001). Enhanced K^+ leak conductance sets the membrane

potential at hyperpolarized voltages below the activation threshold of voltage-gated channels. However, suppressing the K^+ leak conductance enables membrane depolarisation and excitation. K^+ leak channels dominate the membrane conductance during resting state, and are responsible for maintaining the resting membrane potential at negative values close to the E_K.

Molecular identification reveals three major families of K^+ channels with distinct structures: (1) voltage-gated K^+ channels; (2) Inward-rectifier (Kir); and (3) two-pore domain K^+ channels (K2P). Voltage-gated K^+ channels become active by depolarisation, enabling the outward passage of K^+ in depolarized cells, which leads to the repolarization of membrane potential succeeding the upstroke of an action potential. In contrast, Kir channels become blocked by Mg^{2+} and polyamines, and pass very small amplitude K^+ current under conditions of high intracellular and low extracellular K^+ concentration in which the electrochemical gradient of K^+ directs outward currents (O'Connell et al, 2002). Once the resting membrane potential drops to more negative values, the Kir blockage removes, resulting in inward K^+ currents (Goldstein et al, 2001). This is why it is named the "inward rectifier" K^+ channel.

Current passage *via* K2P channels is governed primarily by electrical force and chemical gradient of K^+ across the cell membrane. Moreover, their open state probability is voltage-insensitive and thus this group of K^+ channels are categorized as background K^+ channels, and are rather insensitive to a wide range of classical potassium channel blockers, such as tetraethylammonium (TEA), 4-aminopyridine (4-AP) and Ba^{2+} (O'Connell et al, 2002; Stojilkovic et al, 2010, Lesage, 2003). The molecular structure of K^+ leak channels is known to have two pore-forming domains (2p) in each subunit (Goldstein et al, 2001).

Even though K^+ leak channels pass K^+ over a wide range of membrane potentials, their conductance can be regulated by various agents such as serotonin and cyclic nucleotide (c-AMP) which have been shown to close K^+ leak channels in Aplysia sensory neurons, and noradrenaline that opens K^+ leak channels in guinea-pig submucosal neurons (Siegelbaum et al, 1982; Shen et al, 1997). Additionally, other researchers have reported oxygen-sensitive and GABA (B)-modulated K^+ leak

channels in mammals (Buckler, 1997; Wagner et al, 1997). Further investigations have revealed that these channels are also modulated by pH, stretch, heat, GPCRs and anaesthetics (O'Connell et al, 2002).

1.4.2 Non-selective cationic leak conductance

As discussed above, even though K^+ leak channels make the dominant contribution to the resting conductance of pituitary cells (and neurons), the resting membrane potential of pituitary cells is between -65 to -45 mV (around 20 to 40 mV more depolarized than the equilibrium potential of K^+). This indicates the existence of other cationic leak conductances contributing to the resting membrane potential of pituitary cells (and neurons). Hypothetically, a tonic inward leak current of cations including Ca^{2+}, Mg^{2+} and H^+ fulfil this role, however too much leak of these ions into the cells is destructive to them due to the high sensitivity of cellular homeostatic mechanisms to these cations, which is not the case with Na^+. The most evident role of background Na^+ conductance detected in recordings of all pituitary cell types (Liang et al., 2011; Zemkova et al., 2016; Kucka et al., 2010; Sankaranarayanan and Simasko, 1996; Simasko, 1994; Tomic et al., 2011) is to counteract the K^+ leak conductance to tune the RMP, which would be around -85 mV in pituitary cells and other neurons if there was only basal K^+ leak. By varying the basal permeability of Na^+/K^+ leak conductance, pituitary cells can have a broad range of RMPs among various cell types and within the same cell type, a heterogeneity observed in the intrinsic properties of pituitary cells (Stojilkovic et al, 2010). This is because marginal discrepancies in the expression of background Na^+ leak channels in each individual cell could set the RMP at a different level. It is well established that gene expression in eukaryotic cells is stochastic and associated with noise, and thus the noise emerging from transcription considerably influence protein levels within a clonal population and results in heterogeneity (Blake et al, 2003).

The presence of the basal Na^+ leak conductance was initially found in the giant axon of squid more than 70 years ago by Hodgkin and Katz, and it was estimated to be 4% of basal K^+ leak conductance (Hodgkin and Katz, 1949). Since then, researchers have been looking at these subthreshold cationic conductances

and have reported the existence of several cellular devices contributing to the resting background Na^+ conductance: (1) sodium-dependent cotransporters (such as Na^+-glucose co-transporters and Na^+-phosphate cotransporters) and electrogenic Na^+ transporters (which only carry ion charges) enable Na^+ to enter the neurons; (2) in some neurons as well as pituitary cells, hyperpolarisation-activated and cyclic nucleotide-dependent Na^+ channels (HCN with I_h) are present and conduct Na^+ in a certain subthreshold voltage range, and while they are not fully K^+ selective they have a GYG (glycine-tyrosine-glycine) sequence; (3) the persistent Na^+ current produced by voltage-sensitive Na^+ channels *via* the "window" currents or through non-inactivating ion channels (reviewed by Ren, 2011). However, the subthreshold voltage-sensitive Na^+ conductance is very sensitive to changes in membrane voltage and are blocked by TTX (tetrodotoxin) in the central nervous system (Ren, 2001). Finally, many neurons show a TTX-resistant, voltage-independent "real" background Na^+ current or Na^+ leak current.

1.4.3 NALCN channel: protein structure and function

During the 1980s and 1990s, molecular cloning combined with exogenous expression led to the discovery of 20 four-domain α-subunits superfamily recognized as voltage-dependent Na^+ and Ca^{2+} channels. The family of voltage-gated Na^+ channels includes ten ion channels: $Na_V1.1$-1.9 voltage-gated channels and the non-voltage-gated NaX. The family of voltage-gated Ca^{2+} channels also has ten members: the L-type $Ca_V1.1$-1.4, P/Q type $Ca_V2.1$, N-type $Ca_V2.2$, R-type $Ca_V2.3$, and T-type $Ca_V3.1$-3.3 channels (Figure 1.5) (Lu et al, 2007; Snutch and Monteil, 2007). The pore-forming α subunit of all the channels is composed of four homologous domains each of which consists of 6 transmembrane spanning fragments: a pore loop, external and internal connecting loops (4×6TM). In 1999 however, Lee and colleagues reported the cloning of a cDNA encoding for a new protein from rat brain with a similar predicted topology as voltage-gated Na^+ and Ca^{2+} channels, and referred to as *Rb21*. The *Rb21* mRNA is predominantly expressed in the brain, moderately in the heart and has a relatively weak expression in the pancreas (Lee et al, 1999). In spite of their extensive attempts in expressing the newly cloned cDNA into two expression

systems: Xenopus oocytes and the mammalian cell line tsA201 (Human embryonic kidney cells), they could not detect any currents from the putative channel (Lee et al, 1999). This discovery introduced a third branch to the four-domain voltage-dependent ion channels phylogenetic tree with unknown physiological, biophysical and pharmacological properties (Figure 1.5). Later on, Dejian Ren's laboratory conducted a series of very interesting studies in which they generated *Rb21* (now called NALCN) gene knock-out mice to evaluate their physiology and comprehensively assess the electrophysiological characteristics of the Rb21 ion channel (Lu et al, 2007). Ren and colleagues observed that all the new-born homozygous knockout mice died within 24 hours of birth due to a severe disruption in the respiratory pattern accompanied by enhanced periods of apnoea resulting in hypoxia and neonatal death of all mice (Lu et al, 2007). The interrupted respiratory rhythm in the knockout mice was due to the loss of rhythmic bursting pattern of electrical activity and reduced firing frequency in the C4 (cervical) nerve root of the brain stem that innervates the diaphragm, and is responsible for its contraction and regulation during normal respiration (Lu et al, 2007). Moreover, the authors reported that the resting membrane potential of hippocampal neurons was reduced by 10 mV and was insensitive to the changes in extracellular Na^+ concentration. The background Na^+ leak current was significantly reduced, and the TTX- and Cs^+-resistant Na^+ leak current was not detected in the mutant hippocampal neurons (Lu et al, 2007). Using heterologous expression in HEK293 cells Ren and colleagues were able to record constitutively active, voltage-independent and nonselective cationic current which is identical to the properties of the long-sought neuronal background Na^+-leak channel/nonselective and thus it was named NALCN (Lu et al, 2007). It is worth noting that Lee and colleagues in their 1999 paper, stated that "there was no significant inward current in *Rb21* (so called NALCN)-injected oocytes" similar to the one elicited from voltage-gated Ca^{2+} and Na^+ channels. This led them to conclude that there is no detectable functional expression of the novel protein in their expression systems (Lee et al, 1999). Their report suggests that they were expecting to observe a large inward current similar to the one recorded from the voltage- gated channels, and presumably they may have attributed the observed few pA increase in the leak

current to the leaky or loose seal rather than a physiological phenomenon. However, Ren and colleagues demonstrated that the increase in the leak current in HEK293 cells is physiological by replacing the extracellular Na^+ with the large impermeable cation $NMDG^+$ which led to a significant reduction of the leak current in HEK cells (Lu et al, 2007). Therefore, they could show that the observed increase of the leak current in HEK293 cells is indeed due to the expression of the injected *Rb21* cDNA (NALCN cDNA) and is a physiological phenomenon.

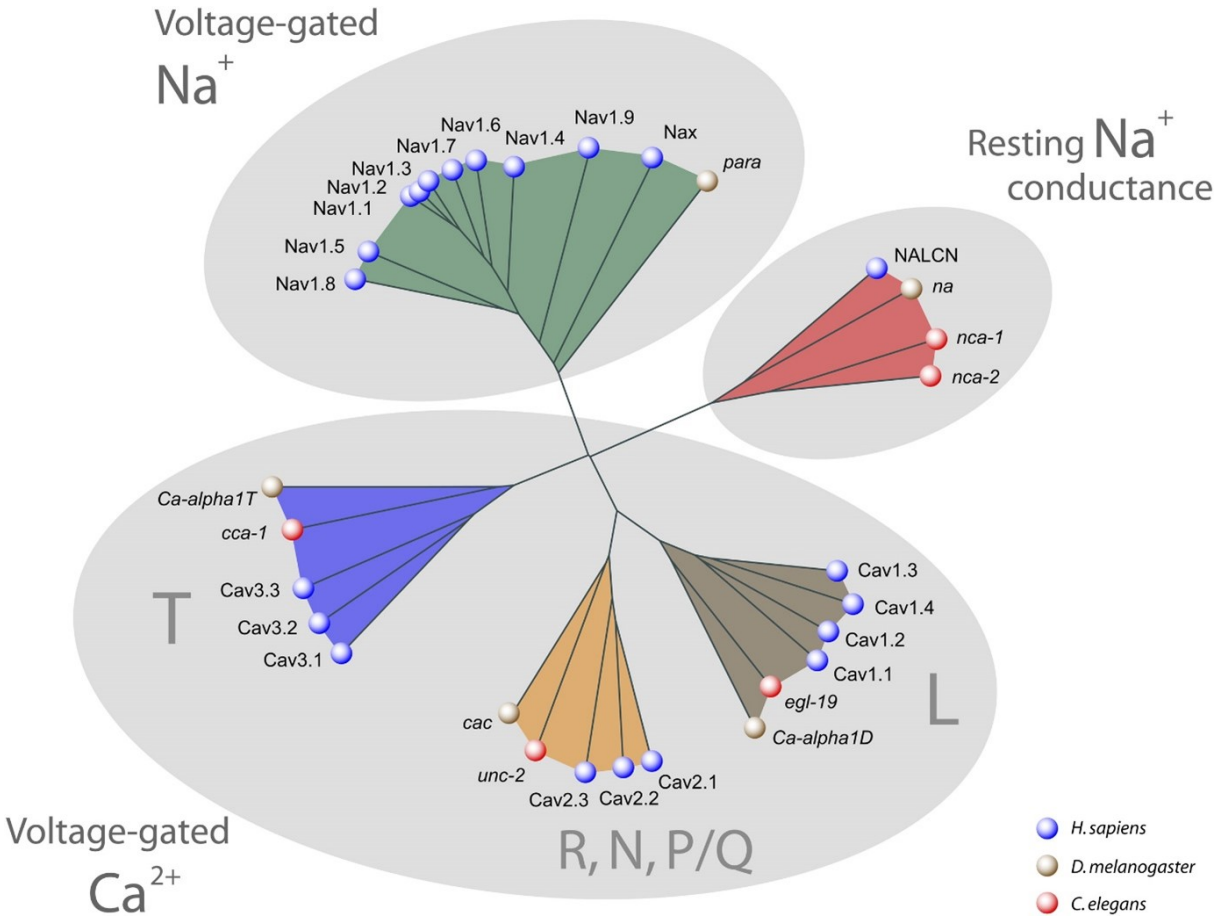

Figure 1.5: Classification of the pore-forming α-subunit of the four-domain ion channel family, as depicted for three species: *Homo sapiens, D. melanogaster and C. elegans.*
Ten α-subunit genes express the mammalian family of voltage-dependant Na^+ channels (Nav1.1–1.9, Nax), ten α-subunit genes express the mammalian voltage-dependant Ca^{2+} channels (Cav1.1–1.4, Cav2.1–2.3, Cav3.1–3.3). The third branch expresses the discovered background Na^+ conductance NALCN which tunes the resting membrane potential at more depolarised levels than the equilibrium potential of K^+. (The figure is reproduced from Snutch and Monteil, 2007).

As previously mentioned, structurally, voltage-dependent Na^+ and Ca^{2+} channels consist of four homologous domains, each of which is composed of 6 transmembrane segments (S1-S6) (Hille, 2001). Their selectivity filter is made up of extensions of S5-S6 pore (p) loops incorporated by each transmembrane domain (Figure 1.6) (Hille, 2001). In voltage-gated Ca^{2+} channels, the Ca^{2+} selective pore needs acidic amino acids which can bind Ca^{2+} in the canal of the pore. These amino acids are four glutamate [E] or aspartate [D] residues coming from each individual of the four homologous domain called EEEE and EEDD motifs (Figure 1.6). The selectivity filter in voltage-dependant Na^+ channels contains the DEKA locus composed of aspartate, glutamate, lysine and alanine which face the pore canal and are located in analogous positions (Figure 1.6) (Heinemann et al, 1992; Koch et al, 2000).

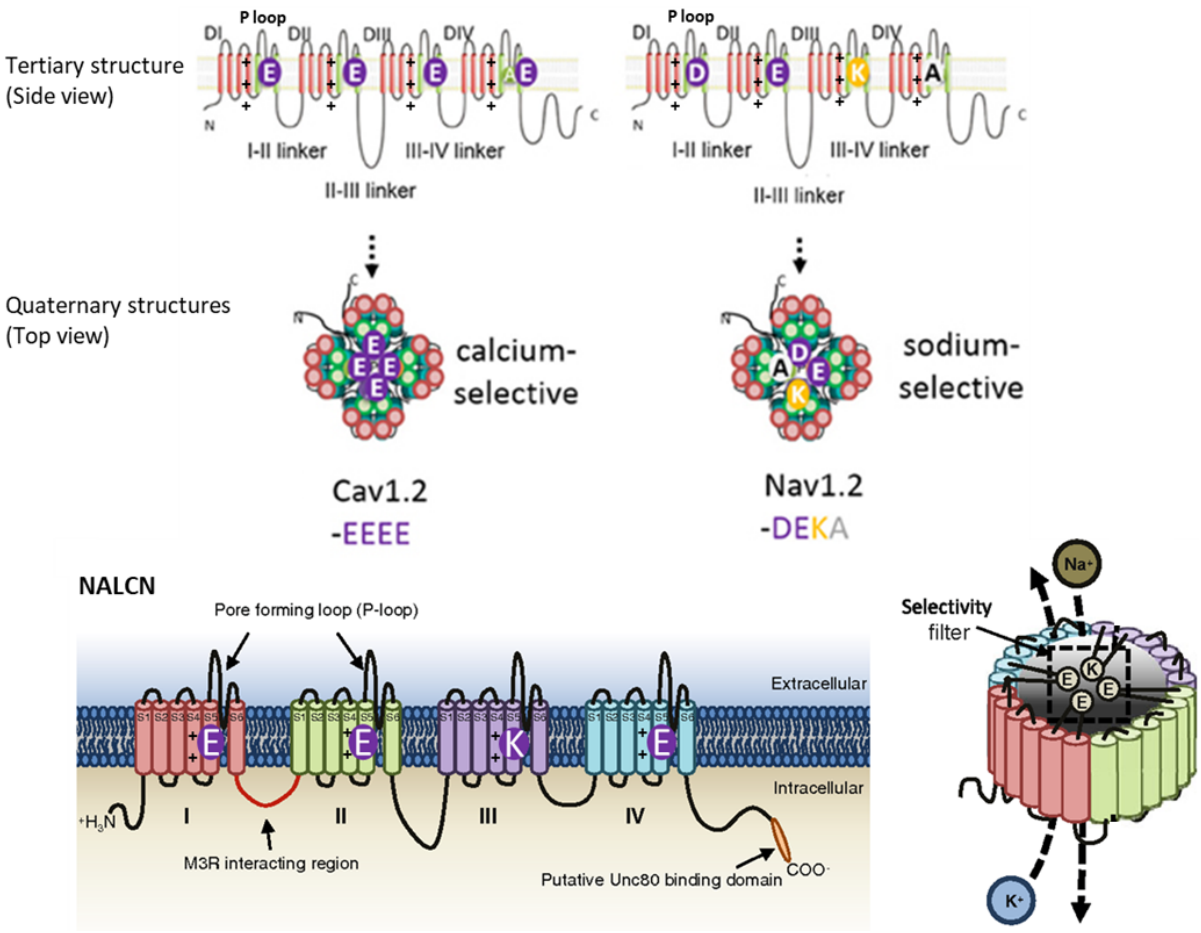

Figure 1.6: The molecular structure of the pore-forming α-subunit of the four-domain 6 transmembrane (4px6TM) ion channel family in eukaryotic cells.

Voltage-gated Na^+ and Ca^{2+} channels as well as NALCN all have four homologous domains each of which is composed of six spanning transmembrane segments (S1-S6). Four pore forming loops (P loops) extending from S5 to S6 makes the ion conductance and selectivity filter. The main difference between the voltage-gated channels and NALCN structure is 1) the number of positively charged residues on S4 of each 6TM domain, which is considerably higher in the voltage-sensitive channels than NALCN (21 vs 13), 2) the type of residues forming the selectivity filter (motif) which determines the unique permeability of each ion channel and 3) the pore size which is the narrowest in voltage-gated Na^+ channels. Mutation experiments revealed that UNC_{80} directly binds the C-terminal of NALCN. Moreover, it showed that M3R (muscarinic M3 receptors) connects to NALCN through cytoplasmic loop between domain I and II. (The diagram for the voltage-gated channels is adapted from Stephens et al, 2015; the diagram for NALCN is adapted from Lu and Feng, 2012).

In mammals, the NALCN ion channel is a protein made of 1738 amino acids that has a topology similar to voltage-activated Na^+ and Ca^{2+} channels but with distinct features (Lu et al, 2007). In the voltage-sensing S4 transmembrane segments of each of the four domains of NALCN, there are less positively charged amino acids (13 versus the 21 discovered in $Na_V1.1$ or $Ca_V1.1$) (Figure 1.6) (Lee et al, 1999, Lu et al, 2007). This can explain the voltage insensitivity of the NALCN channel. Interestingly the pore region of NALCN is composed of an EEKE motif which is a mixture between the pore motif of the voltage-gated Na^+ (DEKA) and that of the voltage-gated Ca^{2+} channel (EEEE or EEDD) (Figure 1.6) (Lu et al, 2007). This hybrid motif endows NALCN a selectivity pore with a unique permeation property. Lu and colleagues proved that NALCN protein forms the channel structure itself by mutating its selectivity filter from EEKE to EEKA. This led to a reduction in Ca^{2+} selectivity ratio from PCa=0.5 to PCa=0.1 (Lu et al, 2007).

1.4.4 NALCN auxiliary subunits

In a similar manner to many ion channels, NALCN is linked (directly and indirectly) with numerous proteins, forming a large complex (Figure 1.7). The networking proteins are UNC_{79}, UNC_{80}, Fam155A or Nlf-1, Src tyrosine kinase family and G-protein coupled receptors, which are involved in the folding, stabilization, cellular localization, and activation of NALCN (reviewed in Cochet-Bissuel et al, 2014).

UNC_{80} and UNC_{79}

UNC_{80} and UNC_{79} are large proteins composed of approximately 3300 amino acids and 2800 amino acids respectively, without any known transmembrane segments or functional domain (reviewed in Cochet-Bissuel et al, 2014). It has been demonstrated that the UNC_{80} gene expresses a highly conserved protein which is necessary for the neuronal localization and expression level of the NCA-1 and NCA-2 ion channel subunits in *C. elegans*, which are the orthologues of NALCN in mammals (Jospin et al, 2007). In this study, it was shown that UNC_{80} loss-of-function mutants are sluggish and move occasionally, spending most of their time lying still on plates. If the animals were triggered by external stimulants, they would only move two body lengths and quickly stop, a phenotype known as "fainting" (Yeh

et al, 2008). Moreover, it was shown that NCA-1 and UNC_{80} are both required in *C. elegans* for transmitting depolarisation signals from cell bodies to synaptic regions. Loss of function UNC_{80} and UNC_{79} mutants exhibited the same phenotype as observed in NCA loss-of-function mutants, which was a decreased synaptic transmission at the neuromuscular junctions resulting in regular fainting (halting in locomotion) in *C. elegans* (Yeh et al, 2008). Interestingly, the same group found that the loss-of-function of either the UNC_{79} or UNC_{80} gene is enough to revert the coiler phenotype observed in NCA gain- of-function mutants to that of fainters (exaggerated body bends during movements leads to a phenotype called coiler) (Yeh et al, 2008). Their further investigation using *in vivo* calcium imaging showed that while the cytosolic Ca^{2+} transients in cell bodies of the mutants' motor neurons are not changed by altered NCA activity, synaptic Ca^{2+} oscillations are remarkably decreased in loss of function mutants, and increased in gain-of-function mutants (Yeh et al, 2008). Additionally, the use of fluorescence probes (immunostaining) indicated an enriched co-expression of UNC_{80}, UNC_{79} and NCA in non-synaptic regions along the axons in *C. elegans*. Overall, this implies that first, NCA is required for signal transmission along the axon; secondly, its localisation and functionality relies on UNC_{80} and UNC_{79} and thirdly, NCA (NALCN), UN80 and UNC_{79} co-localize in the same channel complex (Yeh et al, 2008). Later, Lear et al (2013) uncovered more details regarding the interdependency between NALCN, UNC_{79} and UNC_{80} to better comprehend the function and modulation of the NALCN channel. They generated UNC_{79} and UNC_{80} loss-of-function mutants in Drosophila melanogaster (Lear et al, 2013). They discovered that the mutants exhibit severe deficiencies in circadian locomotor rhythms which are not distinguishable from NA mutant phenotypes (the NARROW ABDOMEN channel in *D. melanogaster* is orthologous to the mammalian NALCN). Using molecular techniques, they detected that the loss of function of each individual gene - NA, UNC_{79} or UNC_{80} - results in reduced expression of all three proteins in pacemaker neurons, with an insignificant effect on mRNA levels. These results suggest an inter-reliant post-transcriptional modulatory relationship amongst the three gene products. Interestingly, despite this relationship, they found that the need for UNC_{79} and UNC_{80} in generating circadian rhythm

in *D. melanogaster* cannot be circumvented by enhancing NA protein expression (Lear et al, 2013). Moreover, immunoprecipitation experiments demonstrated that UNC_{79} and UNC_{80} form a complex with NA in *D. melanogaster* neurons (Lear et al, 2013). Collectively, these results indicate essential requirements for UNC_{79} and UNC_{80} proteins which are indispensable to produce a functional cationic leak channel protein. Further, the data highlights that UNC_{79} and UNC_{80} support NA protein localization/maturation during translational stage after transcription.

However, this regulatory interaction in invertebrates may not be entirely conserved in mammals. In fact, it has been reported that while loss of function UNC_{79} mutant mice do not show detectable amounts of UNC_{80} proteins, they do display high levels of NALCN (Lu et al, 2010; Speca et al, 2010). More investigations revealed that UNC_{80} behaves as a scaffold protein for UNC_{79} and Src family tyrosine kinases (Figure 1.7) (reviewed in Cochet-Bissuel et al, 2014). Indeed, NALCN is able to interact with UNC_{80} in the absence of UNC_{79}, and UNC_{79} interacts with UNC_{80} in the absence of NALCN. This implies that UNC_{80} is a scaffolding protein between NALCN and UNC_{79}. Additionally, the interaction between NALCN and UNC_{80} is mandatory for NALCN activation and inhibition by G-protein coupled receptors (Wang and Ren, 2009; Lu et al, 2010). Moreover, it is demonstrated that the presence of UNC_{80} is sufficient for NALCN to operate normally in mouse primary neurons, and is able to bypass the need for UNC_{79} (Lu et al, 2010; Lear et al, 2013).

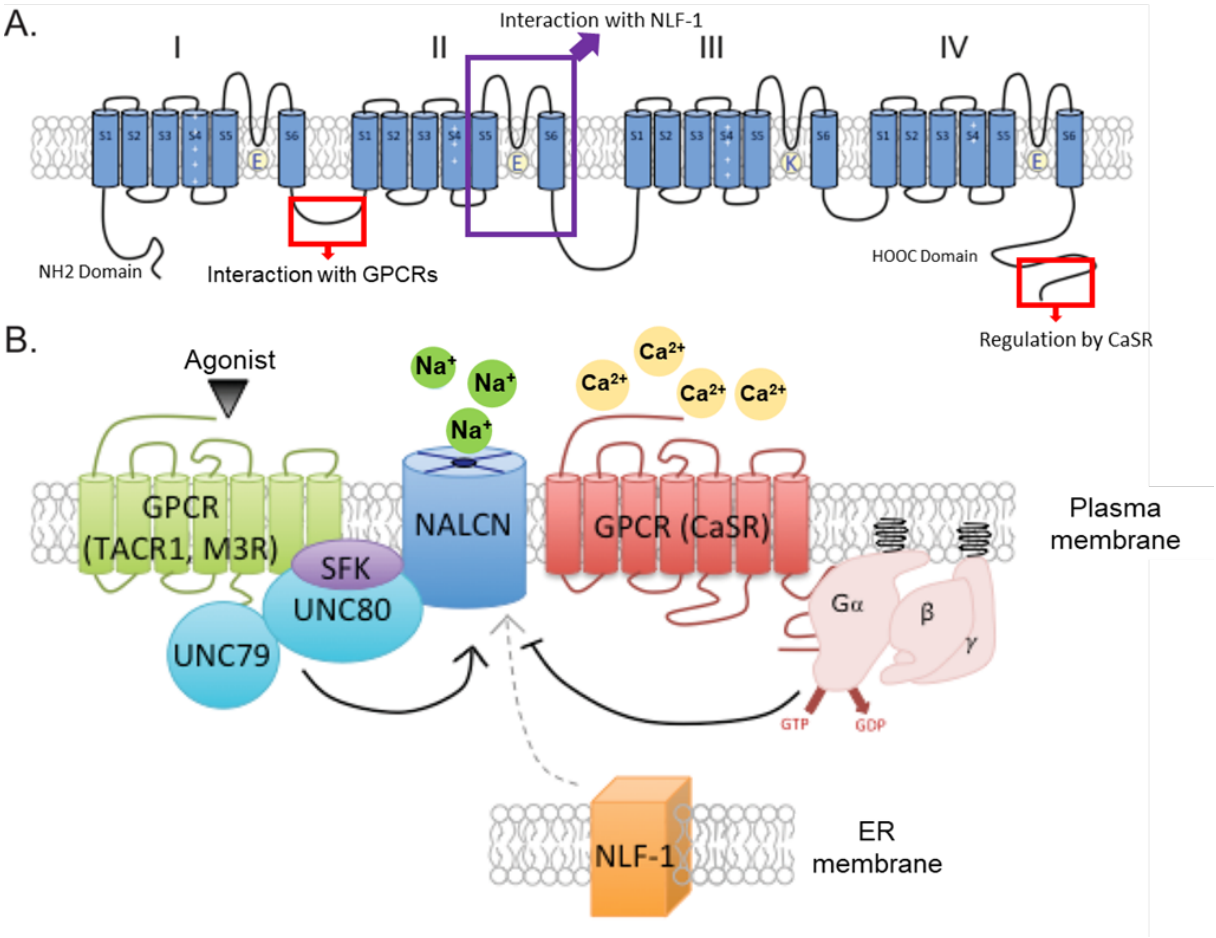

Figure 1.7: Schematic representation of NALCN and the associated proteins.
A) The intracellular loop of NALCN connecting domains I and II links with M3R (Swayne et al, 2009). The downstream molecular cascade of CaSR (Ca^{2+} sensing receptor) interact with cytoplasmic carboxy-terminus (Lu et al, 2010). The loop extended from S5 to S6 of transmembrane domain II is necessary for the interaction with NLF-1 (Xie et al, 2013). **B)** NCA localization factor-1 (NLF-1) or FAM155A (mammalian orthologue of NLF-1) engages in rapid assembly and delivery of NALCN to the plasma membrane where NALCN interacts with G-protein coupled receptors such as Tachykinin receptor 1 (TACR1) and Muscarinic receptor 3 (M3R). Once activated by their agonists substance P and acetylcholine respectively, they increase NALCN conductance which results in enhanced NALCN currents *via* SFK (*src* family kinases)-coupled pathway. The presence of UNC_{79} and UNC_{80} is mandatory for SFK dependant pathway. NALCN current is suppressed at a normal extracellular Ca^{2+} level (2 mM) through a G-protein coupled Ca^{2+} sensing receptor (Lu et al, 2010), however Chua and colleagues (2020) have provided evidence showing that extracellular Ca^{2+} directly inhibit the NALCN pore (The figure is modified from Reinl, 2016).

1.4.5 NLF-1 (NCA Localisation Factor-1, also termed FAM155A)

NLF-1 or FAM155A is a protein with 438-468 amino acids (depending on the species) which interacts with premature sodium leak channel NALCN to stabilise and facilitate its native conformation and membrane localization. It has been recently reported that robust functional heterologous expression of NALCN requires co-expression of FAM155A, UNC80 and UNC79 to recapitulate the hallmarks of non-selective cationic leak currents (Bouasse et al, 2019; Chua et al, 2020). The NALCN–FAM155A structure has shown several features with distinguished physiological implications. FAM155A produces a large extracellular dome that may accumulate cations towards the selectivity filter and shields attack from peptide neurotoxins (Kschonsak et al, 2020). The NALCN–FAM155A interface is extensive and evolutionarily conserved (Kschonsak et al, 2020). It is suggested that FAM155A probably has evolved to regulate the organised assembly/folding and function of NALCN (Kschonsak et al, 2020)

Mei Zhen and her team performed a genetic screen to identify genetic suppressors that can revert the coiler phenotype observed in gain-of-function NCA mutants (referred to as NCA (gf)) in *C. elegans* to a wild-type phenotype, in order to identify subunits or effectors of the newly discovered ion channels NCA (NALCN in mammals). Through screening genetic suppressors for NCA (gf), they found another gene NLF-1 (NALCN localization factor 1) whose loss-of-function rescues the coiler phenotype displayed by NCA (gf) worms (Xie et al, 2013). As mentioned before, while NCA (gf) show exaggerated body curves over movements leading to periodic coiling (Yeh et al, 2008), NCA (gf)::NLF-1 loss-of- function indicate normal movements and body bends, and do not coil (Xie et al, 2013). Further qualitative and quantitative behavioural evaluations (e.g. relative idle/active state and rhythmicity in motor pattern) revealed that NLF-1 (loss-of- function) mutants show hallmarks for movement deficits which determines fainters, similar to what is observed in NCA (loss-of-function) mutants (Xie et al, 2013). Thus, they included NLF-1 in the same genetic cascade as NCA gene. Similar to NCA, NLF-1 also shows a high level of expression predominantly in the *C. elegans* nervous system (Xie et al, 2013). Ad-

ditional molecular work indicated the presence of an endoplasmic reticulum (ER) retention motif (RXR) in NLF-1 protein. This was further confirmed by detection of colocalized NLF-1::GFP with numerous ER reporters such as CP450::mCherry, SP12::mCherry and TRAM::mCherry in neurons of *C. elegans*, whereas the NLF-1::GFP neither colocalized with cell membrane reporter GPI::YFP nor with Golgi membrane reporter ManII::mCherry (Xie et al, 2013).

The next question was how does an ER protein modulate membrane excitability? Ion channels are synthesised and assembled in the endoplasmic reticulum prior to their shipment to the cell membrane (Deutsch, 2003). Zhen and colleagues explored if NLF-1 protein resides at the ER and is mandatory for the folding, assembly and delivery of the NCA leak channel. Their results show that in NLF-1 null mutants, all the discovered NCA subunits including NCA-1::GFP, NCA-2::GFP, UNC_{79}::GFP and UNC_{80}::RFP have a significant decrease in axonal membrane localisation. Interestingly, in NLF-1 null mutants, a heat-shock drove a short pulse of NLF-1 expression which was enough to rescue the axonal localisation of NCA-1::GFP and NCA-2::GFP as well as the fainting phenotype (using *in vivo* fluorescence microscopy combined with behavioural analysis) (Xie et al, 2013). An acute rescue of the NLF-1 mutants' phenotype under a stressful condition implies a direct role of NLF-1 in fast assembly and/or shipment of the NCA channels to the axon membrane, making it behave as a chaperone. Chaperones are a large group of protein families that interact with unfolded or partly folded protein subunits to stabilize non-native conformation and mediate the proper folding of premature proteins/or unfolding native proteins for degradation. Chaperones uncouple from the folded proteins once they have reached the native and functional state. They are essential for viability and their expression usually is enhanced by cellular stress (Lehninger et al, 2013).

Electrophysiological recordings from neurons of the NLF-1 mutants exhibited a drastic reduction in the inward depolarising leak current as well as a hyperpolarised resting membrane potential (by 10 mV) in premotor interneurons of *C. elegans*, which led to the fainting behaviour (Xie et al, 2013). Furthermore, Zhen and colleagues successfully cloned the NLF-1 homologue in mice (called FAM155A), which shares moderate homology with the one in *C. elegans*, particularly at the central

region called the NLF domain. Similarly, this homologue has an ER retention signal (RXR) as well as an ER transmembrane segment (Xie et al, 2013). Zhen and colleagues cloned the NLF domain of mice and triggered its expression in *C. elegans* using *C. elegans* NLF-1 promoter, and that rescued the NLF-1 (loss-of-function) phenotype in *C. elegans* mutants. This further confirms how conserved the role of NLF-1 is across invertebrates and vertebrates.

Further investigation has also revealed that NLF-1 function is highly conserved across several species including *C. elegans*, mouse, *D. melanogaster* and Yeast, and its regulatory interaction with the sodium leak channel NALCN dates back to a billion years ago (Ghezzi et al, 2014). In *D. melanogaster*, the expression profile of the NLF-1 homolog CG33988 is highly correlated with NALCN (called na in the fly) (Ghezzi et al, 2014). More interestingly, Michael Rosbash and his team revealed that CLOCK (CLK), which is a master transcriptional regulator of the circadian clock in *D. melanogaster*, directly targets hundreds of genes, one of which is CG33988 (NLF-1 ortholog in *D. melanogaster*) to regulate its circadian transcription (Abruzzi et al, 2011). This implies that NALCN function is under the regulation of clock genes. Flourakis and colleagues (2015) monitored the expression dynamic of NLF-1, NALCN, UNC_{79} and UNC_{80} in both *D. melanogaster* and mice clock neurons using qRT-PCR at different time points (Flourakis et al, 2015). Their results showed that only NLF-1 transcription exhibits a circadian oscillation and not the other subunits, consistent with Rosbash's findings.

1.4.6 NALCN pore selectivity and pharmacology

Removal of more than 90% of bath Cl^- and replacing it with methane sulfonate (MES), does not noticeably alter the magnitude or equilibrium potential of NALCN current (Lu et al, 2007), confirming that NALCN is not permeable to anions but is conducting cations. In contrast, reducing extracellular Na^+ from 155 mM to 15.5 mM decreases the amplitude of the inward current (recorded with ramp from -100 to +100 mV) and changes the reversal potential, indicating Na^+ as a permeant ion (Lu et al, 2007). NALCN selectivity motif clearly shows that it should also be permeable to Ca^{2+} and K^+ ions. Lu et al, (2007) used the equilibrium potential of

NALCN current under different bi-ionic conditions (in which only two crucial ion species – an extracellular divalent cation and an intracellular univalent cation are involved in the process of excitation) to calculate the approximate ion selectivity of the NALCN channel in HEK cells where only NALCN was expressed. Their results show that PNa = 1.3 > PK = 1.2 > PCs = 1.0 > PCa = 0.5. Hence, NALCN is a nonselective cation conductance and is permeable to Na^+, K^+ and Ca^{2+} with highest conductivity for Na^+. However, Chua et al (2020) found that NALCN does not conduct any divalent cations such as Ca^{2+}, and that Ca^{2+} is a pore blocker. Using heterologous expression of NALCN and all of its known auxiliary subunits UNC_{79}, UNC_{80} and FAM155A in HEK cells, Chua and colleagues first showed that NALCN current directionality and equilibrium potentials were sensitive to the replacement of extracellular or intracellular Na^+ with $NMDG^+$. However, it was not sensitive to the substitution of extracellular Cl^- with large impermeable anion methane sulfonate consistent with previous reports (Chua et al, 2020). Further, they evaluated the permeability of monovalent and divalent cations by creating equimolar concentrations of test cations on the extracellular space, and the impermeable $NMDG^+$ in the intracellular space. They observed no permeability to divalent cations such as Ca^{2+}, Mg^{2+} and Ba^{2+}.

TTX, a well-known highly selective voltage-gated Na^+ blocker, does not block NALCN current (up to 10 μM TTX), whereas several voltage-gated Ca^{2+} blockers could partly block NALCN with low affinity (IC50: 0.15 mM for Cd^{2+}, 0.26 mM for Co^{2+}, and 0.38 mM for verapamil) (Lu et al, 2007). Interestingly, Gd^{3+}, which is a high-affinity blocker for stretch-activated channels, significantly blocked NALCN current with IC_{50} of 1.4 μM (IC_{50} is a concentration at which there is a half maximum inhibition). Finally, the general characteristics of NALCN current (such as voltage insensitivity, current-voltage relationship, permeability and pharmacology) are different to those of transient receptor potential cation channels (TRP), or non-specific leaks, confirming the functional presence of the NALCN channel as a background Na^+ current (Lu et al, 2007)

1.4.7 Role of NALCN in cell physiology

Following comprehensive reports by Ren, more knockout (conditional) and knock down studies in the central nervous system have been conducted to unravel the role of NALCN (Lutas et al, 2016; Flourakis et al, 2015; Philippart and Khaliq, 2018). These reports provide rigorous evidence that NALCN is the major contributor to the resting Na^+ leak conductance, and thus significantly impacts the basal excitability of GABAergic neurons of substantia nigra pars reticulata, neurons of superchiasmatic nucleus and dopaminergic neurons of substantia nigra pars compacta (Lutas et al, 2016; Flourakis et al, 2015; Philippart and Khaliq, 2018). Without NALCN's contribution, they showed that the resting membrane potential is remarkably hyperpolarized leading to either reduced firing frequency or silenced electrical activity in neurons; this noticeably impacts the physiology and viability of organisms (Flourakis et al, 2015; Lutas et al, 2016; Philippart and Khaliq, 2018). However, the conditional knockout of each member of TRPC channels individually (e.g. TRPC1,TRPC2,. . . , TRPC7) and the entire family of TRPC at once, did not significantly alter the excitability or RMP of GABAergic neurons of the substantia nigra pars reticulata in mice (Lutas et al, 2016). There are many more regions in the nervous system with neurons generating autonomous firing activity including cerebellar Purkinje neurons (Raman and Bean, 1997; Raman et al, 2000), cerebellar nuclei neurons (Raman et al, 2000), cerebellar unipolar brush cells (Russo et al, 2007) and dopaminergic neurons of ventral tegmental area (in mid brain) (Khaliq and Bean, 2010). The capability of producing periodic firing in these neurons has been shown to be an intrinsic property of the cell as it continues in dissociated neurons in culture and ex vivo (in slices) in the presence of synaptic transmission blockers (Häusser et al, 2004; Llinas, 1988). Therefore, there have been investigations regarding the properties of subthreshold conductances responsible for maintaining the membrane potential close to the threshold (such as -50 mV) above which voltage-gated ion channels become active, or to depolarize the membrane potential to the activation threshold during inter-spike intervals for triggering the generation of rhythmic firing (Khaliq and Bean, 2010). Their reports indicate the involvement of a TTX-insensitive and voltage-independent Na^+ leak channel which is relatively non-selective since the re-

versal potential of the extrapolated I-V curve relationship (current-voltage) is near 0 mV. These observed biophysical and pharmacological properties of the conductance are very similar to that of NALCN. However, whether they are primarily mediated through NALCN needs further investigation through for example knock down or knockout studies.

1.4.8 NALCN is regulated by GPCRs

Beside the maintenance of an autonomous generation of action potentials in neurons, the background Na^+ conductance of NALCN is also both negatively and positively modulated by external stimuli to regulate the resting membrane potential. It has been found that NALCN current is activated by neurotransmitters, substance P (SP) and neurotensin, *via* the *src* family of tyrosine kinase (SFK)-dependent and G protein-independent pathway in the murine hippocampal and ventral tegmental area of mid brain neurons (Lu et al, 2009). Alongside suppressing K^+ currents, including M-current, neurotransmitters can trigger neuronal excitation through the activation of background Na^+ conductance (reviewed in Ren, 2011). In contrast with these data, NALCN does not mediate a basal background Na^+ current in a pancreatic β-cell model (MIN6) but facilitates an acetylcholine-activated Na^+ current (Swayne et al, 2009). Utilising heterologous expression in HEK293 cells, Swayne and colleagues demonstrated that acetylcholine-triggered NALCN current requires the M3 muscarinic receptor (M3R), whose activation is conducted through a *src* family of tyrosine kinase-dependent and G-protein independent pathway (Swayne et al, 2009). The muscarinic modulation of NALCN was also described in substantia nigra pars reticulata neurons of midbrain (Lutas et al, 2016). In these neurons, NALCN not only regulates RMP and firing rate but also is modulated by muscarinic acetylcholine receptor and glycolysis (Lutas et al, 2016).

To sum up, even though NALCN is insensitive to voltage, its activity can be further regulated by neurotransmitters and other extracellular stimuli through controlling its accessory proteins (Ren, 2011). As a result, NALCN activity can be positively regulated by neurotransmitters such as substance P, neurotensin and acetylcholine through corresponding G-protein independent *src* family of tyrosine

kinase-dependent pathway. Additionally, NALCN can be negatively modulated by neurotransmitters such as dopamine (D2 receptor) and GABA (GABA-B receptors), and by alterations in extracellular Ca^{2+} through G-protein dependent pathways.

1.5 Background Na^+ leak conductance in pituitary cells

In pituitary cells, maintaining the RMP at depolarised levels close to the activation threshold of voltage-gated ion channels is a crucial task of background Na^+ leak channels, without which cell functionality is disrupted. It has also been shown that background Na^+ conductance regulates the membrane potential in response to external stimuli (Liang et al, 2011; Tomić et al, 2011). Moreover, background Na^+ leak conductance is responsible for the generation and/or maintenance of spontaneous firing in all pituitary cells (reviewed in Kwiecien and Hammond, 1998; Stojilkovic et al, 2010; Fletcher et al, 2018). Autonomous firing and associated cytosolic Ca^{2+} transients is clearly an intrinsic property of pituitary cells as it persists in dissociated pituitary cells in culture (Stojilkovic et al, 2010) and in pituitary slices in the presence of gap junction blockers (Guerineau et al, 1998; Bonnefont and Mollard, 2003). Further, animals bearing ectopic pituitary grafts (the connection between the hypothalamus and pituitary gland is cut) secrete high amounts of PRL and a low level of luteinizing hormone (LH) for a long period of time resulting in pseudopregnancy (Stojilkovic et al, 2005). It also has been shown that the activation of protein kinase A (PKA) in pituitary cells increases the TTX-resistant background Na^+ current, which results in sustained depolarisation (Rawlings, 1999). There has been speculation regarding the origin of Na^+ leak conductances in endocrine pituitary cells, such as hyperpolarisation-activated and cyclic nucleotide-modulated channels (HCN) with a resulting current depicted as I_h. However, it is unlikely that this current has a major function in generating spontaneous electrical activity or regulating resting membrane potential in anterior pituitary cells. Firstly, these channels become active at potentials more negative than -60 mV, with minor activation at resting membrane potential in a lacto-somatotrophs cell line (Kucka et al, 2012). Additionally, the application of HCN channel blockers including ZD7288 and

Cs^+ to these cells and to lactotrophs entirely inhibits I_h whereas it neither stops the spontaneous electrical activity nor affects the resting membrane potential (Kucka et al, 2012). Another potential candidate could be persistent Na^+ currents which are produced by voltage-gated Na^+ channels through the "window" current; however, the addition of Riluzole, a blocker of the persistent sodium current, does not inhibit spontaneous electrical activity in endocrine pituitary cells (Tomić et al, 2011). Moreover, the generation of a window current *via* voltage-gated Na^+ channels is impacted by the voltage dependence of the channel's activation and inactivation. Further work by Kucka and colleagues shows that the mRNA transcript for TRPC1 (transient receptor potential canonical) channel is greatly expressed in pituitary cells; they reported that the blockers of TRPC channels 2-APB and SKF96365 hyperpolarised the cell membrane and stopped spontaneous firing of action potentials as well as associated $[Ca^{2+}]_i$ transients and basal prolactin secretion (Kucka et al, 2012). However, the problem with SKF96365 as a known blocker of TRPC channels is that it is not highly specific to TRPC channels. It has been reported that there are significant overlapping physiological associations between TRPC channels and low-voltage-gated Ca^{2+} channels (known as T-type Ca^{2+} channels) (Singh et al, 2010). Using recombinant DNA technology, Singh and colleagues showed that SKF96365 blocks both T-type and L-type Ca^{2+}channels at concentrations normally used to evaluate TRPC function, which is 10 μMolar (Singh et al, 2010). Thus, the use of the pharmacological blocker SKF96365 does not confirm the molecular identity of the background sodium leak channel. Overall, there is not yet rigorous evidence confirming the molecular identity of the major background Na^+ leak conductance and its contribution to cell excitability in endocrine anterior pituitary cells.

1.6 Overview of the thesis

The overall goal of the thesis is to gain a better understanding of the regulatory components of the pattern of electrical activity intrinsic to pituitary cells, which will in turn help scientific researchers to better understand hormone secretion.

In **Chapter 2**, there is a full explanation of the general materials, methods and statistical tests that were used in the presented studies.

Chapter 3:

Hypothesis: Small variations in Na^+ and K^+ leak conductance significantly modulate the excitability of endocrine pituitary cells.

Using dynamic clamp combined with calcium imaging, the contribution of Na^+ leak conductance is *quantified*, as well as that of the K^+ leak, in determining the pattern of electrical activity and cytosolic Ca^{2+} transients in anterior pituitary cells. Dynamic clamp allows the investigator to precisely modify the various biophysical parameters of ion channels in real time to decipher the role of each individual biophysical property in shaping the pattern of electrical activity. In fact, dynamic clamp allows the precise manipulation of those parameters (e.g. activation, inactivation, gating kinetics and conductance) that cannot be manipulated by other experimental methods such as the use of pharmacological agents or knock out models.

Chapter 4:

Hypothesis: NALCN is the main Na^+ leak channel in endocrine pituitary cells, which mediates the major inward Na^+ leak current.

Using lentiviral transduction, the molecular identity of the major Na^+ leak conductance in pituitary cells is discovered. Further, its key role in tuning the resting membrane potential as well as in regulating cytosolic Ca^{2+} concentration is reported.

In **Chapter 5**, the overall conclusions of the study are summarised, and future directions of the work is discussed.

Chapter 2

Materials and Methods

2.1 Cell culture: GH4 cell line

Cell line

The GH4-C1 cell line (or GH4) was purchased from DSMZ (Deutsche Sammlung von Mikroorganismen und Zellkulturen). The cell line was developed in 1972 from a successively passaged GH3 cell population that secreted little or no detectable amount of growth hormone. GH4-C1 cells mainly secrete prolactin and have been used to study the molecular pathways of signal transduction and receptor modulation (Stojilkovic et al, 2010). These cells are also utilised for assessing electrophysiological properties of the plasma membrane as well as cytoplasmic calcium homeostasis in endocrine pituitary cells, and are used as a model for lacto-somatotroph pituitary cells.

Cell culture

GH4 cells were maintained in culture conditions in Ham's F-10 Nutrient Mix medium (Gibco, Thermo Fischer Scientific, #11550043) supplemented with 15% Horse Serum, 2.5% FBS and 1% Glutamax (all from Gibco, Thermo Fisher Scientific, #26050088, #16140063 and #35050061 respectively) in a humidified environment of an incubator with 37°C temperature, 95% air and 5% CO_2. Cells used in this research were from a passage range between 3 and 10.

2.1.1 Passage of cell line

Cells were passaged once a week at around 70-80% confluence and kept in 25 cm^2 Corning polystyrene flasks. For passaging the cells, first the medium was removed,

and then 3 mL Versene-EDTA solution (Gibco, #15040066) was added for gentle non-enzymatic cell detachment from the bottom of the flask. Then, the flask was incubated for 2-3 minutes until the majority of the cells were detached. Dissociated cells were resuspended in an extra 7 mL of F10 medium in a 15 mL Falcon tube and were then centrifuged for 10 minutes at 120xg. After centrifugation, the supernatant was removed and the cell pellet was resuspended in 4 mL F10 medium and counted using the Trypan Blue dye exclusion method (a commonly used technique to determine the number of viable cells in a cell suspension based on the principle that live cells have integrated and intact membrane which exclude specific dyes such as Trypan blue while dead cells do not). Then, one million cells were transferred to a new sterile 25 cm^2 flask and fresh supplemented F10 was added to make a final volume of 5 mL. For single-cell electrophysiological recording, GH4 cells were plated on 15 mm round uncoated coverslips (Thermo Fisher Scientific) at a density of 10^4 cells per coverslip located in a 12-well plate (Sigma-Aldrich), and then used for up to 5 days after passaging. Recording from GH4 cells started 24 hours after plating on coverslips.

2.1.2 Cell storage in liquid nitrogen tank and recovery of the cells from storage

For storage, cells cultured in 25 cm^2 flasks at approximately 80% confluence were collected and counted. Afterwards, the cells were suspended in the supplemented F10 comprising 10% dimethyl sulphoxide (DMSO) to reach a final dilution of 1×10^6 cells per mL. Subsequently, cells were aliquoted into 1 mL cryotubes (polypropylene tube, capacity 2.0 mL, from Merck) and maintained at -80°C overnight. The next day, the cells were transferred to liquid nitrogen. To thaw the frozen cells, a cryotube was taken from the liquid nitrogen tank and kept in a 37°C water bath for a short period of time. Cells were immediately transferred into 9 mL fresh F10 medium and topped up with F10 medium to make a final volume of 10 mL. To remove DMSO, the suspension was centrifuged for 10 minutes at 120xg, after which the supernatant was removed, and fresh supplemented F10 was added. The cell suspension was transferred to a 25 cm^2 flask and maintained in a 37°C incubator.

2.2 Primary cell culture

2.2.1 Animals

Murine anterior pituitary cells were cultured from wild-type C57BL/6J mice as required (provided by the University of Exeter animal house). Mice were kept in groups of two to four under standard circumstances at the University of Exeter animal unit: Lights on at 6:00 AM, lights off at 6:00 PM at 21 ± 2 °C, tap water and food were available *ad libitum*. The adult mice aged between two to six months were selected randomly regardless of their sex. All animal studies were conducted in accordance with the UK Animals in Scientific Procedures Act 1986 (ASPA) and study plans were approved by an institutional Named Animal Care and Welfare Officer (NACWO) at the University of Exeter.

2.2.2 Primary culture protocol

Three or four mice were culled *via* cervical dislocation and then were decapitated in accordance with Schedule 1 procedures of Home Office England. After removing the brain, the sellar diaphragm (a flat piece of dura matter) was gently removed using the tips of tweezers and then the pituitary gland was removed from the sella turcica (bony cavity) and placed in a 100x21mm culture dish (Thermo Fisher Scientific) containing 150 μL 4°C DMEM (Dulbecco's modified Eagle's medium with high glucose and 25mM HEPES from Sigma Aldrich-#D6171-500ML) located on ice. Under a dissection microscope, the intermediate and posterior lobes were removed using a scalpel blade (size 10), and the anterior lobes were chopped to small pieces manually. Subsequently, the chopped tissues were transferred into a 50 mL Falcon tube containing 2.5 mL of DMEM supplemented with 207 TAME Units/mL trypsin (Sigma Aldrich, #T9935) and 36 Kunitz Units/mL DNase I (Sigma Aldrich, #D5025), and then incubated in a 37°C water bath for 10 minutes. Every 5 minutes, the tube was shaken to disperse the tissue pieces evenly to achieve a thorough digestion. After 10 minutes, the suspension was gently triturated 20-30 times using a 1 mL pipette tip. At the end of the digestion step, an inhibition solution containing 5 mL DMEM supplemented with 0.25 mg/mL lima soybean trypsin inhibitor (Sigma Aldrich, #T6522), 100 kallikrein units of aprotinin (Sigma Aldrich, #10820)

and 36 Kunitz Units/ml DNase I was added to the digestion solution, and the cell suspension was left for a few minutes to inactivate the trypsin enzyme activity. The resulting suspension was finally filtered through a cell strainer with 70 μm nylon mesh (Merck-#CLS431751-50EA) and was centrifuged at 100×g for 10 minutes. The pellet was resuspended in 500-600 μL DMEM solution and then 60 μL of the resuspended cells was plated on each 15 mm diameter round coverslip in a 12-well plate. After 20 minutes, once the cells were securely attached to the bottom of coverslips, 1 mL of growth medium (DMEM + 2.5% FBS + 0.1 % fibronectin (Sigma #F1141) + 1% penstrep antibiotic) was added to each well and then incubated at 37°C in a 5% CO_2 incubator. The culture medium was replaced with antibiotic-free growth-medium 6 hours later. The growth medium was refreshed every two days. Experiments for chapter 3, started 24 hours after tissue harvesting. Pituitary cells in culture were used up to 5 days post harvesting.

The initial trypsin concentration tested was 15 μl in 2.5 mL DMEM, which was subsequently reduced to 12, and then 10 μl to avoid over-digestion. Enzymatic treatment digests the connective tissue and basement membrane or extracellular matrix which is a very thin layer separating connective tissues from the underlying cells. To achieve a very high seal resistance between pipette rim and cell membrane, and to reduce the leakage shunt, the cell membrane needs to be clean. However, over-digestion can make the membrane fragile. Therefore, through an optimisation process, the optimal trypsin concentration for maintaining a stable seal on the pituitary cell membrane for a long time-period of recording (30 to 60 minute) was 10 μL in 2.5 mL for three mouse pituitary glands. For the second part of the study, testing the NALCN knock down effect (Chapter 4), cells were transduced with lentivirus. A concentrated suspension of lentivirus (5-10 μL) was added to the medium in each well of a 12-well plate. Fresh growth medium was substituted 24 hours after transduction. Green fluorescent cells were usually observable 2-3 days after transduction, and the brightest GFP-positive cells regardless of the cell size were selected for electrophysiological recording. An ideal extra step to confirm NALCN KD in pituitary cells would be ICC or qRT-PCR on pituitary cells treated with the virus. However, in the present study, NALCN KD was confirmed functionally using electrophysiology

and calcium imaging. Each batch of primary pituitary cell culture was utilised for up to 5 days after transduction for electrophysiological recordings. After 5 days, the cell membrane would typically become fragile and thus it was difficult to maintain a Gigaseal and a stable recording.

2.3 Generation of lentiviral construct

Genetic manipulation using lentiviral gene delivery systems has been widely used due to its unique high transduction efficiency and the capability to integrate DNA into the genome of host cells regardless of their proliferation status. In fact, lentivirus can infect both actively dividing and non-dividing (terminally differentiated) cells both *in vivo* and *in vitro*. For safety reasons, the lentiviral genome is edited and is split across three plasmids each of which is replication incompetent. In this study, a second generation lentiviral gene delivery system was used, which is comprised of three separate plasmids: a packaging plasmid, an envelope plasmid and a transfer (or transducing) plasmid (Figure 2.1). The gene of interest is inserted into the transfer plasmid. In second generation lentivirus systems, the viral accessory genes such as vpu, vpr, vif and nef are removed. Although these accessory genes are necessary for the propagation of HIV-1 virus in primary cells, or *in vivo*, they are not necessary for lentiviral production.

The packaging plasmid used in this study was pCMV delta R8.2 (#12263, Addgene) which expresses HIV Gag, Pol and all the virus functional proteins required for infection, under the control of the cytomegalovirus (CMV) immediate early promoter. HIV Gag and Pol encodes group-specific antigen and viral enzymes such as reverse transcriptase, integrase and protease (Figure 2.2). The envelope plasmid pCMV-VSV-G (#8454, Addgene) expresses a vesicular stomatitis viral glycoprotein (VSV-G) (Figure 2.3). The VSV-G envelope is normally used in generating lentiviral particles since it has a broad tropism over a wide variety of species and cell types. Lentiviral tropism is defined by the capability of the viral envelope antigens to couple with the host cell receptors (Cronin et al, 2006). This therefore confers the virus the ability to bind and enter into the host cell. Moreover, VSV-G is less toxic for mammalian cells (Farley et al, 2007) and has high structural stability which al-

lows the viral particle to endure the ultracentrifugation essential to obtain high titre (Akkina et al, 1996). In order to prevent the generation of replication-competent lentivirus during vector preparations, the packaging signal ϕ and LTRs (long terminal repeats) are not included in the envelope plasmid. They are commonly included, along with the RRE (Rev-responsive element) in the transfer plasmid.

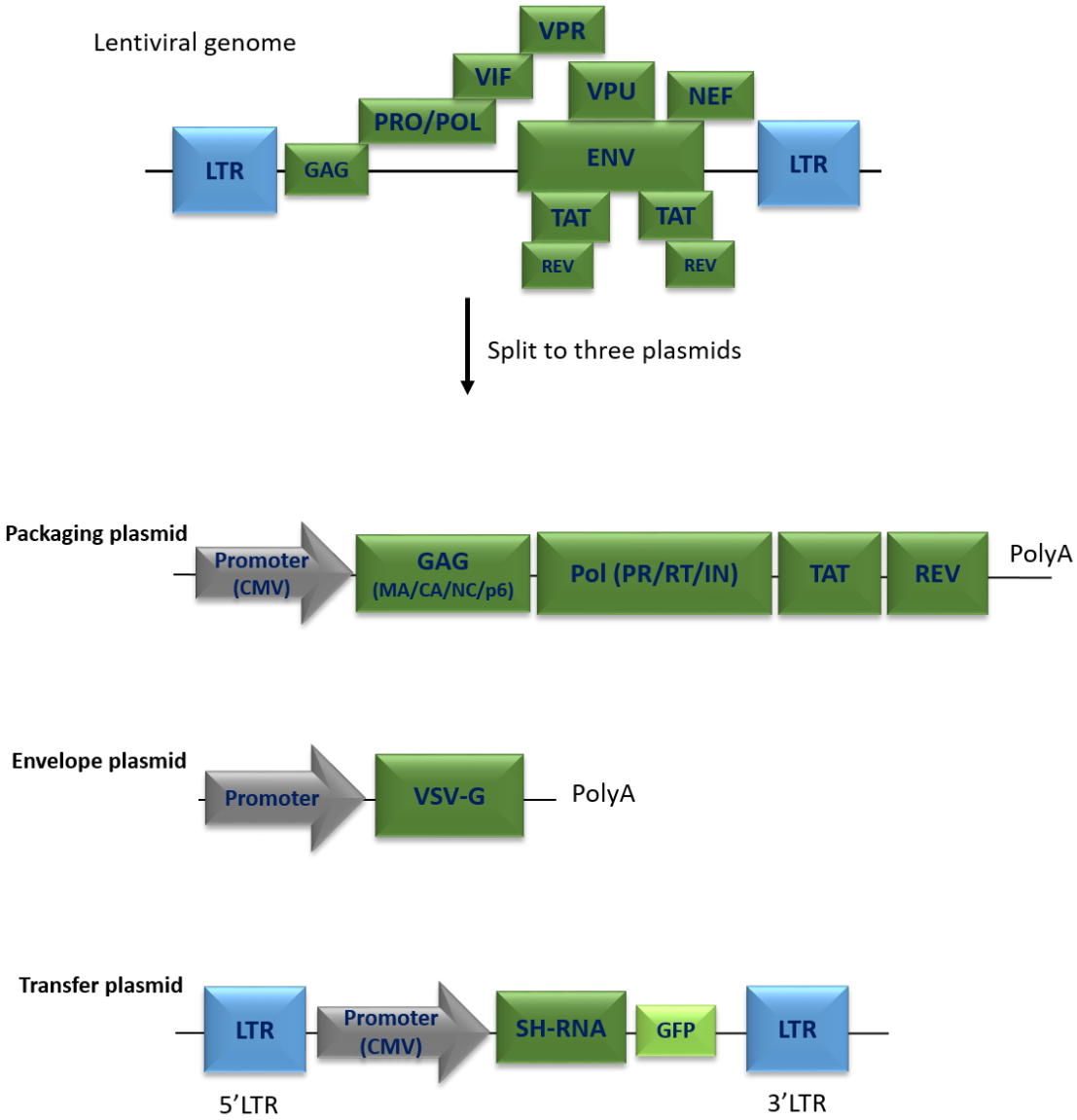

Figure 2.1: Second generation lentivirus system expresses only 4 of 9 HIV genes: Gag, Pol, Tat and Rev.
In the second generation lentiviral system, the viral genome is edited and split into three separate plasmids including packaging plasmid, envelope plasmid and transfer plasmid. The gene of interest is inserted into the transfer plasmid. The transfer plasmid, on its own, can be used for transient infection in cell culture. **Gag** is a polyprotein and is an acronym for Group Antigens. **Pol** gene products include the HIV-1 reverse transcriptase, an integrase and the late-phase protease. **Tat** stands for trans-activating factor and is essential for viral replication whose function is to increase transcription elongation from the viral promoter. **Rev** is a transactivating protein that is critical to the regulation of HIV-1 (and other lentiviral) protein expression.

The transfer plasmid pGIPZ was provided by Dr Arnaud Monteil (The Institute of Functional Genomics, Montpellier France) (Figure 2.4). The gene of interest (short hairpin RNA referred to as sh-RNA) was inserted in the downstream region of the CMV promoter after the turbo GFP gene (improved green fluorescent protein obtained from pontellina plumata). Virus packaging signal, CMV promoter and the downstream genes are flanked by long terminal repeats (LTR) which mediate the incorporation of transfer plasmid genes into the host genome. The LTRs and the sequences between them are integrated into the genome of the host cell upon viral transduction (HIV-1 virus tends to select highly transcriptionally active sites of the host genome for integration (Wang et al, 2007, Berry et al, 2006). As previously mentioned, transfer plasmid includes Rev which expresses a protein that controls the splicing and export of virus transcripts; Rev protein also binds to the Rev-responsive- element (RRE) to mediate the nuclear export of viral mRNAs. MicroRNA-adapted shRNA based on miR-30 for specific NALCN silencing cloned in the lentiviral pGIPZ plasmid and targeting the 5'-GCAACAGACTGTGGCAATT-3' region of the rat NALCN encoding RNA obtained from a commercial source (Dharmacon #V2LMM_90196). A non-silencing control (scramble shRNA) was used in my experiments (Dharmacon #RHS4346). HpaI/BamHI (Figure 2.4) are the restriction sites in pGIPZ plasmid between which the NALCN silencing shRNA was inserted. The non-silencing scramble shRNA was inserted in the same site in a separate pGIPZ plasmid. Both plasmids were provided by Dr Arnaud Monteil (The Institute of Functional Genomics, Montpellier France). The lentiviral constructs were made by the author under the supervision of Dr Mariusz Mucha.

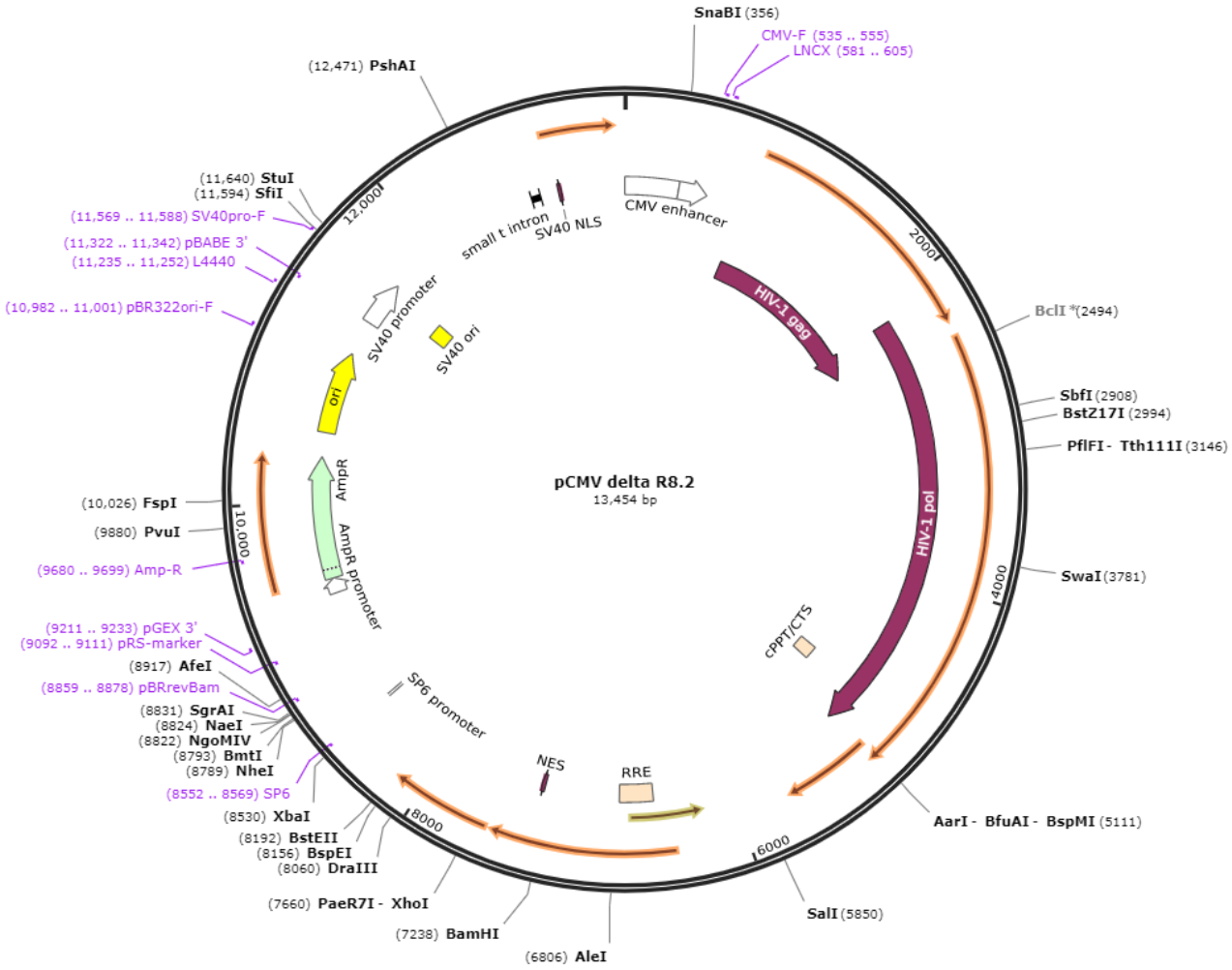

Figure 2.2: Schematic representation of the packaging plasmid.
In the second generation lentiviral system, the packaging plasmid only contains HIV Gag, Pol, Tat and Rev genes under the control of the CMV promoter. Gag firstly, is transcribed into an unspliced mRNA which later is spliced into three different transcripts encoding three main viral proteins such as matrix, capsid and nucleocapsid proteins. Pol expresses viral protease, reverse transcriptase and integrase. Tat expresses transactivators necessary for starting the viral transcription. Rev encodes a protein that modulates the splicing and export of viral transcripts. Additionally, Rev mediates nuclear export of viral mRNA's. Taken from https://www.addgene.org/browse/sequence/267403.

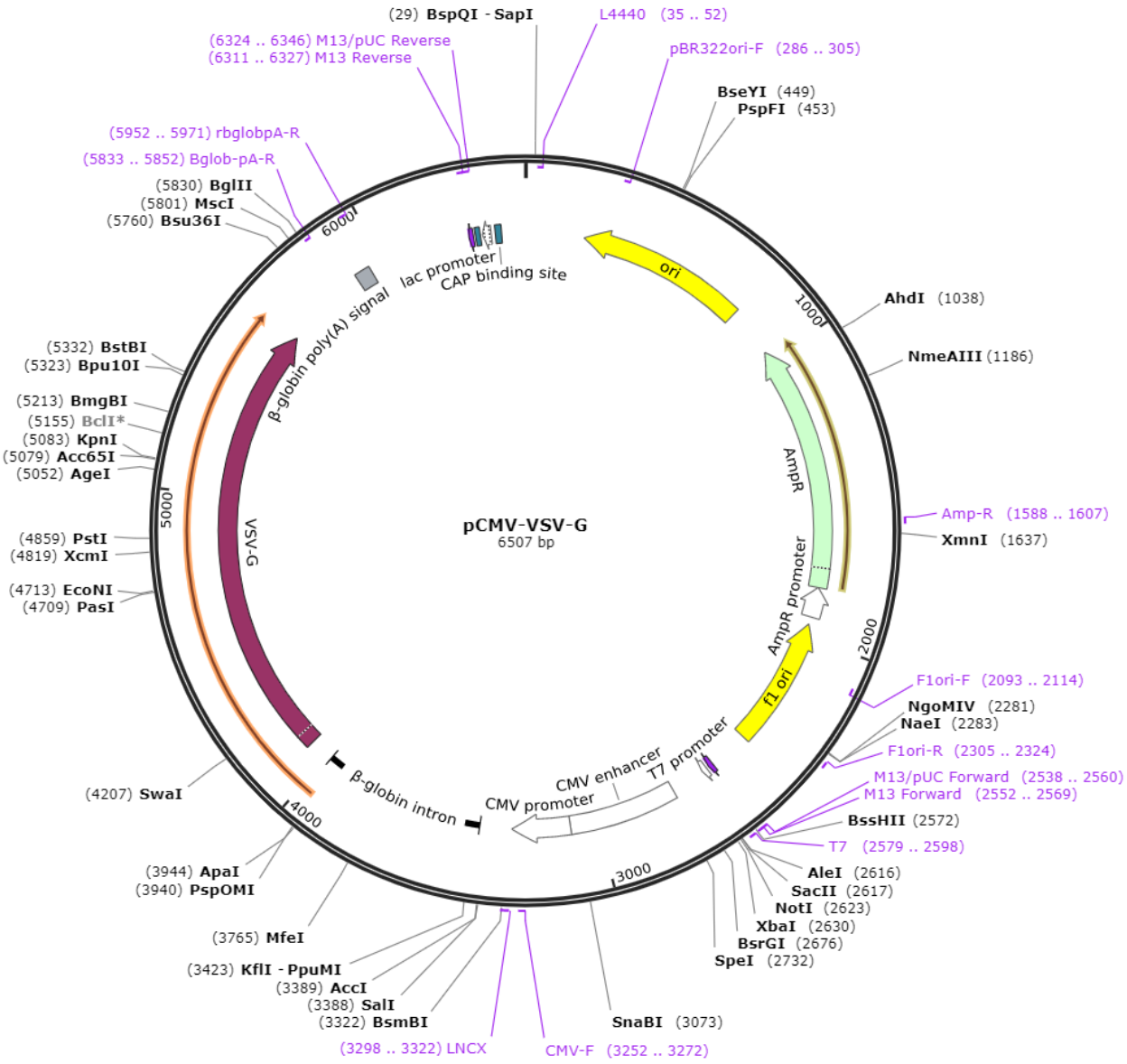

Figure 2.3: Schematic representation of envelope plasmid.
The envelope plasmid contains VSV-G gene encoding viral surface glycoprotein responsible for the recognition of the host cell surface receptors, and subsequently attachment and entry into the host cell. Taken from https://www.addgene.org/browse/sequence/244397.

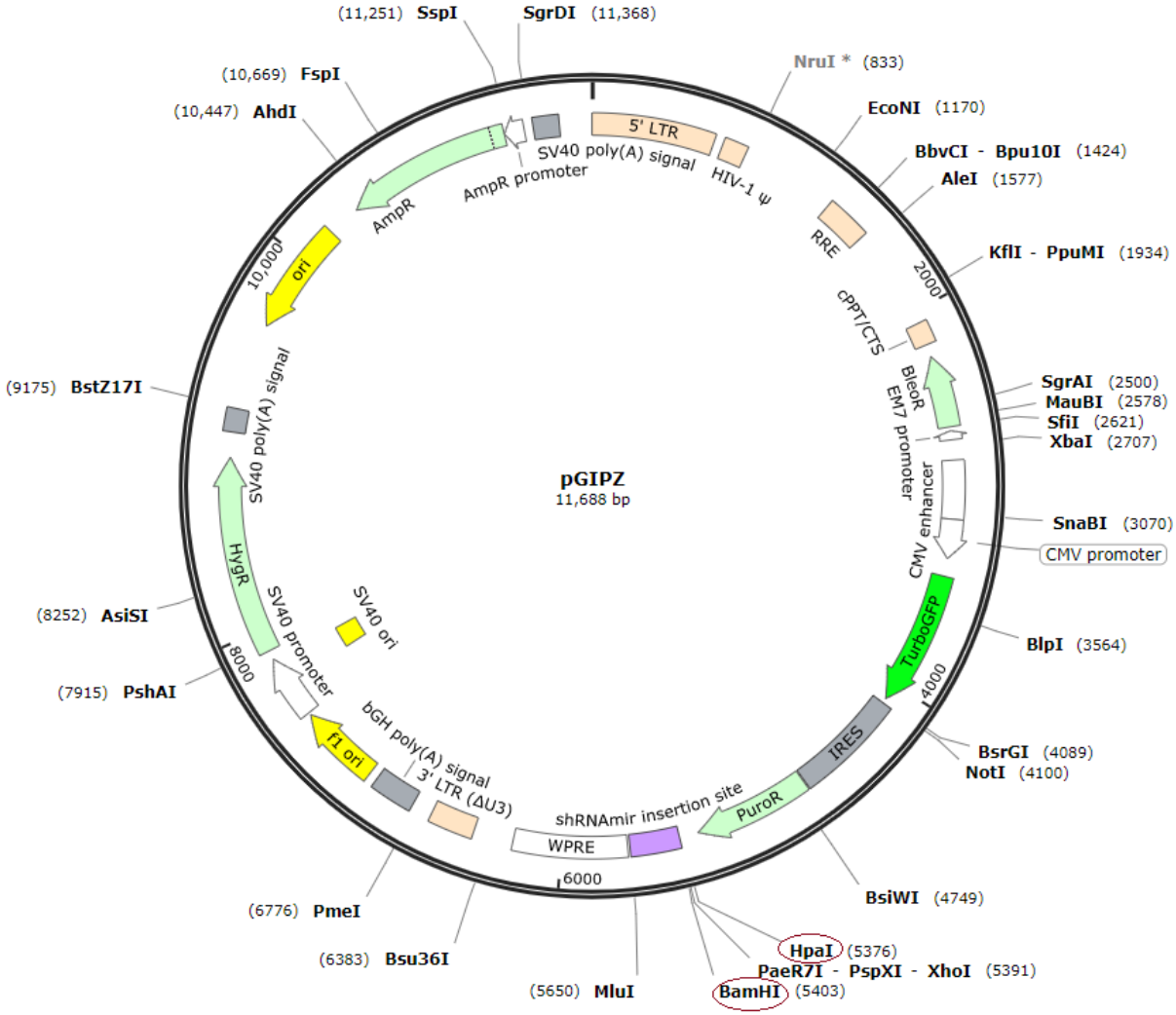

Figure 2.4: Schematic representation of the structure of the transfer plasmid provided by Dr Arnaud Monteil, Montpellier, France.
The transfer plasmid contains the gene of interest (shRNA) inserted under the control of CMV promoter after TurboGFP. The transfer plasmid is ampicillin resistant. The inserted gene will be transcribed to shRNA which will target NALCN mRNA to stop its translation in the host cell pituitary cells. HpaI/BamHI are the restriction sites in pGIPZ plasmid between which the shRNA was inserted.

2.3.1 DNA plasmid transformation into electro-competent bacteria

Electro-competent bacteria (NEB® 10-beta #C3020, New England Biolab) were taken from a -80°C freezer and thawed on ice, and were then diluted 1:1 with ice-cold 10% glycerol in dH_2O (glycerol creates an osmotic pressure appropriate for bacteria). The suspension (50 μl) was transferred to sterile electroporation cuvettes (Bio-Rad). Approximately 1 ng of each DNA plasmid (sh-RNA and scr-RNA) was added to each cuvette and incubated for 5 minutes on ice. Afterwards, the cuvettes were transferred to the electroporation system (BioRad) and a 1.8 kilo volt electrical field was applied for 5.2 ms. The application of electrical field results in a transient movement of charged particles across the cell wall and thus it creates transient holes on the cell wall allowing the plasmids to penetrate into the bacteria. The suspensions were immediately pipetted with 950 μL LB (Lysogeny broth) growth medium and successively transferred into a 15 mL Falcon tube, and incubated in a shaking incubator for an hour at 30°C for recovery. This step also allows the antibiotic resistance gene in the plasmid to express. Afterwards, 100 μl cell suspension was spread onto an ampicillin-resistant selective LB agar (1% agar) plate (containing 100 μg/ml ampicillin) and wrapped in foil (to preserve the humidity) and then incubated overnight at 30°C.

2.3.2 Plasmid amplification

After 24 hours a high number of single colonies started to appear. Five colonies from each plate were picked using sterile tips (passed over fire quickly) and inoculated into five separate 50 mL Falcon tubes containing 5 mL of LB medium with ampicillin (100 μg/ml) and incubated diagonally for 24 h at 30°C in a shaking incubator (30°C is chosen to reduce the probability of plasmid recombination. In fact, the lower temperature slows down the speed of DNA replication and thus the cells have sufficient time to repair any mutation or recombination).

2.3.3 Bacterial stocks

Bacterial suspension (0.7 mL) was diluted with 0.3 mL of 100% sterile glycerol in a cryotube, and then immediately transferred to a -80°C freezer for long-term storage for later use.

2.3.4 Alkaline lysis for purifying DNA plasmid

After 24 hours, the bacterial suspension was transferred to centrifuge tubes and centrifuged at 23000 x rpm for 5-10 minutes. The supernatants were then removed and the pellets resuspended in alkaline lysis buffer. The DNA plasmids were subsequently extracted and purified utilising the Genejet Plasmid Mini kit from Thermo Fisher, according to the manufacturer's instructions. Alkaline lysis is a method of choice for harvesting circular plasmid DNA or RNA from bacterial cells. The general principle of this method is to lyse the bacterial cells and subsequently perform selective alkaline denaturation of high molecular weight chromosomal DNA while ensuring the DNA plasmids stay double-stranded. The next step is neutralisation of the pH, upon which the chromosomal DNA renatures to make an insoluble clot. This will leave the DNA plasmids in the supernatant (Birnboim and Doly, 1979).

2.3.5 Quantifying the DNA yield

After extracting the plasmids, a Thermo Scientific NanoDrop 2000/2000c Spectrophotometer was used to evaluate the quantity and quality of the acquired DNA. This was achieved by measuring the ratio of optical absorbancy of the DNA solution at 260 nm (OD260) and 280 nm (OD280). The OD260:OD280 ratio indicates the purity of the obtained DNA. The appropriate ratio is 1.8, signifying pure double stranded DNA, whereas values below 1.8 indicate phenol contamination, and/or the presence of protein. Values higher than 1.8 reveal RNA contamination. The shape of the obtained graph should be similar to a bell shaped curve with a sharp peak. The two ends of the bell curve indicate the contamination with proteins and salts. The DNA concentration was derived using the NanoDrop software and it was usually in the range of 200-400 ng/μl.

2.3.6 HEK293T cell culture

The human embryonic kidney cell line (HEK 293T) is easily transfected and allows high levels of viral protein expression and thus was routinely utilised to produce a high titre (>10^7 ifu/ml) of lentiviral particles in this study (See Barde et al, 2010, Protocols for Neuroscience, Chapter 4: Unit 4. 21). The HEK293T cells were seeded into 75 cm^2 corning flasks, and then Dulbecco's Modified Eagles Medium (DMEM + 4.5 g/L glucose ("high-glucose") from Thermo Fisher Scientific) supplemented with 10% foetal calf serum (FCS; Sigma) and 1% pen-strep antibiotics (Sigma) were added. Afterwards, the flasks were incubated at 37°C in a 5% CO_2 incubator until a confluency of 80% was achieved.

2.3.7 Transient transfection of HEK293T cell line with three plasmids

One aliquot of HEK293T cells was thawed and plated on a T75 Corning flask in DMEM supplemented with 10% FCS and 1% antibiotic, and was incubated in a 37°C 5% CO_2 incubator. After the confluency reached 70-80%, the cells were passaged onto four T75 Corning flasks. This was done *via* trypsinisation (3 mL of 1x trypsin-EDTA was added for approximately 5 minutes) and centrifugation for 5 minutes at 120xg. After the confluency reached 70-80%, the cells were further passaged onto sixteen 90 mm petri dishes (Thermo Fisher). Cells on the petri dishes reached 70-80% confluency on the day of transient transfection. The medium was replaced with 10 mL fresh supplemented DMEM. Then, 10 μg of transfer plasmid plus 10 μg of packaging plasmid and 5 μg of envelope plasmid (2:2:1) were diluted in 1.1 mL of serum-supplemented (and antibiotic free) DMEM in 1.5 mL Eppendorf tubes (x16). Subsequently, 125 μl of polyethylenimine (PEI) (linear M.W: 25,000 Dalton; 3 mg/ml) was added, then vortexed for 10 seconds, spun down briefly and incubated at room temperature for 10 minutes. Afterwards, this solution was added to each HEK293T petri dish and incubated for 48 hours at 37°C (5% CO_2) until the fluorescent signals were visible (Figure 2.5). Efficiency of the cell transfection was indicated by the expression of fluorescent protein (GFP) visible under the microscope. In each preparation, above 85% of transfected HEK cells were GFP positive.

Validation of GFP expression in HEK cells between preparations was used in the absence of viral titre measurements.

2.3.8 Isolation and concentration of lentiviral particles

The plates were shaken well (causing some cells to detach) and the medium was collected into 50 mL Falcon tubes and spun down for 7 minutes at 1500 x g to remove all the debris and detached cells. Afterwards, the supernatant was filtered using 0.45 μm low protein affinity filters (Sigma) into single use 36 ml ultracentrifuge tubes (Thermo Fisher Scientific; PP thin-wall). Then, 1:1000 1 Molar sterile $MgCl^2$ and 2.6 μl of 15 μg/μl DNase I (RNase-free) was added to each tube. The tubes were then wrapped with Parafilm and incubated at 37°C for 15 minutes. Following this, the tubes were balanced using a milligram precision scale and then ultracentrifuged at 115,000 rpm for 90 minutes at 4°C. In the meantime, the paper towels were sterilized with UV for approximately 15-20 minutes. After centrifugation, the supernatant was removed and the tubes were held upside-down for a few minutes on the paper towels to allow the medium leftovers to leak out. Subsequently, 70 μl of sterile ice-cold PBS (phosphate buffer saline) was added to each tube. The tubes were then incubated on ice for 2 hours, after which the viral suspensions were combined and centrifuged at 8000 rpm for 30 seconds (benchtop centrifuge). Finally, 15 μl aliquots were prepared and immediately stored at -80°C.

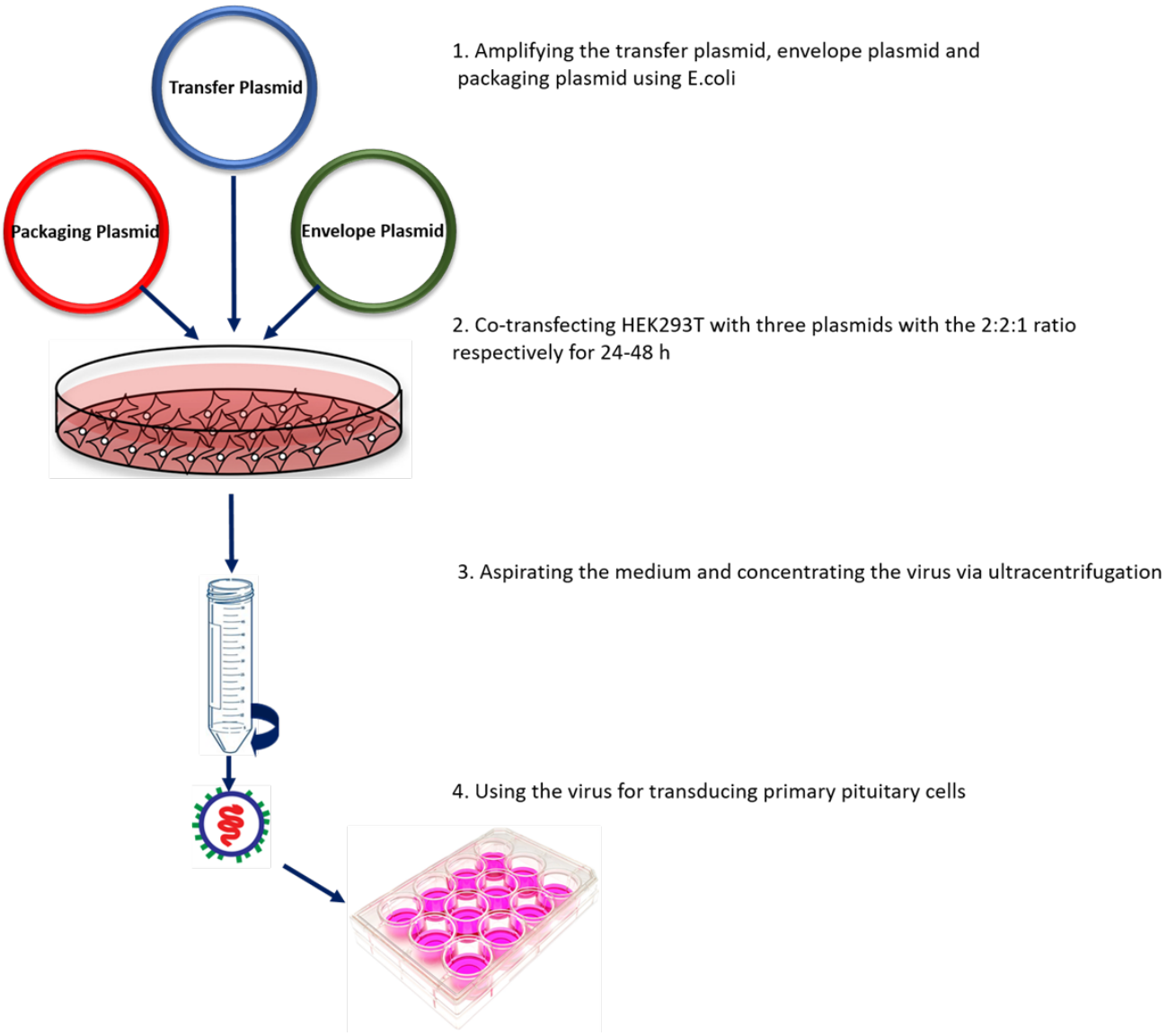

Figure 2.5: Co-transfecting HEK293T cells with the three plasmids to produce lentiviral particles.
Transfer plasmid, envelope plasmid and packaging plasmid were cloned using electrocompetent E. coli and then were added to the HEK293T cell culture for 24-48 hours. Once the green fluorescent signal appeared, the virus was harvested and stored at -80°C freezer in 15 μl aliquots. They were later used to transduce primary pituitary cells in culture.

2.4 Electrophysiology

Patch-clamp electrophysiology is a technique to study ion flow across the cell membrane as well as ion channel activity in live cells and tissues. Voltage-clamp is a mode in which the membrane potential is held at various voltages using a feedback amplifier. This enables us to measure the ion flow or electrical current across the cell membrane at certain voltages. In contrast, current-clamp allows us to measure firing activity and membrane potential by injecting different amounts of current to cells using the feedback amplifier. The critical characteristics of patch-clamp technique are: (1) the formation of a tight seal (giga ohm) between the cell membrane and the tip of a micropipette; and (2) high temporal resolution (in micro second range). A capillary glass micropipette filled with intracellular-like solution is gently located on top of a small patch of plasma membrane. A gentle suction is successively applied resulting in the formation of a tight seal with a very high resistance (called cell-attached mode) between the micropipette and the patch of the membrane. This seal is termed a "gigaseal" which means the resistance between the membrane and the micropipette exceeds 10^9 Ω. The gigaseal has a high mechanical stability enabling the recording of currents passing through single channels. The high resistance is the key to minimise the background electrical noise, facilitating the recording of the very small currents (pico ampere range) flowing across the plasma membrane. The intracellular-like solution in the pipette may come to contact the cytoplasm by applying a second suction (or electrical pulses) to rupture the small patch of plasma membrane enclosed by the micropipette tip's rim. This is called whole cell recording. Alternatively, the fluid continuity can be achieved *via* "perforating" the membrane patch by the addition of an exogenous pore-forming antibiotics to the micropipette solution to create pores on the patched membrane (termed perforated patch-clamp recording). In this study, the perforated patch-clamp technique was used to study the electrical properties of the murine anterior pituitary cells and a clonal pituitary cell line (GH4). When the micropipette solution and cytoplasm come into contact with each other, there will be some molecule (e.g. ATP) and ion exchange (from more concentrated liquid to less concentrated) leading to the activation of some leak channels, and a shift in the voltage which is called the liquid-liquid

junction potential. However, using perforated patch-clamp technique helps to stop molecule exchange and to reduce the ion exchange by preventing the large ions from equilibrating across the pipette tip, and only very small ions (e.g. Cl^-) can pass through. In the present studies, perforated patch-clamp mode was chosen to minimize dialysis artefacts during long-lasting electrical recordings. A junction potential of approximately 8 mV (calculated by the offset mode of Pclamp software) was not corrected.

2.4.1 Electrophysiological recording

Electrophysiological recordings from pituitary cells were performed at room temperature using single-cell amphotericin-perforated patch-clamp technique. The recordings were obtained using an Axopatch 700B amplifier and Clampex 10.1 (Molecular Devices) with a sampling rate of 10 kHz and filtered at 2 kHz (lower pass). Patch pipettes were fabricated from borosilicate glass with filament (outer diameter: 1.50 mm and inner diameter: 0.86 mm, Warner Instrument-multi channel system distributer) and pulled using a micropipette puller (Sutter Instruments, model P-97). Pipette tips were then fire polished and had a resistance ranging from 4 to 6 MΩ. Once a high resistance seal was formed (>10 GΩ), usually within 10 minutes of patching, the access resistance (also known as series resistance) would reduce to less than 50 MΩ, and then the recording started. If the seal resistance was less than 10 GΩ, the cell was discarded. In current clamp mode, series resistance was compensated by Bridge-Balance and was usually less than 40 MΩ. Junction potential was not corrected. In voltage clamp mode, compensated series resistance was normally less than 50 MΩ (electronic compensation was done *via* whole-cell mode of multiclamp 1440). The median capacitance of patched GH4 cells was 5.5 pF with a range between 4 and 10 pF. The mean capacitance of patched murine pituitary cells was 4.5 pF with a range between 4 and 6 pF and a standard deviation of 1.7. The majority of isolated murine pituitary cells in my preparation were visually of medium size. During recording, the cells were constantly perfused using a gravity-driven perfusion system, with a flow rate of 0.5 mL/min with extracellular solution containing (in millimolar) 138 NaCl, 5 KCl, 10 alpha-D-glucose, 25 HEPES, 0.7

Na_2HPO_4, 1 $MgCl_2$ and 2 $CaCl_2$. The pH was adjusted to 7.4 with NaOH, 305 mOsmol/L. Patch pipettes were filled with an intracellular solution containing (in millimolar) 10 NaCl, 100 K-Gluconate, 50 KCl, 10 HEPES, and 1 $MgCl_2$. The pH was adjusted to 7.2 with KOH, 295 mOsmol/L. The osmolality of the solutions was maintained by adding an inert ingredient sucrose. 5 μl Amphotericin-B of a stock solution (20 mg/mL in dimethyl sulfoxide) was added to 1 mL of pipette solution to achieve a final concentration of 50 μg/ml. Other concentrations such as 10 μl Amphotericin-B were also tried, however 5 μl resulted in more durability of the recording.

2.4.2 Dynamic clamp

With dynamic clamp I can effectively change the biophysical property of ion channels (such as activation, inactivation, gating kinetics and conductances) as I choose and investigate how these manipulations affect the pattern of electrical activity. In other words, I can establish the contribution of a type of ion channel to regulating various aspects of electrical activity (Milescu et al, 2008).

In this study, a second computer and an analogue-to-digital acquisition card (DAQ) were installed to run the dynamic clamp module in the software QuB (Milescu et al, 2008). In the current clamp mode of the Axopatch 700B amplifier, the membrane potential (V_m) of a patched cell was recorded in real time and passed to the computer running QuB as an input for a mathematical expression of non-selective cationic leak channels (sodium leak channels): I_{NS}=g_{NS} (V_m - E_{NS}) which defines the corresponding current (I_{NS}) going through them. The sodium leak conductance (g_{NS}) was changed manually. The calculated I_{NS} was then injected back to the cell *via* the same DAQ and then the membrane voltage response was recorded. The reversal potential (E_{NS}) for this channel was considered zero since this channel is permeable to different monovalent cations (e.g. K^+ and Na^+) but primarily to Na^+ (Lu et al, 2007; Chua et al, 2020). A similar mathematical expression was used to establish the role of potassium leak channels in the excitability of pituitary cells: I_K=g_K (V_m-E_k) The only difference in this equation is the reversal potential (E_k), which is -85 mV (reversal potential of potassium). Dynamic clamp can be thought

of as a novel extension to the conventional current-clamp technique as the injected current is calculated for a specific voltage at each point in time. Thus, the injected current is varied dynamically, unlike conventional current clamp in which the injected current is constant across all time points.

2.5 Measurement of cytosolic calcium in single pituitary cells

Alterations in the cytoplasmic Ca^{2+} concentration are commonly measured by luminescent or fluorescent Ca^{2+} binding compounds. Two very extensively used Ca^{2+} indicators are Fura-2 and Indo-1 which are derivatives of calcium chelator 1,2-bis(o-aminophenoxy)ethane-N,N,N',N'-tetraacetic acid (BAPTA) developed by Roger Tsien and his colleagues (Grynkiewicz et al, 1985). Both Fura-2 and Indo-1 are excited by ultraviolet light, and exhibit a shift in their excitation and emission wavelengths respectively once they are bound to Ca^{2+}. This feature is beneficial since the Ca^{2+} concentration can be measured from alterations in the ratio of the fluorescence intensities at two excitation or emission spectrums. This ratiometric method cancels out the artefacts arising from bleaching, different dye loadings, changes in focus and variations in laser intensity. Here, Fura-2 dye was used to measure the cytosolic Ca^{2+} transients in pituitary cells.

The coverslips with pituitary cells were bathed in the extracellular solution (containing same ingredients as described in the above electrophysiology section) with 2μM fura-2 AM (Thermo Fisher Scientific, #F1221) for 45 minutes at 37 °C. The cells were then rinsed three times with the extracellular solution using a 2 mL Pasteur pipette. Following this, the coverslips were mounted onto the recording chamber (volume $\approx$ 0.2 mL) on the stage of an inverted microscope (Nikon eclipse Ti). Cells were constantly perfused with the extracellular solution at room temperature using a gravity-driven perfusion system. After a cell was patched and series resistance reduced to lower than 50 MΩ, calcium imaging was performed simultaneously with membrane voltage recording. Cells were excited every 1 second with alternating 340-nm and 380-nm light beams (20 millisecond exposure time) originating from a Lambda DG-4 wavelength switcher (Sutter Instrument Company). Light intensity

was reduced by 50% before hitting the cells using an appropriate filter. The intensity of emission light was measured at 520 nm and images were acquired by a Hamamatsu digital camera C1344 set to 4 × 4 binning. Hardware control was achieved by TI Workbench software developed by T. Inoue (as used by Tabak et al, 2010). Using this software, regions of interest (ROI) were selected around the patched cells that were not overlapping with other cells and a single background ROI was selected in an empty space. Pixel values within each region of interest were averaged for both 340 and 380 excitation wavelengths and then subtracted from the background. Following this, a ratio r was computed according to the formula (as used by Tabak et al, 2010):

$$r = \frac{(ROI_{340} - ROI_{background340})}{(ROI_{380} - ROI_{background380})} \tag{2.1}$$

Image analysis was performed in MATLAB.

2.6 Immunocytochemistry (ICC)

GH4 cells were cultured on 15 mm^2 coverslips ($n = 3$) and incubated at 37°C and 5% CO_2 overnight. The next day, cells were washed three times with 1x PBS (phosphate buffered saline) supplemented with 1 mM Mg^{2+} and 2 mM Ca^{2+} (the presence of Ca^{2+} and Mg^{2+} is necessary for keeping the cells attached to the coverslips). Then, the cells were fixed with 4% paraformaldehyde (PFA) in PBS (with Ca^{2+} and Mg^{2+}) for 30 minutes at room temperature. Subsequently, cells were washed 3 times with PBS. The permeabilization step was skipped since the NALCN antibody was designed to bind the extracellular domain. Therefore, cells were immediately incubated for 60 minutes at room temperature in blocking solution (3% BSA (bovine serum albumin) in PBS + 0.03% TritonTM X-100) on an agitated surface. The primary antibody anti-NALCN/VGCNL1 (extracellular) (#ASC-022) was diluted 1:500 in the blocking solution + 2% serum generated from the host of secondary anti-body (in this case goat), and was applied to the coverslips and incubated at 4°C for 24 hours in a humidified chamber. The negative control coverslips were incubated with only blocking solution and no primary antibody. The anti-NALCN antibody (hosted in rabbit) is a highly specific polyclonal antibody (Ou et al, 2020) targeted directly against an epitope of rat NALCN (amino acid residues 902-914)

located at extracellular S1-S2 domain III (Figure 2.6).

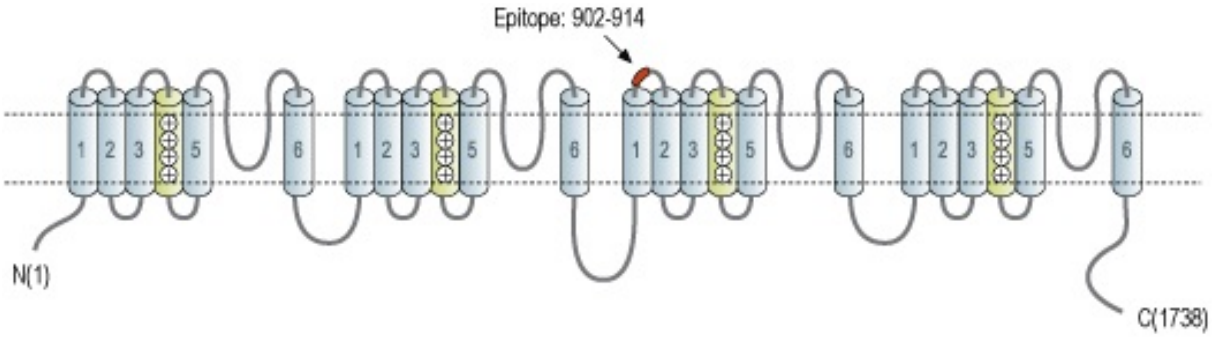

Figure 2.6: Anti NALCN anti body targeted directly against an epitope of NALCN channel extending from S1 to S2 of domain III.
The antibody has been designed to specifically recognize NALCN in mice, rat, and human cells (the figure is reproduced form the manufacturer website alomone.com). The next day, the coverslips were washed with PBS three times (the last time for 5 minutes) and the Alexa-Fluor conjugated antibody (at 1:1000, Molecular Probes) diluted in blocking solution was added to the petri dishes containing the coverslips. Afterwards, the petri dishes were incubated on an agitated surface for 60 minutes at room temperature, and shielded from light using foil wrap. Coverslips were then washed three times with PBS (each time 5 minutes). The nucleic acids present in the dissociated pituitary cells were visualised with TOTO-3 (1:2000, Thermo Fisher). For this purpose, coverslips were incubated with TOTO-3 for 15 minutes on an agitated surface at room temperature, then washed three times (each time 5 minutes) and finally mounted with Fluorsave medium (Calbiochem). The controls were the coverslips where primary antibody was omitted. Images were obtained using a Zeiss LSM 5 Exciter confocal microscope run by Zen software.

The next day, the coverslips were washed with PBS three times (the last time for 5 minutes) and the Alexa-Fluor conjugated antibody (at 1:1000, Molecular Probes) diluted in blocking solution was added to the petri dishes containing the coverslips. Afterwards, the petri dishes were incubated on an agitated surface for 60 minutes at room temperature, and shielded from light using foil wrap. Coverslips were then washed three times with PBS (each time 5 minutes). The nucleic acids present in the dissociated pituitary cells were visualised with TOTO-3 (1:2000, Thermo Fisher). For this purpose, coverslips were incubated with TOTO-3 for 15 minutes on an agitated surface at room temperature, then washed three times (each time 5 minutes) and finally mounted with Fluorsave medium (Calbiochem). The controls were the coverslips where primary antibody was omitted. Images were obtained using a Zeiss LSM 5 Exciter confocal microscope run by Zen software.

2.6.1 Immunohistochemistry (IHC of the pituitary gland)

Pituitary glands were extracted and fixed overnight in 4% PFA in PBS. The following day, 70 μm thick sections were cut using a vibratome (Campden Instruments, UK), placed on Poly-L-Lysine coated microscope slides (VWR) and left to dry. Next, the sections were blocked with 10% FBS in PBST (PBS containing 0.01% Triton X-100) for one hour at room temperature. Primary rabbit anti-NALCN antibody (at 1:500) in 10% FBS/PBST was applied to the sections and incubated in humid chamber at 4°C degrees overnight. The next day, sections were washed 3 times for 15 minutes with PBST and the secondary, 488-Alexa-Fluor conjugated antibody (at 1:1000, Molecular Probes) was applied in 10% FBS/PBST solution for 1 hour at room temperature, followed by a series of three 15 minute washes with PBST. The nucleic acids present in the pituitary gland cells were visualised with TOTO-3 (1:2000, Thermo Fisher). Thus, sections were incubated with TOTO-3 for 15 minutes on an agitated surface, then washed three times (each time 10 minutes) and subsequently mounted with Fluorsave medium (Calbiochem). The controls were the sections where primary antibody was omitted. Images were obtained using a Zeiss LSM 5 Exciter confocal microscope run by Zen software.

2.7 Quantitative Real-Time PCR (qRT-PCR)

2.7.1 NALCN primer design

First, the whole gene sequence of NALCN gene including exons and introns was identified using the Ensemble genome browser: (https://www.ensembl.org/Mus-musculus/Gene/Sequence?db=core;g=ENSMUSG00000000197;r=14:123276634-123627144). The next step was to select two exons with a very large intron (preferably the largest intron) in between. This is to ensure that no DNA contamination in the preparation will be amplified, and that only the cDNA derived from extracted mRNA will be amplified (because mRNA only contains the exons and not the introns). Then, the sequences of both exons were located using Primer3 software to obtain the best primer sequence with 40-60% maximum GC content and 20 nucleotide length. Subsequently, the primer sequence suggested by Primer3 software was blasted using the NCBI website. This is to ensure that the suggested primer sequence blasts 100% with only the NALCN gene in mus musculus (or any other species), but not with any other genes.

The customised NALCN primer (Thermofischer):

Forward: 5'- GGCAGATGCTAGTGCAGAAC

Reverse: 5'- TCAGTAACTGGCTGGGCTTC

The house keeping control gene β-actin primer:

Forward: 5'-TGCTCCTCCTGAGCGCAAGTACTC

Reverse: 5'- TCAGTAACTGGCTGGGCTTC

2.7.2 RNA Purification

Four mice ($n = 4$) were sacrificed *via* cervical dislocation, and then the pituitary glands were harvested, the posterior and intermediate parts were removed, and the anterior parts were immediately submerged in RNalater solution (Qiagen) to prevent RNA degradation. Afterwards, RNA was extracted using RNeasy Lipid tissue mini kit (Qiagen) accordingly to the manufacture's protocol. The obtained RNA was measured using Nanodrop 2000/2000c at A260/A280 ratio with values between 1.8 and 2.1.

2.7.3 Reverse transcription

0.5 μg of RNA was converted to cDNA using EvoScript Universal cDNA Master kit (Roche).

2.7.4 9.4 SYBR® Green qRT-PCR

Next, SYBR® Green qRT-PCR was performed to measure the relative level of NALCN mRNA using fast SYBR green master mix (Thermo Fisher, #4385610). The qRT-PCR conditions for relative mRNA quantitation started with a 15 min denaturation step at 95°C followed by 40 cycles of 95°C – 15 second, 55°C – 30s, 72°C – 30s. The quantitation for each gene was performed three times.

The double delta CT method ($\Delta\Delta$CT) was used to analyse the data. The double delta CT ($\Delta\Delta$CT) values indicate the normalised target gene expression levels relative to the expression levels of housekeeping gene β-actin utilised as a control. Levels of NALCN were normalised to β-actin-coding mRNA levels by subtracting the mean CT of the control (β-actin) from the mean CT of NALCN.

2.8 Data Analysis

The time course of the membrane potential was quantified to evaluate the event duration and inter-event intervals for each cell (as described by Tabak et al, 2011). Briefly, to calculate the duration of each electrical event, the start time and the end time of each event were acquired running a threshold-crossing detection algorithm in MATLAB (Figure 2.7). This algorithm normalised the voltage traces relative to the minimum and maximum membrane voltages of each sequence creating a range between zero and one. This is to reduce the differences amongst the event durations, which can result from differences in event amplitude and voltage offset amongst cells (the base membrane potential in pituitary cells oscillates and is not stable). To measure the inter-event intervals, the data points between the end time of an event and start time of the next event was calculated and then multiplied by the time step (Figure 2.7). The threshold-crossing line to define the beginning of an electrical event was set at 0.5 (start time) which is significantly larger than the noise amplitude in the experiment. The threshold-crossing line to terminate the electrical

event was set at 0.45 (end time) which is below the burst oscillation amplitudes and yet significantly higher than the noise amplitude in the basal membrane potential.

The MATLAB function "findpeaks" was used to objectively determine the number of spikes and bursts in voltage traces. Using this function, first, the voltage traces were normalised as described above, then every peak above a certain threshold (0.5) was identified. If an electrical event had two or more closely spaced neighboring peaks, then the electrical event was defined as a burst. A peak which did not have neighbors (single peak) was defined as a spike. For measuring the event duration, inter-event interval and identifying peaks a range of 120 seconds was selected from each voltage traces.

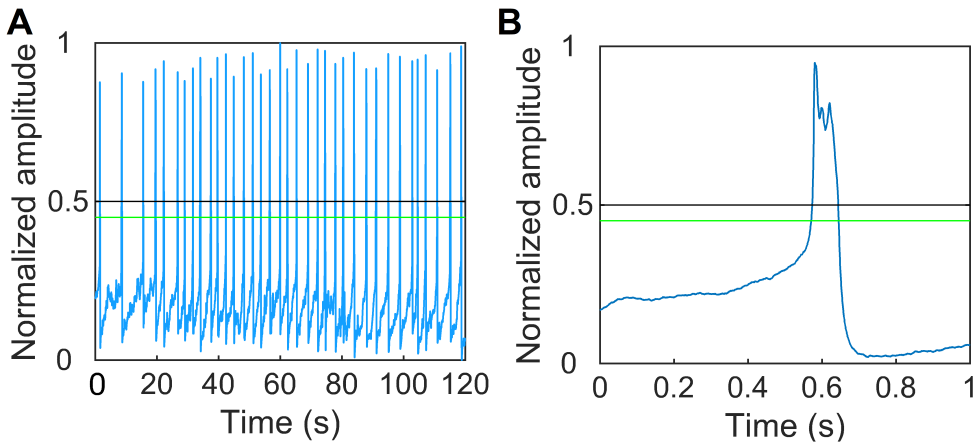

Figure 2.7: Measurement of event duration and inter-event interval in voltage traces.
A) A range of 120 seconds of a normalised voltage trace over which the event duration and inter-event interval were calculated. The black line represents the threshold-crossing line set at 0.5 (start time), and the green line represents the threshold-crossing line set at 0.45 (end time). To measure the inter-event intervals, the data points between the end time of an event and start time of the next event was calculated and then multiplied by the time step. To calculate the duration of each electrical event, the distance between the start time and the end time of each event were measured and multiplied by the time step (dt). **B)** Smaller window (1s) of panel A

2.8.1 Statistical analysis

In order to quantitatively describe the relationship between the changes in the leak-channel conductance and its effect on inter-event interval, event duration and $[Ca^{2+}]_i$, either an exponential or linear model was fitted to the data where it was appropriate. In the exponential model, the effect of varying leak conductance on inter-event interval was analysed in terms of a decay constant (β). The data points corresponding to each single cell were fitted to a one-term exponential model of the form $y = ae^{\beta x} + c$ which returns the distribution of β,α and c (β is the decay constant). Here a, β, and c are fitting coefficients. If the coefficient β is negative it means that the function y has an exponential decay. In contrast, if the coefficient β is positive it means that the function y has an exponential rise. However, for some data sets the relationship between the two variables was linear and thus the exponential fitting function was not a suitable option (determined in the result section). Therefore, the data points corresponding to each single cell in those data sets are fit to a linear model of the form $y = bx + c$ which returns the distribution of b (slope).

In order to measure the significance of b/β (b or β) distribution, first the normality of b/β population was evaluated using a one-sample Kolmogorov-Smirnov test. The null hypothesis was rejected at 0.05 significance in each data set indicating that b/β are not normally distributed. Therefore, the non-parametric one-sample "Wilcoxon signed rank" test was performed to determine the significance of b/β distribution, for which the null hypothesis is rejected if the p-value is below 0.05. Using this test, the distribution of b/β (or histogram of b/β) was compared statistically to a normal distribution centred at zero. Here, zero means no change. The null-hypothesis for one-sample "Wilcoxon signed rank" test is that the median of the data is equal to zero. Using this test, the b/β is ranked from the highest values to the lowest values and then its median is compared with a normal population with median zero.

If the p-value of the test is less than 0.05, it means that very small changes in the conductance of leak-channels results in the substantial changes in inter-event intervals, event duration, RMP and cytosolic calcium level. However, if the p-value is greater than 0.05, it implies that the distribution of b/β is centred around zero and thus the changes in the conductance of leak channels does not create significant

changes. In order to determine whether the fitting function is a suitable function, the r-square (r^2) was evaluated using Matlab software. The r-square indicates the goodness of the fits and its value varies between zero and one. The closer the r-square is to one, the better the fit. The r-square is close to one for most of the fits with only a few fits having low r-square (r-square < 0.8). After removing the data with the low r-square and evaluating the significance of the b/β, the results did not change, and the p-value was still less than 0.01.

This model-based approach was considered over other conventional statistical tests, such as repeated-measures ANOVA, as it takes the inter-individual variability amongst pituitary cells into account. Endocrine pituitary cells and the clonal cell line GH4 cells are heterogeneous in terms of their cell-size, cell capacitance and the magnitude of their response to the same stimuli. As a result, one cell may have a much stronger response to the same changes in leak conductance compared to another cell. Binning or averaging of inter-event intervals at every value of conductance masks the intercellular variability. Moreover, the averaging method can lead to an overall fluctuating trend which is not representative of the behaviour of each individual cell. This spurious behaviour is particularly highlighted when small cell-population sizes are analysed.

Chapter 3

How leak channels control dynamic activity of endocrine anterior pituitary cells

3.1 Introduction

A common feature amongst all the endocrine pituitary cells and their clonal cell lines is the spontaneous (independently of external stimuli) generation of electrical activity which can be modulated by hypothalamic and intrapituitary factors as well as feedback signals coming from the periphery (reviewed by Fletcher et al, 2018). The critical role of spontaneous firing in all pituitary cells is to activate voltage-gated calcium channels (VGCCs), either to directly drive hormone release (stimulus-secretion coupling) or to maintain the intracellular calcium stores at responsive state to facilitate receptor-controlled secretion (reviewed by Stojilkovic, 2012).

The ability of pituitary endocrine cells to generate action potentials spontaneously relies on the presence of a group of subthreshold (background) cationic currents which tune the resting membrane potential at levels close to or above the activation threshold of VGCCs. An inward background cationic current carried by Na^+ (I_{Nab}, also known as nonselective cationic current I_{NS}) is responsible for maintaining the resting membrane potential at depolarised levels away from the K^+ equilibrium potential in all pituitary cells as well as related cell lines (Simasko, 1994; Sankaranarayanan and Simasko, 1996; Kwiecien and Hammond, 1998; Tsaneva-Atanasova et al, 2007; Kucka et al, 2010; Liang et al, 2011; Tomic et al, 2011; Kucka et al, 2012; Zemkova et al, 2016; Kayano et al, 2019). Impairing the function of background sodium channels in these cells, for example by replacing the extracellular

Na^+ with the large impermeant cation $NMDG^+$, hyperpolarises the membrane potential close to the K^+ reversal potential. Therefore, this leads to the silencing of electrical activity and abolishment of calcium influx and basal hormone secretion. The constitutively active background sodium channels can be further modulated by the extracellular signals. Several research groups have reported that the background Na^+ currents potentiate the stimulatory response caused by excitatory hypothalamic factors through increasing the slope of slow depolarisation phase prior to the generation of action potentials (Liang et al, 2011; Zemkova et al, 2016; Kretschmannova et al, 2012). Additionally, the blockade of inward cationic currents has been shown to substantially delay the stimulatory response of CRH (corticotropin releasing hormone) by approximately 13 minutes (Liang et al, 2011). These reports pinpoint background sodium conductance as an essential component for both maintaining the spontaneous generation of action potentials and modulating receptor-controlled membrane depolarisation in endocrine pituitary cells. However, the molecular identity of the background Na^+ channels in pituitary cells remains unknown.

This inward depolarising current is counterbalanced by an outward hyperpolarising current carried by K^+ (background K^+ current or I_{Kb}) which participates in adjusting the resting membrane potential in pituitary cells (Fletcher et al, 2018). One candidate for playing this role is the inwardly rectifying K^+ channel family (Kir) which are active near resting level, pass large inward K^+ current upon hyperpolarisation, and are blocked by magnesium and spermine during strong depolarisation (Stanfield et al, 2002). The constitutively active Kir has a crucial role in modulating the resting membrane potential as well as the frequency and amplitude of cytoplasmic calcium oscillation in endocrine pituitary cells (Charles et al, 1999). These channels are inhibited by excitatory hypothalamic factors such as TRH, CRH and GHRH to enable depolarisation, and are activated by inhibitory hypothalamic factors such as dopamine and somatostatin to facilitate hyperpolarisation (Barros et al, 1997; Corrette et al, 1996; Shorten et al, 2000; Xu et al, 2002; Einhorn et al, 1991; Sims et al, 1991; Thomas and Smith, 2001). Therefore, it is expected that a GPCR like the D2 receptor that inhibits background Na^+ channels also activates background K^+ channels to induce hyperpolarisation. Conversely, GPCRs that ac-

tivate background Na^+ channels also inhibit background K^+ channels such as Kir channels in order to induce depolarisation.

Collectively, these studies suggest a hypothetical role for fine-tuning of cation-currents near the resting membrane potential to pivot between excitation and inhibition of endocrine cells, allowing for acute control of hormonal secretion. One way in which hypothalamic factors can tune the electrical excitability of endocrine pituitary cells is by shifting the balance between these sodium and potassium background conductances (Fletcher et al, 2018). What is not known, however, is precisely how much change in these background conductances is required to alter the electrical activity of these cells. Because pituitary cells have a very high input resistance (on the order of 5 GΩ [Dubinsky and Oxford, 1984]; that is, a total conductance around resting membrane potential on the order of 0.2 nS), I hypothesised that even a very small change in one of these conductances may shift this balance enough to have a significant impact on electrical excitability.

Here, I quantified the change in Na^+ and K^+ leak conductances required to significantly alter the electrical excitability of endocrine pituitary cells. To do so, I used the dynamic clamp technique to precisely and reliably induce small changes in the leak conductances of living cells (first in the lacto-somatotroph cell line GH4 and later in murine primary anterior pituitary cells). This enables the investigator to observe how manipulating leak channel conductance affects both the pattern of electrical activity and cytosolic Ca^{2+} levels.

3.2 Results

3.2.1 Authentication and characterization of GH4 cell line

The GH4 cell line was developed from a successively passaged GH3 cell population originated from norwegian rat pituitary adenoma. GH4 cells secrete mainly prolactin hormone (PRL), and little or no detectable amount of growth hormone (Stojilkovic et al, 2010). Two primary characteristics of GH4 cells are their excitatory response to the hypothalamic neurohormone thyrotropin releasing hormone (TRH) as well as the secretion of PRL.

Electrical and $[Ca^{2+}]_i$ activity of GH4 cells in response to TRH

In the current study, the electrical and $[Ca^{2+}]_i$ activity of GH4 cells were evaluated in response to TRH. It is well-established that TRH induces an initial release of Ca^{2+} from intracellular Ca^{2+} stores into the cytosol followed by increased cellular Ca^{2+} uptake through voltage-gated calcium channels. Therefore, TRH stimulates prolactin secretion in GH4 cells by enhancing intracellular Ca^{2+} via two mechanisms: first, mobilization of $[Ca^{2+}]_i$ from intracellular Ca^{2+} stores; second, Ca^{2+} influx through voltage-gated calcium channels (Albert et al, 1984; Gershengorn and Thaw, 1985; Kruskal, 1984; Schlegel, 1984). These reports were in agreement with the results obtained by Ozawa, 1981 and Ozawa, 1985 who performed electrophysiological experiments to show that TRH-induced release of $[Ca^{2+}]_i$ from intracellular Ca^{2+} stores triggers the acute activation of calcium-gated potassium channels, which results in the membrane hyperpolarisation in GH4 cells. Ozawa, 1981 and Ozawa, 1985 also reported that the subsequent increase in Ca^{2+} influx via voltage-gated calcium channels is associated with an increased firing activity for an extended period of time in GH4 cells. Consistent with the previous reports, I could demostrate the typical biphasic electrical and $[Ca^{2+}]_i$ response of GH4 cells to TRH using electrophysiology and calcium imaging techniques (Figure 3.1). The addition of 10 nM TRH to GH4 cells recorded in current-clamp (I=0) resulted in membrane hyperpolarisation followed by a depolarisation and increased firing activity (Figure 3.1A, n=12, each cell was obtained from different coverslips across several experimental sessions). In a separate experiment using a different GH4 cell passage-number, the $[Ca^{2+}]_i$ activity in respone to 10 nM TRH was investigated (n=35). The measurement of $[Ca^{2+}]_i$ in GH4 cells indicated a transient increase of $[Ca^{2+}]_i$ from the resting level after the addition of 10 nM TRH. This peak was followed by a decay to the resting value within the next few minutes (Figure 3.1B). My results showed that 100% of the recorded GH4 cells responded to TRH.

Detecting the PRL expression in GH4 cells using immunocytochemistry

Next, I investigated the PRL expression in GH4 cells using rabbit monoclonal anti-PRL (Abcam, # ab188229). My results indicated that more than 99% of stained

GH4 cells (n=3 coverslips) were PRL positive (Figure 3.2). Taken together, my results confirmed that the provided GH4 cell line by "Deutsche Sammlung von Mikroorganismen und Zellkulturen" company is functional and authentic, and exhibit the features assigend to GH4 cell line.

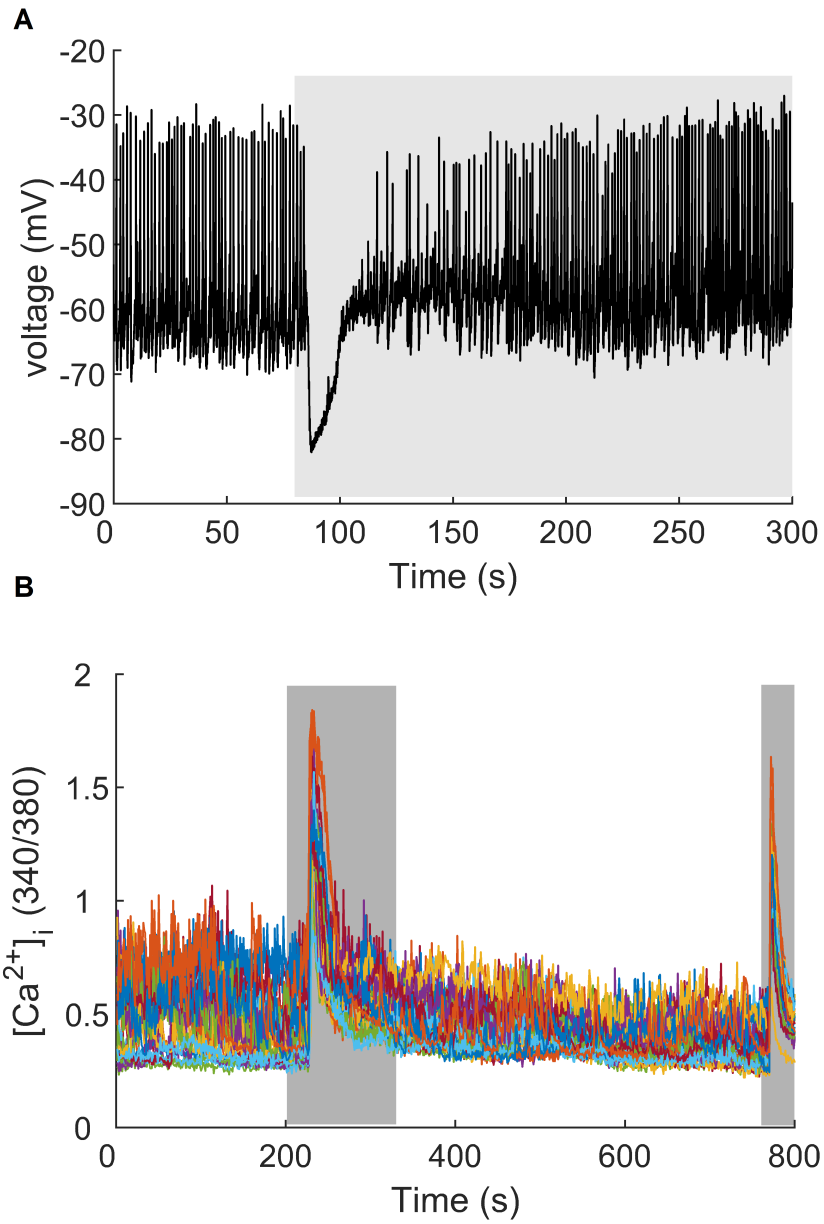

Figure 3.1: The biphasic electrical and $[Ca^{2+}]_i$ response of GH4 cells to 10 nM TRH.

A) A representative voltage trace recorded from a GH4 cell. The application of 10 nM TRH significantly hyperpolarised the membrane potential and subsequently depolarised the cell membrane in all recorded GH4 cells (n=12, each cell was obtained from independent coverslips). **B)** The application of 10 nM TRH resulted in a transient increase of $[Ca^{2+}]_i$ from the resting level (n=35). This peak was followed by a decay to the resting value within the next few minutes. The last peak is extracellular K^+ (15 mM)-induced increase in Ca^{2+} influx to check the viability of GH4 cells, which shows all the cells are alive and functional.

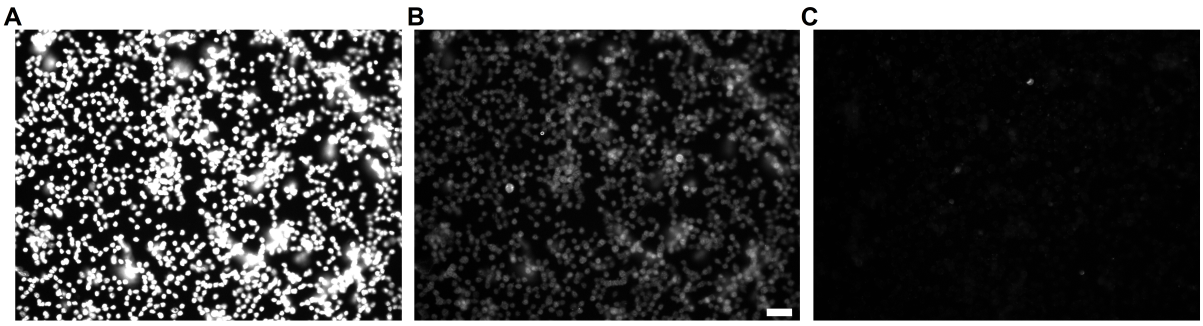

Figure 3.2: The stained GH4 cells were PRL positive.
A) The DNA staining with DAPI, excited by 360 nm light. **B)** PRL staining with rabbit monoclonal anti-PRL(1:1000) + Goat anti-rabbit polyclonal secondary antibody (1:1000, Alexa Fluor) excited by 488 nm light. **C)** Negative control where the primary antibody is omitted. All the graphs are imaged under 10X magnification and 200 ms exposure time. The scale bar in panel B is 50 μ M

3.2.2 GH4 cells have a relatively high input resistance

First, I showed that GH4 cells have a high input resistance. Using perforated patch-clamp electrophysiology, voltage steps ranging from -80 to -50 mV (with 10 mV increments, holding potential: -60 mV, duration for each step: 500 ms) were applied in GH4 cells to record the leak currents at potentials in which the voltage-gated ion channels are not active. A linear I-V (current-voltage) relationship was obtained, allowing to evaluation of the the passive properties of the cells (e.g. conductance, input resistance etc.). From the slope of the linear I-V relationship (Figure 3.3), the input resistance was found to be on average 7 Giga Ohm (minimum of 3.12 GΩ and maximum of 10.21 GΩ, n=16), which is considerably greater than previously reported (e.g. 170-500 Mega Ohms in Dufy et al, 1979; Taraskevich and Douglas, 1980; and 2-4 Giga ohms in Hagiwara and Ohmori, 1982; Dubinsky and Oxford, 1984). This discrepancy in the obtained input resistance may be due to the leakage of the current at the site of the membrane rupture by microelectrodes in conventional whole-cell and intracellular recording techniques used in previous studies. However, perforated patch-clamp is a less invasive technique in which the cell membrane is not ruptured. Instead, small pores are created by antibiotics (amphotericin-B) and thus the amount of current leakage is significantly reduced. The recording temperature is another factor that can affect the input resistance of the cells, however all the above experiments were performed at room temperature. This high input resistance of GH4 cells during rest implies a high sensitivity of these cells to very small changes in the leak conductances. For instance, in a cell with 5 GΩ input resistance, injection of 1 pA positive current is sufficient to depolarize the membrane potential by 5 mV.

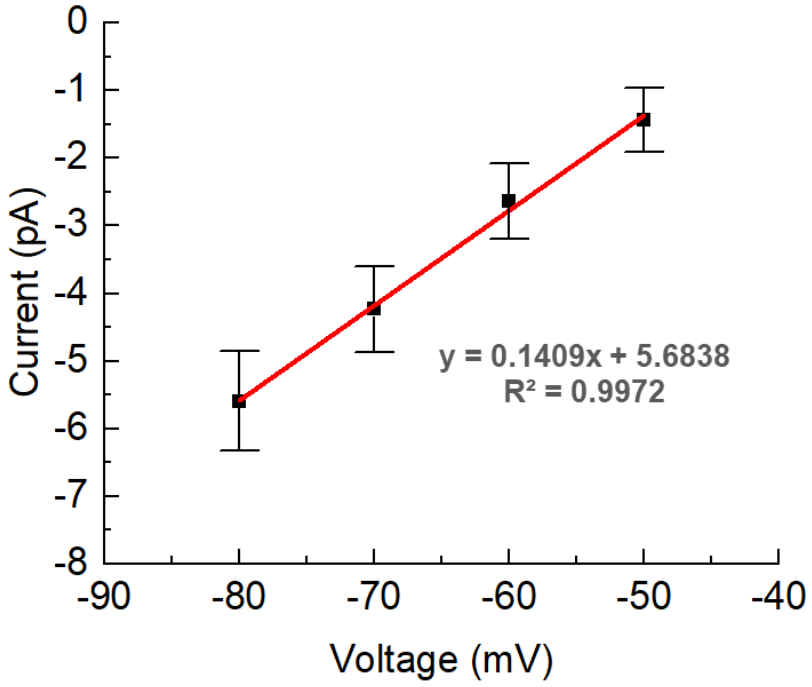

Figure 3.3: The input resistance of GH4 cells.
The voltage steps ranging from -80 to -50 mV (with 10 mV increments, holding potential: -60 mV, duration for each step: 500 ms) were applied to record the currents from GH4 cells at different potentials (n=16, cells were obtained from several coverslips throughout numerous experimental sessions). In this range, voltage-gated channels are not activated in GH4 cells. After achieving a Gigaohm seal ($R_t > 10$ GΩ, Ih (holding current) <4 pA and V_h (holding potential) = -60 mV), once the access resistance (Ra) reached below 50 MΩ the voltage step protocol initiated. The red line is a linear regression fitted to the measured data points using excel. The R^2 indicates the goodness of the fit. The bars represent the standard deviation. The slope is 0.1409.

3.2.3 Removing extracellular sodium eliminates a tonic inward leak current and supresses the generation of electrical events

To confirm that there is a small background Na^+ current depolarising GH4 cells, I replaced most extracellular Na^+ by impermeable cation $NMDG^+$. Consistent with previous reports (reviewed in Fletcher et al, 2018), replacing 135 mM of extracellular Na^+ with $NMDG^+$ in current-clamp mode ($I = 0$), hyperpolarised the GH4 cells close to -70 mV and stopped the generation of electrical activity ($n = 5$, Figure 3.4A,B). $NMDG^+$ has the same number of positive charge [or valence] as sodium ions so it can maintain the osmolarity of extracellular solution. However, it has a much greater molecular size and thus does not pass through the Na^+ leak channels. Redoing the same experiment in voltage-clamp mode (voltage was held at -60 mV), eliminated the tonic inward current by about 1 to 5 picoamperes (pA) across different cells ($n = 4$, Figure 3.4C,D). This suggests that reducing only 1 to 5 pA positive inward current is sufficient to hyperpolarise GH4 cells close to the K^+ reversal potential and abolish the electrical activity. Therefore, the next experiments were conducted to precisely quantify the exact contribution of leak conductances to the pattern of electrical activity and $[Ca^{2+}]_i$.

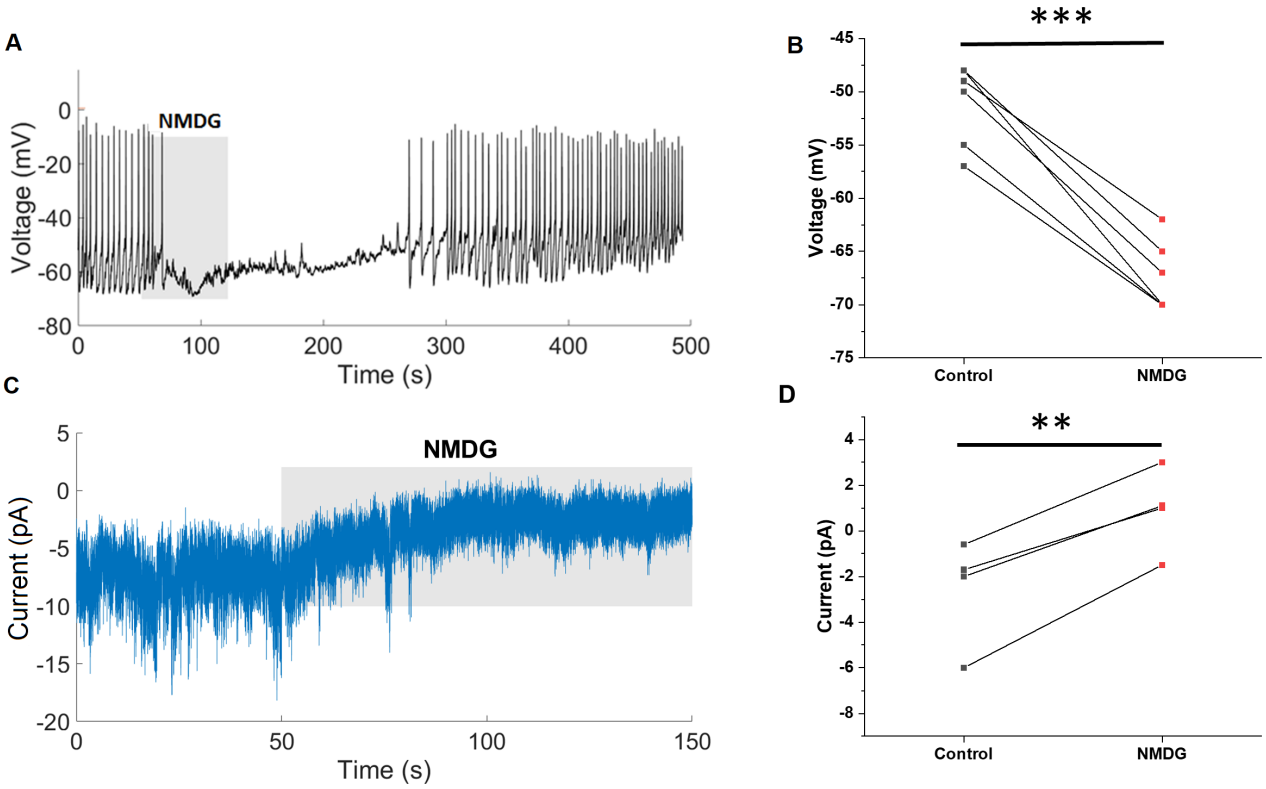

Figure 3.4: The effect of removing extracellular Na^+ on the spontaneous generation of electrical activity, and on the inward leak current in GH4 cells.

A) In current clamp mode ($I = 0$), the replacement of $[Na^+]_o$ (extracellular Na^+) with $NMDG^+$ stopped the generation of electrical events and hyperpolarised the example cell from ≈ -55 to -70 mV. The grey area is the period during which the $NMDG^+$ was present in the recording chamber.**B)** Membrane potential values before and after the replacement of $[Na^+]_o$ with $NMDG^+$ in GH4 cells (Vm before $NDMG^+$: -51.8 mV ± 3.8; Vm after $NMDG^+$: -68 mV $\pm 3.5, n = 5, p < 0.001$, paired t-test). **C)** Replacement of $[Na^+]_o$ with $NMDG^+$ eliminates the tonic inward leak current by approximately 5 pA in this example cell (membrane potential is held at -60 mV). **D)** Inward leak currents before and after the replacement of $[Na^+]_o$ with $NMDG^+$ (leak current before $NMDG^+$: -2.8 pA ± 2; leak current after $NMDG^+$: -0.8 pA $\pm 1.1, n = 4, p < 0.01$, paired t-test). All data are represented as mean $\pm$ SD. Single asterisk is $p < 0.05$, double asterisk is $p < 0.01$ and triple asterisk is $p < 0.001$.

3.2.4 The reversal potential of background Na^+ conductance tends to zero in GH4 cells

To measure the reversal potential of the present background Na^+ current in GH4 cells, a cocktail of drugs (containing 1 μM Nimodipine, 1 μM TTX, 10 mM TEA-Cl, 2 mM $CsCl_2$, 12 nM Erg-toxin and 2.5 μM T-type calcium channel blocker TTA-A2) was added to the cells recorded under current-clamp mode to isolate the background Na^+ current. Therefore, all the voltage-gated calcium and sodium channels,voltage-gated potassium channels, potassium leak channels and HCN channels were blocked pharmacologically. Once the spontaneous firing activity was fully inhibited and the level of membrane potential remained stable the voltage-clamp recording started. The voltage step protocol ranging from -70 to 10 mV with 10 mV increment and holding potential of -60 mV was applied, and the elicited Na^+ leak current was recorded. The duration of each step was 400 ms and only the last 50 ms in every step was selected to be averaged for plotting current-voltage (I-V) graph across different GH4 cells (Figure 3.5, n=7). The average X intercept signifiying the voltage at which the net current flow is zero was found to be approximately -10 mV and tends towards zero (Figure 3.5).

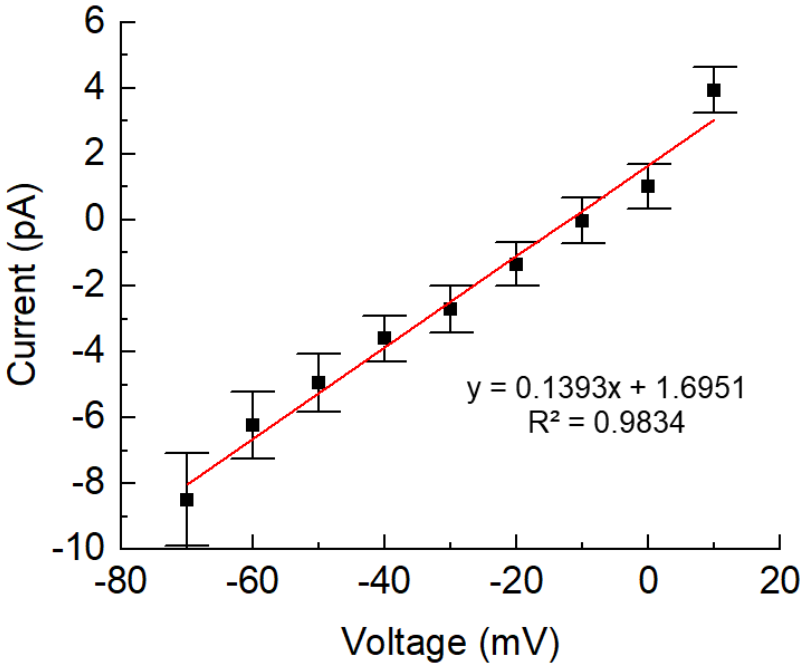

Figure 3.5: The reversal potential of background Na^+ conductance tends to zero and is approximately -10 mV in GH4 cells.
Voltage steps ranging from -70 to 10 mV with holding potential of -60 mV was applied and the elicited leak currents were recorded (n=7). The duration of each step was 400 ms and only the last 50 ms was selected to be measured. The I-V curve shows a linear trend and X intercept (reversal potential) was measured at -10 mV. The R^2 indicates the goodness of the fit. The bars represent the standard deviation.

3.2.5 Minute alterations in background Na^+ conductance substantially impact electrical and $[Ca^{2+}]_i$ activity in GH4 and primary pituitary cells

Using dynamic clamp combined with Ca^{2+} imaging technique, it was possible to alter (increase or decrease) the conductance of background Na^+ leak channels artificially, and record the effect this alteration has on electrical activity and $[Ca^{2+}]_i$ in real time. This is achieved using the mathematical expression of Na^+ leak currents $I_{NS} = g_{NS}$ (V_m-E_{NS}) which mimics the function of Na^+ leak conductance in endocrine pituitary cells (see 2.4.1.1, section on dynamic clamp in Materials and Methods; E_{NS} was set to 0 mV since the background conductance is non-specific). I first quantified the contribution of leak conductances to electrical and $[Ca^{2+}]_i$ activity in GH4 cells, and subsequently in mixed populations of primary murine anterior pituitary cells. My results showed that minute alterations in Na^+ leak conductance (g_{NS}) ranging from -0.1 to 0.12 nanosiemens (nS) were sufficient to substantially change the frequency of electrical activity, resting membrane potential and cytoplasmic calcium level ($[Ca^{2+}]_i$) in GH4 cells as well as in mixed populations of primary murine pituitary cells (Figures 3.6, 3.7 and 3.9, 3.10).

GH4 cells

Under control conditions in GH4 cells (and in the majority of primary pituitary cells), two types of electrical events were observed: 1) spikes and 2) pseudo-plateau bursts (hereafter referred to as burst), for which the pattern is determined by the duration and amplitude of the electrical events (Figure 3.6A,B). Spikes have high amplitude and short duration (a few milliseconds to a few tens of milliseconds; Figure 3.6A) similar to what is observed in neurons. However, bursts are composed of electrical pulses with longer duration (several tens to several hundreds of milliseconds; Figure 3.6B) and lower amplitude than spikes. During a burst, the membrane potential oscillates around the depolarised level after reaching the peak amplitude of an action potential, and repolarises after a few hundred milliseconds.

Increasing g_{NS} *via* dynamic clamp by fractions of a nano Siemen (0.02 to 0.12 nS) could significantly reduce the inter-event intervals in GH4 cells ($p<0.001$, exponential fitting function followed by sign rank test, n=36, Figure 3.6 & 3.7 A-C). More-

over, it increased the resting membrane potential substantially ($p < 0.001, n = 36$, Figure 3.7E), and consequently enhanced $[Ca^{2+}]_i$ ($p < 0.01, n = 11$, Figure 3.7F). In the majority of recorded cells (30 out of 36), increasing the g_{NS} by 0.12 nS, resulted in depolarisation block. Depolarisation block is a silent state where the membrane potential stays around highly depolarised levels relative to the resting membrane potential. Therefore, during depolarisation block, the voltage-gated ion channels responsible for generating action potentials (electrical events) remain in inactivation mode and need to reach hyperpolarised levels to come out of inactivation mode. This occurs when cells are exposed to excessive excitation either by excitatory stimuli or upon applying too much positive current.

In contrast, reducing g_{NS} by -0.02 to -0.08 nS showed the opposite effect: it markedly decreased the frequency of electrical activity (Figure 3.7A-C), resting membrane potential (Figure 3.7E) and $[Ca^{2+}]_i$ (Figure 3.7F). In 16 out of 36 GH4 cells, subtracting g_{NS} by only -0.04 nS entirely abolished the electrical events and hyperpolarised the resting membrane potential by more than 15 mV (Figure 3.6C, 3.7E). This indicates that very minute changes in g_{NS} have a visible effect on the electrical activity, demonstrating a high sensitivity of GH4 cells to the changes in the conductance of Na^+ leak channels.

Changing g_{NS} also significantly altered the event duration in GH4 cells ($p < 0.01$, Figure 3.7D). Indeed, an increase in g_{NS}, induced a noticeable decrease in the event duration, and the opposite effect was also observed. Of note, 24 of 36 recorded GH4 cells predominantly produced bursts with burstiness factor above 80% (bf >80%, bf is the percentage of bursts produced by cells)(Figure 3.18A). The rest of the cells predominantly produced spikes (bf <20%) whose event duration did not show consistent and strong changes upon changes in g_{NS}. The median capacitance of patched GH4 cells was 5.5 pF with a range between 4 and 10 pF. This reflects that a wide distribution of cell size was present in the experiment, which may explain the heterogeneity obsreved in the data.

Further, linear correlation coefficient analysis (MATLAB) revealed that the alterations in the inter-event intervals as a function of g_{NS} strongly correlates with changes in the cytosolic Ca^{2+} content and RMP as expected (Figure 3.8A,B). Also,

there is a correlation between event duration and RMP (Figure 3.8C). However, my findings show that there is no strong and consistent correlation between event duration and $[Ca^{2+}]_i$ (Figure 3.8D). Thus, the impact that the event duration has on $[Ca^{2+}]_i$ as a function of g_{NS} is random and secondary to the effect of inter-event interval on RMP and $[Ca^{2+}]_i$, as a function of g_{NS}.

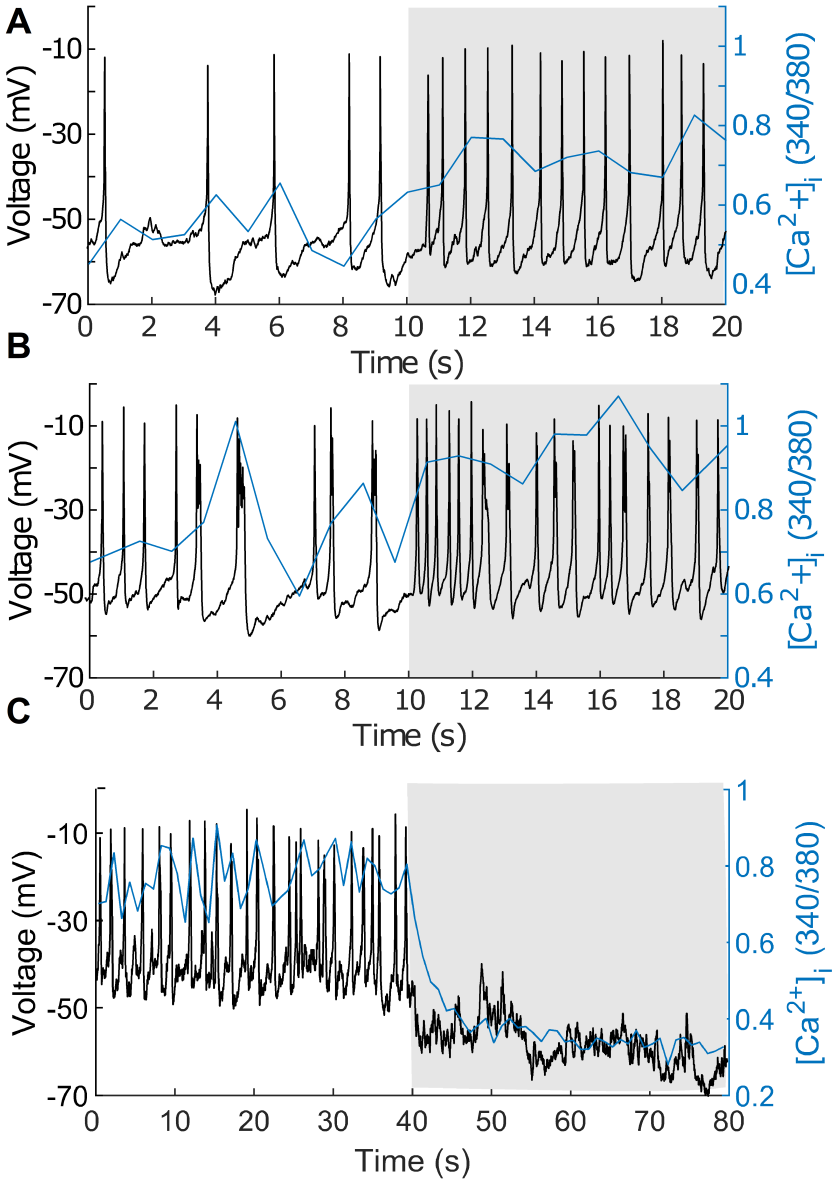

Figure 3.6: Representative traces demonstrating increasing the Na^+ leak conductance (g_{NS}) by very small amounts stimulates electrical activity and Ca^{2+} influx substantially in GH4 cells.
Examples of simultaneous recording of electrical activity and $[Ca^{2+}]_i$. **A)** The grey area indicates the addition of 0.04 nS g_{NS} to a cell which predominantly produces spikes (spiker). **B)** Addition of 0.04 nS g_{NS} to a cell that mainly generates bursts (burster). **C)** Subtraction of 0.04 nS (g_{NS} from a GH4 cell entirely abolished firing and $[Ca^{2+}]_i$ activity and hyperpolarised the cell drastically.

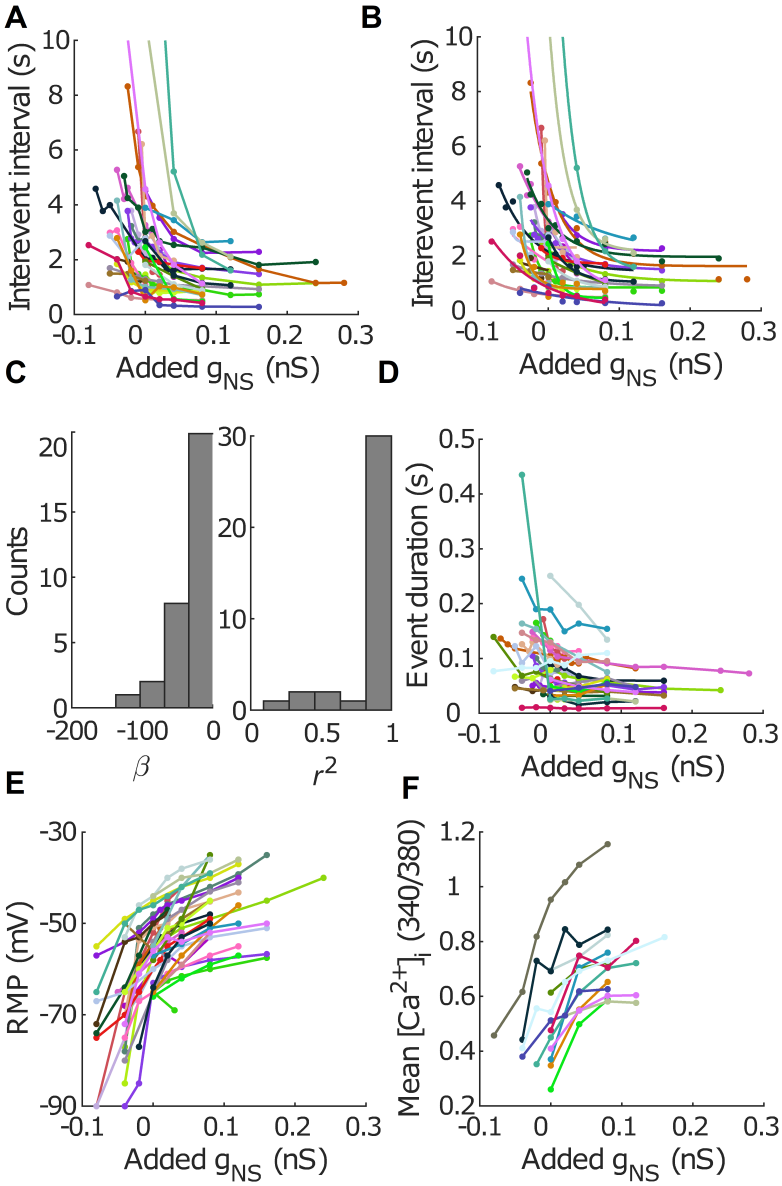

Figure 3.7: Quantitative analysis demonstrating increasing the Na^+ leak conductance (g_{NS}) by very small amounts stimulates electrical activity and Ca^{2+} influx substantially in GH4 cells.
A) Alterations in g_{NS} ranging from -0.1 to 0.12 results in significant changes in the frequency of electrical events in GH4 cells (the bigger the inter-event interval the lower the frequency). Values of g_{NS} above 0.12 nS did not induce further changes in the firing frequency. In contrast, reducing the g_{NS} by more than -0.04 nS (e.g. -0.05 nS) entirely abolished the firing activity and hyperpolarised the cells drastically. Some data (n=3) on the Y axis rise significantly above the Y limit of 10 s but have not been shown in the figure. The Y limit of 10 s was selected to better demonstrate the data trend in the lower values. **B)** The data points corresponding to each single cell are fitted to a one-term exponential model of the form $y = ae^{\beta x} + c$. This statistical approach takes into account the inter-individual heterogeneity amongst GH4 cells (discussed in more detail in Materials and Methods, statistics, section 2.6.1). **C)** Distribution of the decay constants (β) of the exponential fits indicates a decreasing trend of inter-event intervals as a function of g_{NS} ($p < 0.001, n = 36$). Distribution of r-squared values (r^2) for each fit, indicating excellent exponential fit. **D)** The increase in g_{NS} reduces the event duration and vice versa noticeably ($p < 0.01, n = 36$, exponential fitting function). **E)** The small alterations in the g_{NS} markedly changed the resting membrane potential ($p < 0.001, n = 36$, exponential fitting function). **F)** In a subset of recorded GH4 cells, the $[Ca^{2+}]_i$ was simultaneously monitored as g_{NS} was changed ($p < 0.001, n = 11$, exponential fitting function).

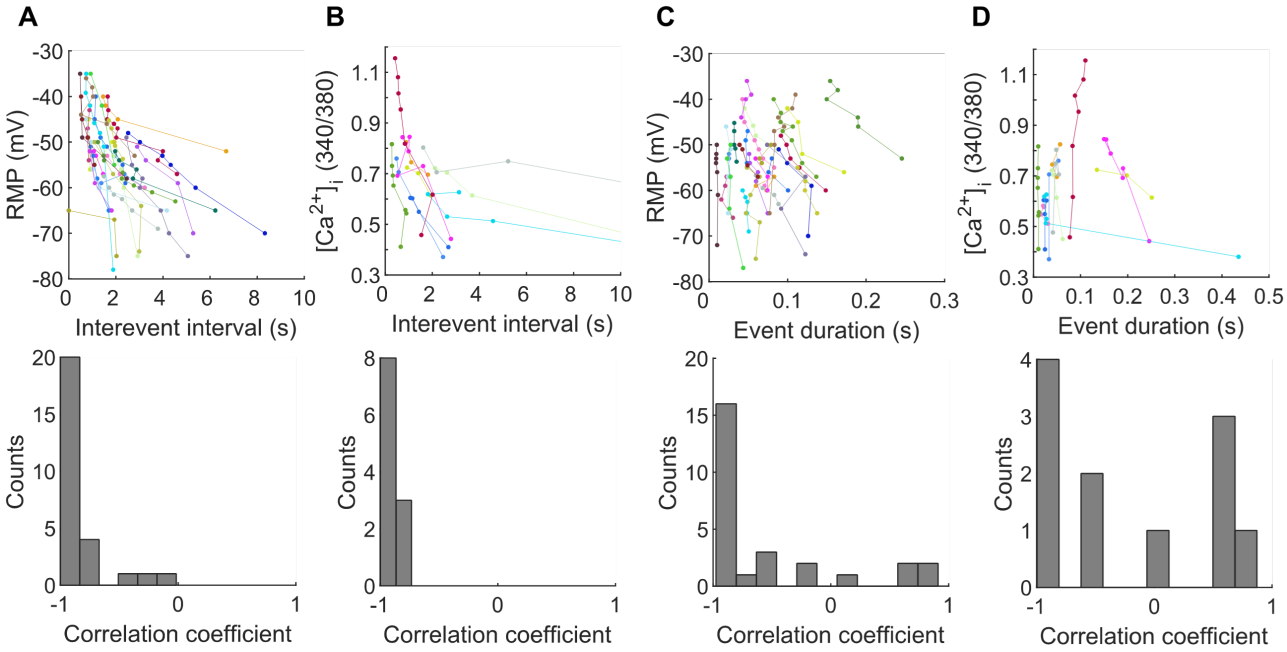

Figure 3.8: Linear correlation coefficient analysis.
A,B) There are strong correlations between the changes in inter-event interval and RMP as well as $[Ca^{2+}]_i$. In A,B bottom panels, the distribution of the correlation coefficient values are skewed towards -1 which means there is a strong and opposite correlation between inter-event interval and RMP, and inter-event interval and $[Ca^{2+}]_i$. **C)** There is also a correlation between changes in event duration and RMP in the majority of the cells. **D)** The distribution of correlation coefficient values are sporadic indicating no strong and consistent correlation between event duration and $[Ca^{2+}]_i$. The bottom panels are histogram distributions of the correlation coefficient values.

Murine primary pituitary cells

After evaluating how the Na^+ leak conductance affects the pattern of electrical activity and $[Ca^{2+}]_i$ of GH4 cells, I next investigated whether the role of Na^+ leak channels could be extended to primary endocrine pituitary cells (Figure 3.9 & 3.10). My results showed that primary pituitary cells are even more sensitive to small variations in g_{NS} than GH4 cells. Indeed increasing the g_{NS} by only 0.02 to 0.04 nS could significantly reduce inter-event interval ($p < 0.001$, exponential fitting function followed by sign rank test, n=16, Figure 3.10A-C). This also increased RMP ($p < 0.001, n = 17$, exponential fitting function, Figure 3.10E) and $[Ca^{2+}]_i$ ($p < 0.01, n = 11$, linear fitting function, Figure 3.10F). Further increase in g_{NS} by 0.08 nS and above resulted in depolarisation block in the majority of pituitary cells (14 out of 16 cells, Figure 3.9C, 3.10E). In contrast, subtracting g_{NS} by -0.02 to -0.04 nS considerably increased the inter-event interval ($p < 0.001, n = 16$), RMP ($p < 0.001, n = 17$) and $[Ca^{2+}]_i$ in pituitary cells ($p < 0.01, n = 11$). Similarly to what was observed in GH4 cells, subtracting g_{NS} by -0.04 nS or more entirely abolished the firing activity in 14 out of 16 recorded pituitary cells, and hyperpolarised the RMP substantially (Figure 3.9D, 3.10E).

The increase in g_{NS} tends to decrease event duration in pituitary cells ($p = 0.04, n = 16$, Figure 3.10D, linear fitting function). Of note, 14 of 16 recorded cells were bursters with burstiness factor higher than 70% (Figure 3.18B). The mean capacitance of patched murine pituitary cells was 4.5 pF with a range between 4 and 6 pF and a standard deviation of 1.7. The majority of isolated murine pituitary cells in my preparation were visually of medium size.

Consistent with my findings in GH4 cells, linear correlation coefficient analysis in pituitary cells (Figure 3.11) revealed that the alterations in the inter-event intervals as a function of g_{NS} strongly correlates with changes in the cytosolic Ca^{2+} content and RMP (Figure 3.11 A,B). Moreover, there is a correlation between event duration and RMP (Figure 3.11C). Although the n number for correlation between event duration and $[Ca^{2+}]_i$ is not high enough to deduce a reliable conclusion, the available data (Figure 3.11D) suggests that there is a consistent linear correlation between them.

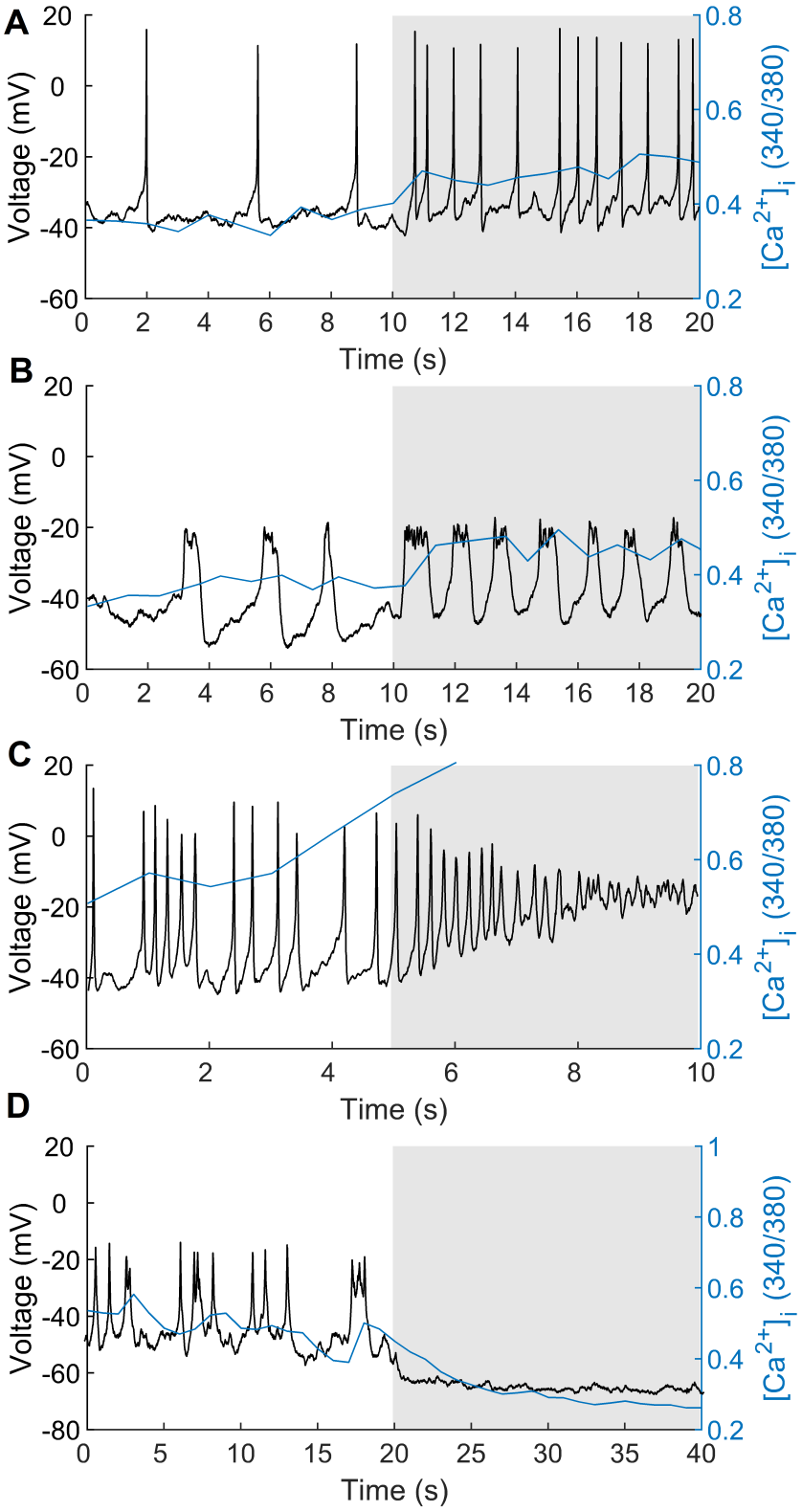

Figure 3.9: Representative traces demonstrating increasing the Na^+ leak conductance (g_{NS}) by very small amounts, stimulates electrical activity and Ca^{2+} influx substantially in primary pituitary cells.
Examples of simultaneous recording of electrical activity and Ca^{2+} influx. **A)** The grey area indicates the addition of 0.04 nS g_{NS} to a cell which predominantly produces spikes.**B)** The addition of 0.04 nS g_{NS} to a cell that mainly generates bursts. **C)** Values of g_{NS} above 0.08 nS did not induce further changes in the firing frequency, and led to depolarisation block. Calcium trace rose significantly above the right Y limit of 0.08 but have not been shown in the figure. The limit of 0.08 was selected to better demonstrate the data trend in the lower values **D)** In contrast, reducing g_{NS} by more than -0.04 nS entirely abolished electrical activity and $[Ca^{2+}]_i$.

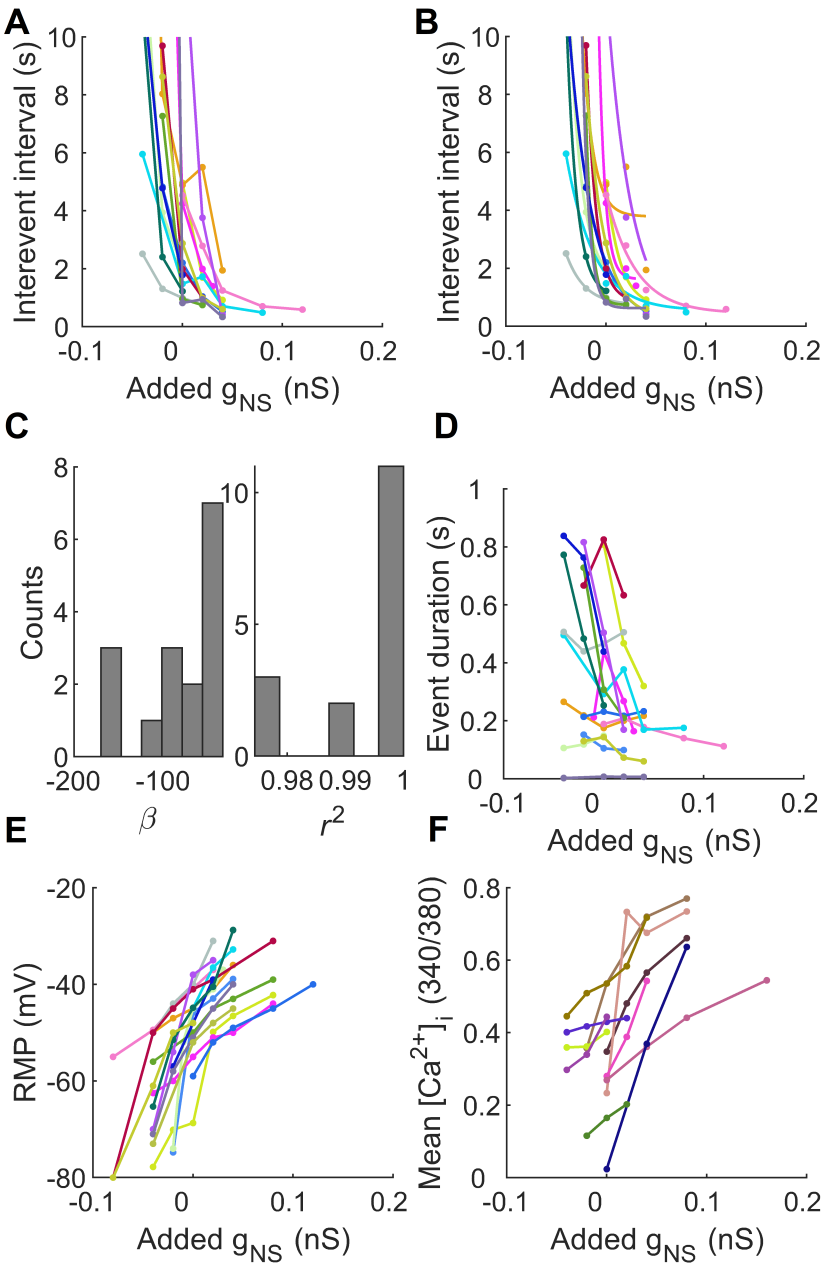

Figure 3.10: Quantitative analysis demonstrating increasing the Na^+ leak conductance (g_{NS}) by very small amounts, stimulates electrical activity and Ca^{2+} influx substantially in primary pituitary cells.
A) Alterations in g_{NS} ranging from -0.08 to 0.12 nS results in significant changes in the frequency of electrical events in pituitary cells.Some data (n=7) on the Y axis rise significantly above the Y limit of 10 s but have not been shown in the figure. The Y limit of 10 s was selected to better demonstrate the data trend in the lower values. **B)** The data points corresponding to each single cell are fitted to a one-term exponential model of the form $y = ae^{\beta x} + c$. **C)** Distribution of the decay constants (β) of the exponential fits indicates a decreasing trend of inter-event intervals as a function of g_{NS} ($p < 0.001, n = 16$). Distribution of r-squared values (r^2) for each fit, indicating excellent exponential fits. **D)** An increase in g_{NS} tends to reduce event duration and vice versa ($p = 0.04, n = 16$, exponential fitting function). **E)** Small alterations in g_{NS} markedly changed the resting membrane potential ($p < 0.001, n = 17$, exponential fitting function). **F)** In a subset of recorded pituitary cells, $[Ca^{2+}]_i$ was simultaneously monitored as g_{NS} was changed. $[Ca^{2+}]_i$ rises significantly as g_{NS} increases by small amounts ($p < 0.01, n = 11$, linear fitting function).

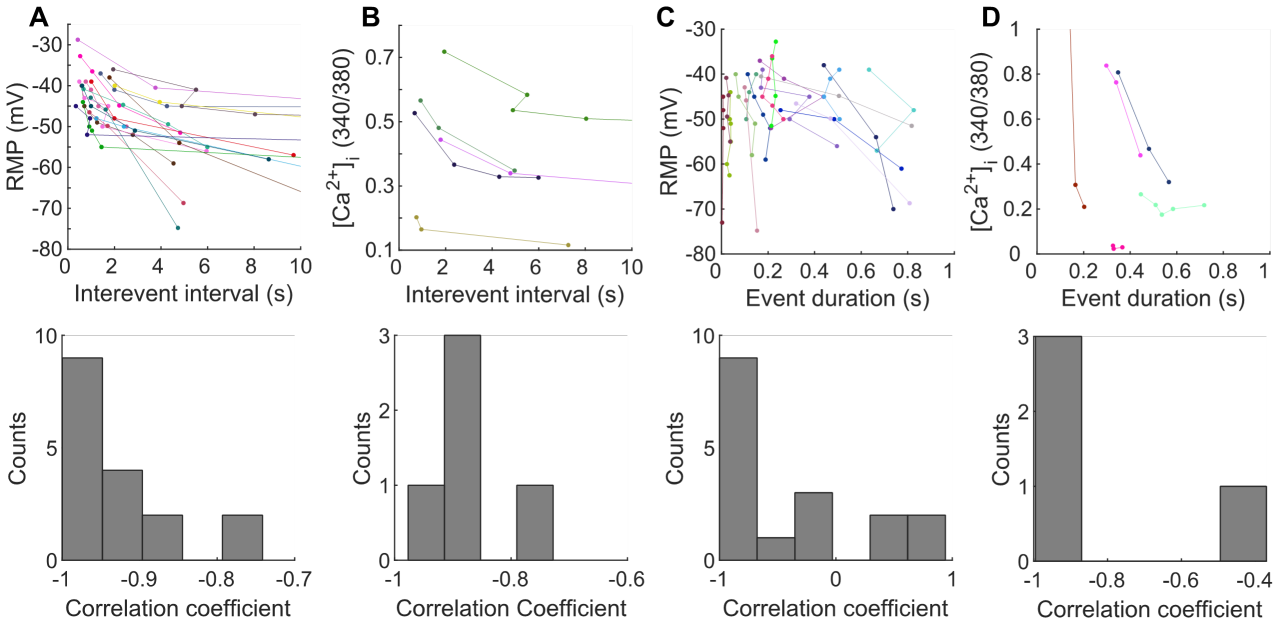

Figure 3.11: Linear correlation coefficient analysis.
A&B) There is a strong correlation between the changes in inter-event intervals and RMP as well as $[Ca^{2+}]_i$.**C)** There is a correlation between event duration and RMP in more than half of the cells. **D)** The histogram shows that there is also a linear correlation between event duration and $[Ca^{2+}]_i$ in these recorded cell.

3.2.6 Minute alterations in background K^+ conductance significantly affect electrical and $[Ca^{2+}]_i$ activity in GH4 and primary pituitary cells

The mathematical expression for the current flowing through K^+ leak channels I_K=g_K $(V_m - E_k)$ was used to inject a K^+ leak conductance through dynamic clamp. In this way, I could evaluate how alterations in the K^+ leak conductance (g_K) determine the pattern of electrical activity and $[Ca^{2+}]_i$ in GH4 cells and in primary pituitary cells.

GH4 cells

Increasing the g_K by 0.02 to 0.12 nS substantially increased the inter-event intervals in GH4 cells ($p < 0.001$, exponential fitting function followed by sign rank test, n=33, Figure 3.12 & 3.13A-C). Additionally, it decreased the resting membrane potential (p < 0.001 n=33, Figure 3.13E), and $[Ca^{2+}]_i$ significantly ($p < 0.001, n = 6$, Figure 3.13F). In 22 out of 33 cells, the addition of 0.08 nS g_K or above, entirely stopped firing activity and hyperpolarised the cells noticeably (Figure 3.12C). In contrast, subtracting g_K by -0.02 to -0.24 nS, markedly increased firing frequency, resting membrane potential and $[Ca^{2+}]_i$. In 21 out of 33 cells, subtracting g_K by -0.16 nS or above resulted in depolarisation block (Figure 3.12D). However, my results demonstrated that changing g_K does not affect the event duration in GH4 cells (p> 0.05, n=33, 3.13D). Of note, 27 out of 33 cells predominantly produced bursts with bf> 80% (Figure 3.18C).

Moreover, linear correlation coefficient analysis revealed that the changes in the inter-event intervals as a function of g_K strongly correlates with changes in the cytosolic Ca^{2+} content and RMP (Figure 3.14 A,B). However, my findings show that there is no strong and consistent correlation between event duration and $[Ca^{2+}]_i$, or RMP (Figure 3.14 C,D).

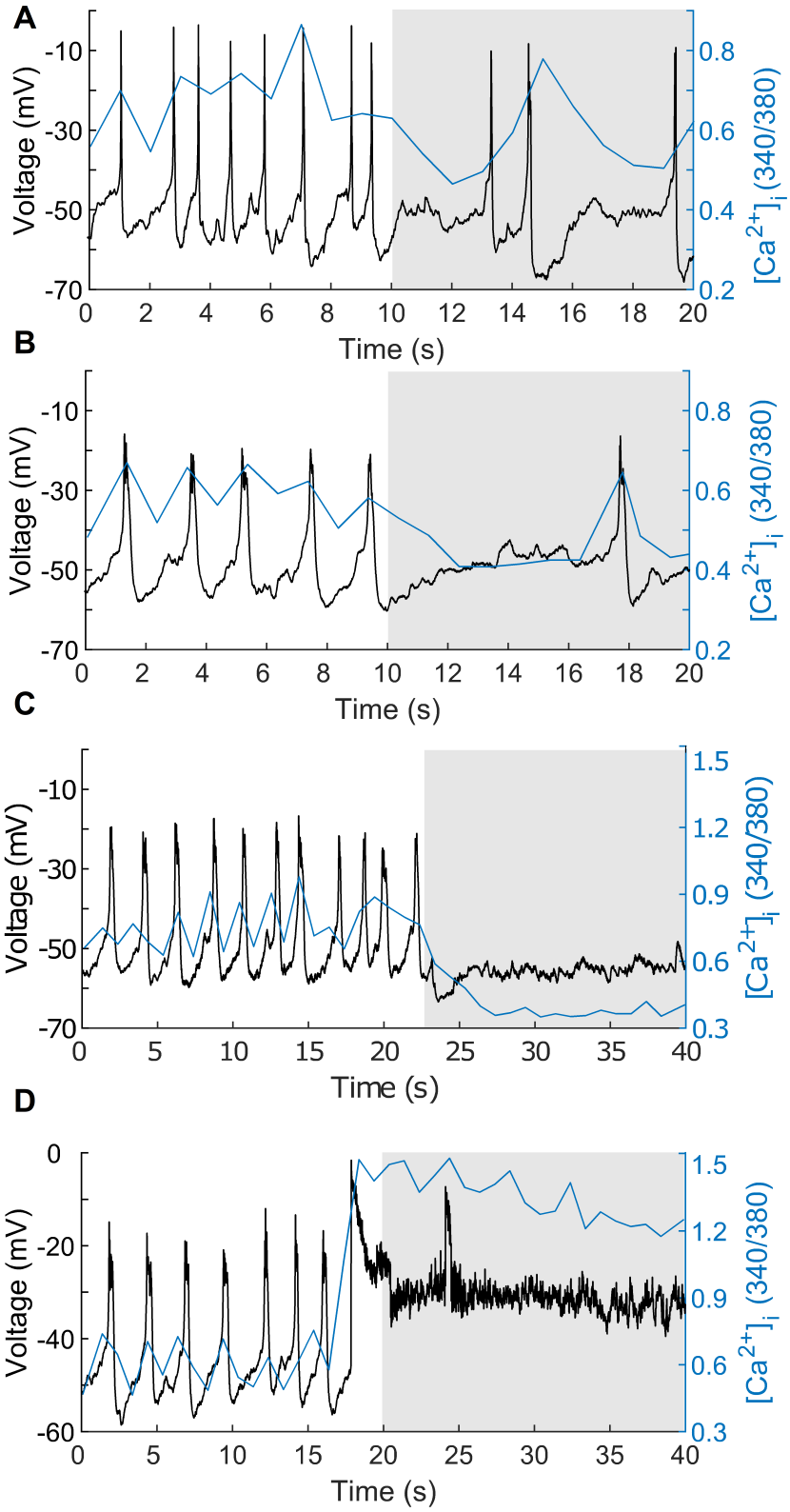

Figure 3.12: Representative traces demonstrating increasing the K^+ leak conductance (g_K) by very small amounts supresses electrical activity and Ca^{2+} influx substantially in GH4 cells.
Examples of simultaneous recording of electrical activity and $[Ca^{2+}]_i$. **A)** The grey area indicates the addition of 0.04 nS g_K to a cell which predominantly produces spikes. **B)** The addition of 0.04 nS g_K to a cell that mainly generates bursts. **C)** Values of g_K above 0.08 nS silenced the cells, and led to the hyperpolarisation. **D)** In contrast, reducing the g_K by more than -0.16 nS resulted in depolarisation block.

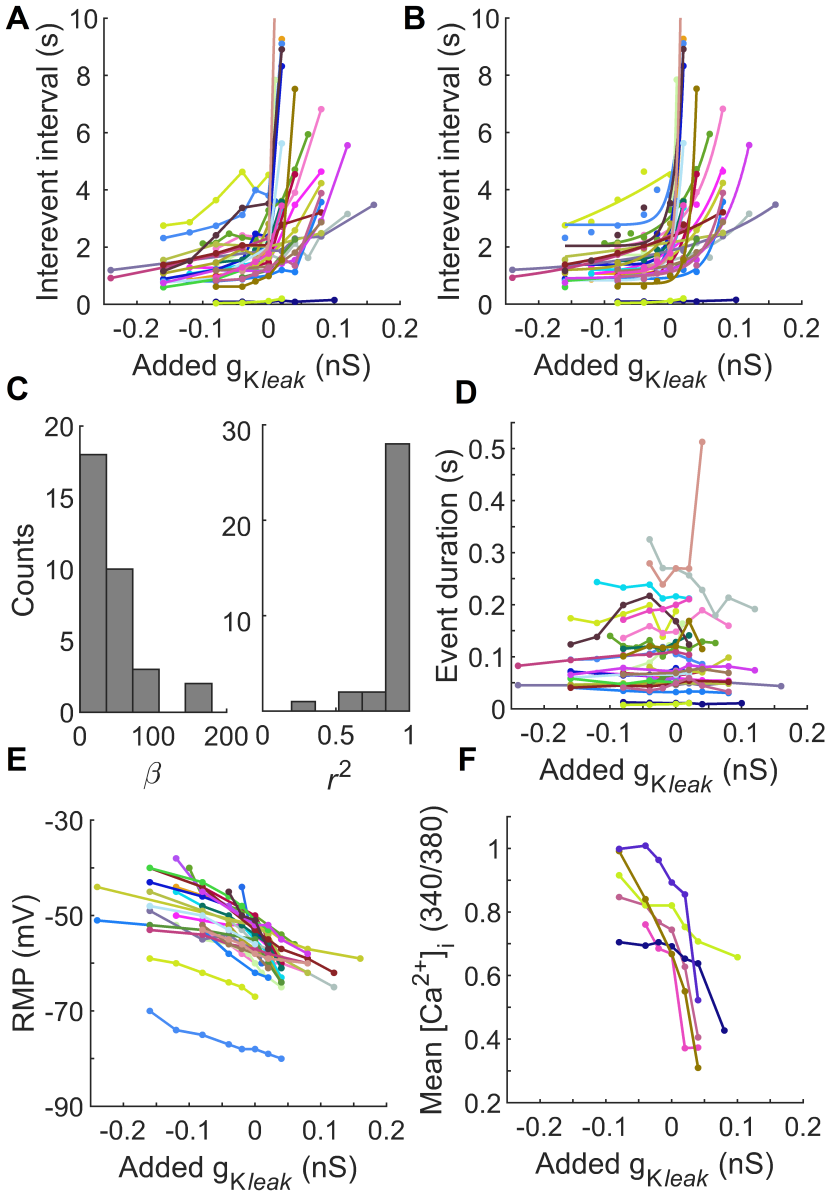

Figure 3.13: Quantitative analysis demonstrating increasing the K^+ leak conductance (g_K) by very small amounts supresses electrical activity and Ca^{2+} influx substantially in GH4 cells.
A) Alterations in g_K ranging from 0.12 to -0.24 nS results in significant changes in the firing frequency of GH4 cells. **B)** The data points corresponding to each single cell are fitted to a one-term exponential model of the form $y = ae^{\beta x} + c$. **C)** Distribution of the decay constants (β) of the exponential fits indicates an increasing trend of inter-event intervals as a function of g_K (p <0.001, sign rank, n=33). Distribution of r-squared values (r^2) for each fit, indicating excellent exponential fits. **D)** The changes in g_K did not affect the event duration ($p > 0.05$, n=33, linear fitting function). **E)** The small alterations in the g_K markedly changed the resting membrane potential (p <0.01, n=33, linear fitting function). **F)** In a subset of recorded GH4 cells, the $[Ca^{2+}]_i$ was simultaneously monitored as g_K was changed (p <0.001, n=6, linear fitting function).

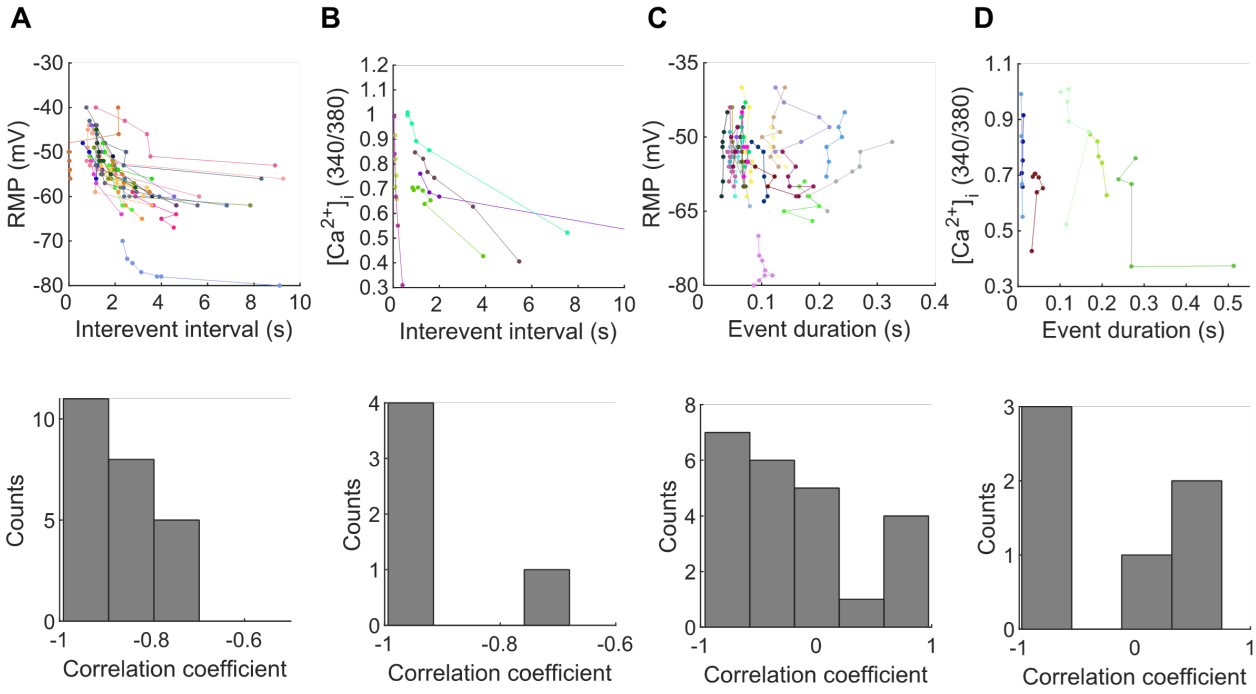

Figure 3.14: Linear correlation coefficient analysis.
A&B) There is a strong correlation between the changes in inter-event intervals and RMP as well as $[Ca^{2+}]_i$ as a function of g_K. **C&D)** There is no consistent correlation between event duration and RMP or $[Ca^{2+}]_i$ as function of g_K in GH4 cells.

Murine primary pituitary cells

I then examined whether my findings with GH4 cells could be extendable to primary pituitary cells. Similarly to what was observed in GH4 cells, increasing g_K by 0.02 to 0.08 nS substantially increased inter-event interval in primary pituitary cells ($p < 0.001$, exponential fitting function followed by sign rank test, $n = 20$, Figure 3.15 & 3.16A-C). Further, it decreased the resting membrane potential ($p < 0.001, n = 20$, linear fitting function, Figure 3.16E), and $[Ca^{2+}]_i$ significantly ($p < 0.001, n = 12$, linear fitting function, Figure 3.16F). In 18 out of 20 cells, the addition of 0.04 nS g_K or above entirely stopped the firing activity and hyperpolarised the cells significantly (Figure 3.15C). In contrast, subtracting g_K by -0.02 to -0.08 nS markedly increased firing frequency, resting membrane potential and $[Ca^{2+}]_i$. In 19 out of 20 cells, subtracting g_K by -0.08 nS or above resulted in depolarisation block and loss of seal. However, consistent with what was observed in GH4 cells, changing g_K did not affect event duration in primary pituitary cells ($p > 0.05, n = 20$, linear fitting function, Figure 3.16D). Of note, 12 out of 20 cells predominantly produced bursts

with bf> 80% (Figure 3.18D). These results indicate that background K^+ leak and Na^+ leak conductances have an opposite effect on the electrical and $[Ca^{2+}]_i$ activity of primary pituitary cells and GH4 cells.

The mean of slopes (absolute values) of the linear regression fitted to the data points of g_{NS}-RMP and g_K-RMP were 148.5 and 87.3 respectively for GH4 cells (r^2 of the fits: 0.86 and 0.96 respectively). The corresponding values in primary pituitary cells were 230.8 vs 129.3 (r^2 of the fits: 0.92 and 0.91 respectively). Hence, Na^+ leak conductance has a much stronger impact on resting membrane potential than K^+ leak conductance.

Linear correlation coefficient analysis revealed that the changes in inter-event interval as a function of g_K strongly correlate with changes in the cytosolic Ca^{2+} content and RMP (Figure 3.17 A,B). However, there is no strong and consistent correlation between event duration and $[Ca^{2+}]_i$, or RMP (Figure 3.17 C,D).

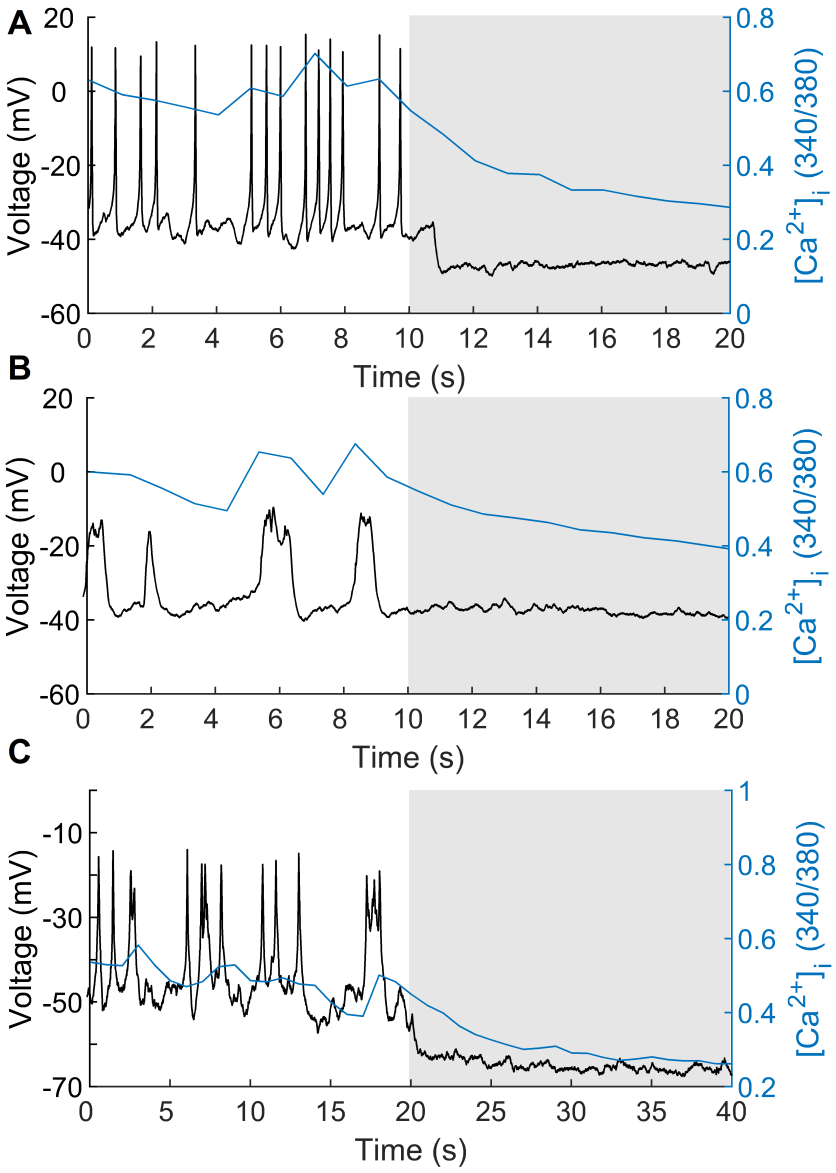

Figure 3.15: Representative traces demonstrating slight increases of the K^+ leak conductance g_K, supress electrical activity and Ca^{2+} influx substantially in murine primary pituitary cells.
Examples of simultaneous recording of electrical activity and $[Ca^{2+}]_i$. **A)** The grey area indicates the addition of 0.04 nS g_K to a cell which predominantly produces spikes. **B)** The addition of 0.04 nS g_K to a cell that mainly generates bursts. **C)** Values of g_K above 0.04 nS (e.g. 0.06) silenced the majority of cells, and led to hyperpolarisation of Vm. In contrast, reducing the g_K by more than -0.08 nS resulted in depolarisation block (due to the substantial depolarisation, the seal was lost and the recording was discontinued).

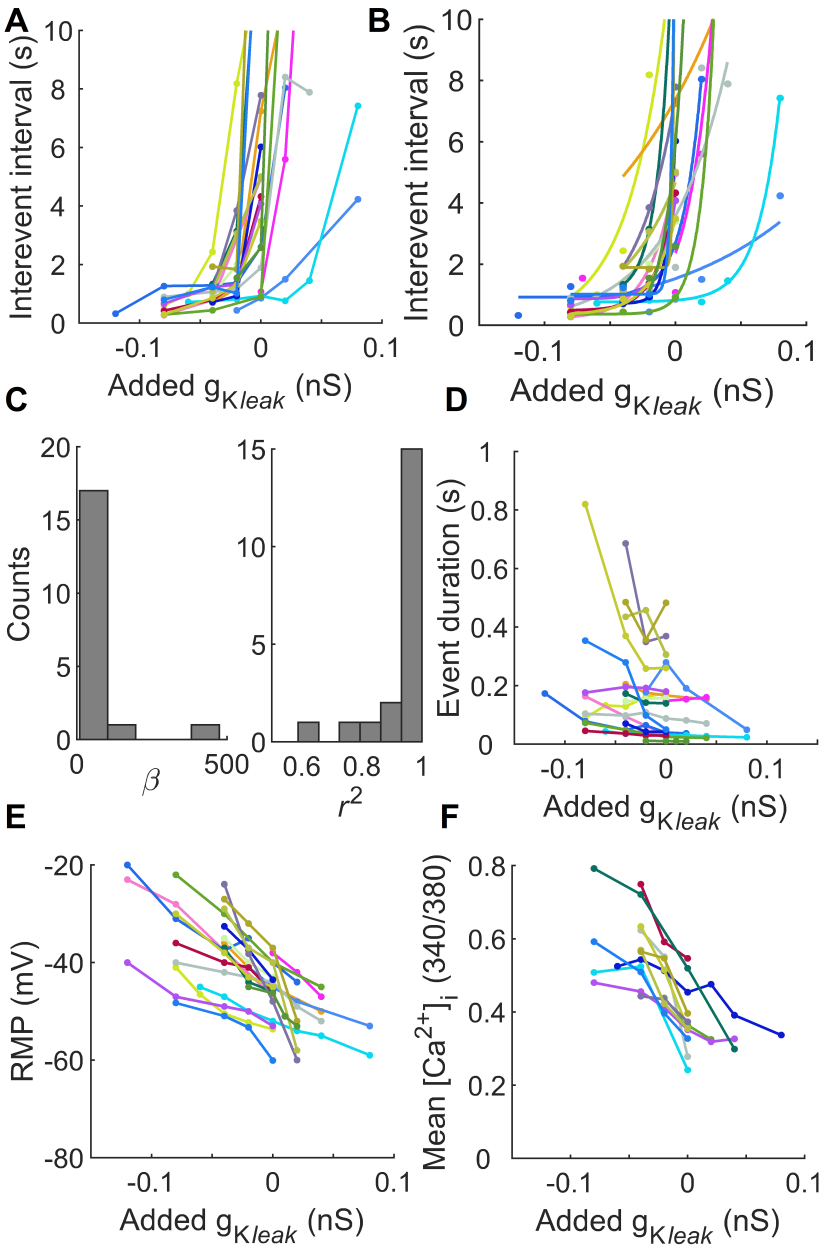

Figure 3.16: Quantitative analysis demonstrating slight increases of the K^+ leak conductance g_K, supress electrical activity and Ca^{2+} influx substantially in murine primary pituitary cells.
A) Alterations in g_K ranging from 0.08 to -0.08 nS result in significant changes in the firing frequency of pituitary cells. **B)** The data points corresponding to each single cell are fit to a one-term exponential model of the form $y = ae^{\beta x} + c$. **C)** Distribution of the decay constants (β) of the exponential fits indicates an increasing trend of inter-event intervals as a function of g_K ($p < 0.001$, sign rank, $n = 20$). Distribution of r-squared values (r^2) for each fit, indicating excellent exponential fits. **D)** The changes in g_K did not affect the event duration significantly ($p > 0.05, n = 20$, linear fitting function). **E)** The small alterations in g_K markedly changed the resting membrane potential ($p < 0.01, n = 20$, linear fitting function). **F)** In a subset of recorded pituitary cells, $[Ca^{2+}]_i$ was simultaneously monitored as g_K was changed ($p < 0.01, n = 12$, linear fitting function).

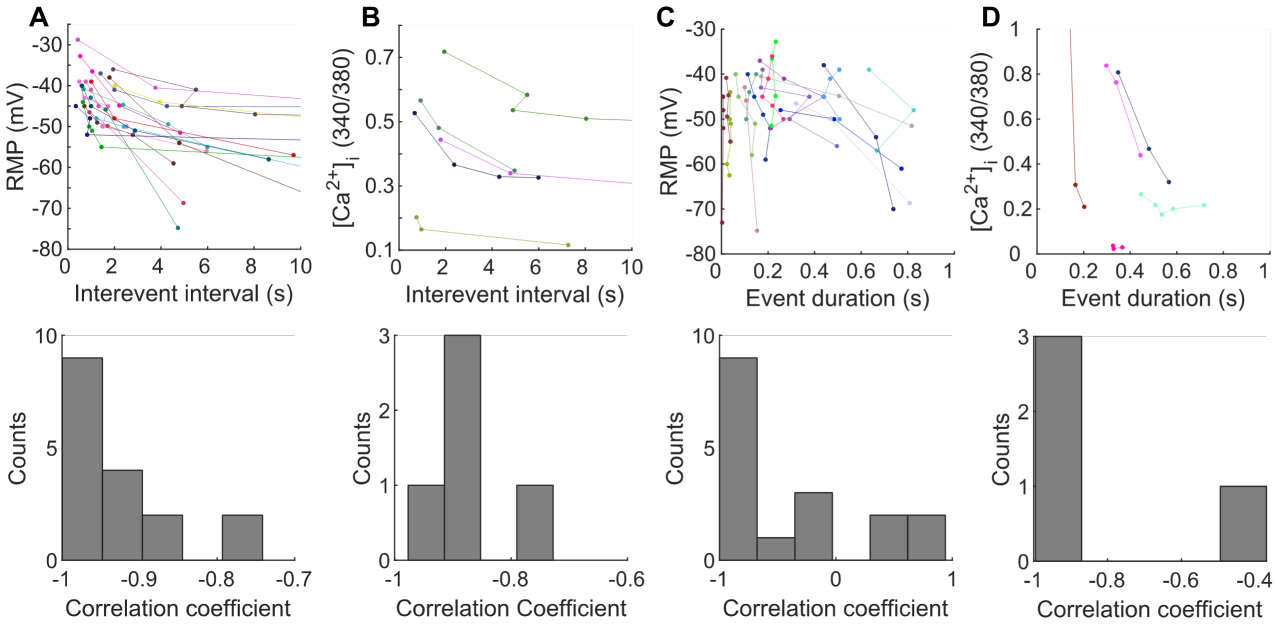

Figure 3.17: Linear correlation coefficient analysis.
A&B) There is a strong correlation between the changes in inter-event intervals and RMP as well as $[Ca^{2+}]_i$.**C)** There is a correlation between event duration and RMP in more than half of the cells. **D)** The histogram shows that there is also a linear correlation between event duration and $[Ca^{2+}]_i$ in these recorded cell.

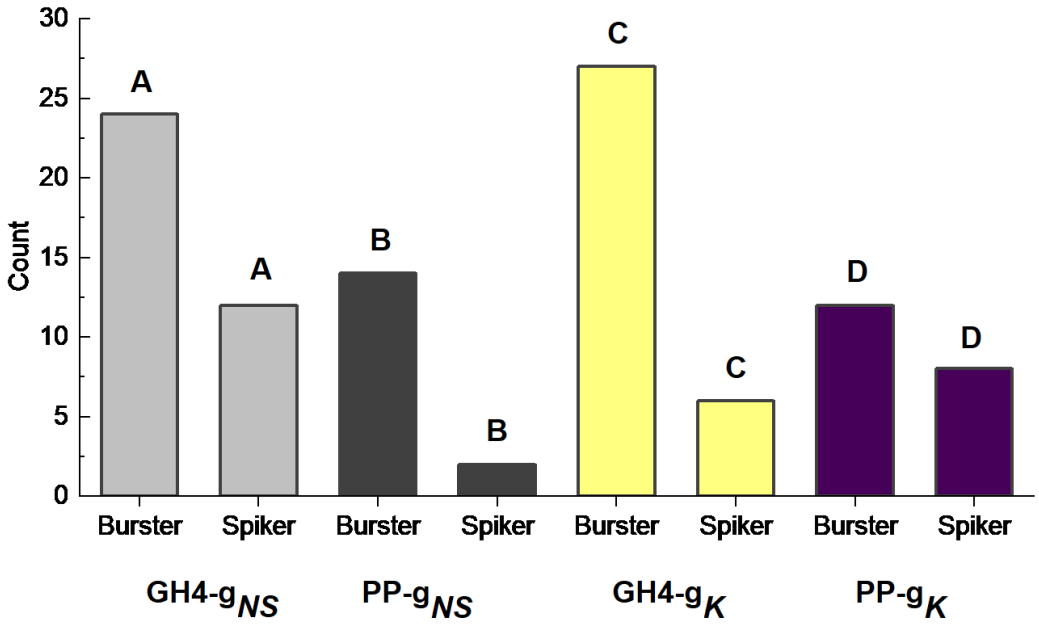

Figure 3.18: Proportion of spikers versus bursters present in the experiment.
The number of bursters vs. the number of spikers in each set of experiment with dynamic clamp is shown. **A)** 24 of 36 recorded GH4 cells for evaluating the effect of g_{NS} on electrical activity, predominantly produced bursts with burstiness factor above 80% (bf $>$ 80%). **B)**14 of 16 recorded primary pituitary (PP) cells for evaluating the effect of g_{NS} on electrical activity, were bursters with burstiness factor higher than 70%. **C)** 27 out of 33 recorded GH4 cells for evaluating the effect of g_K on electrical activity predominantly produced bursts with bf$>$ 80%. **D)** 12 out of 20 recorded primary pituitary cells (PP) cells predominantly produced bursts with bf$>$ 80%.

3.3 Discussion

Using dynamic clamp it has been shown in the present study that very minute alterations in the conductance of Na^+ and K^+ leak channels result in substantial changes in the pattern of electrical activity and $[Ca^{2+}]_i$ in pituitary cells. Increasing the conductance of Na^+ leak channels mediates Na^+ influx leading to the depolarisation of the membrane potential, which in turn increases the excitability of pituitary cells. In contrast, increasing the conductance of K^+ leak channels facilitates K^+ efflux, which hyperpolarises the membrane and consequently reduces the excitability of pituitary cells. Taken together, the results show that endocrine anterior pituitary cells are extremely sensitive to slight changes in Na^+ and K^+ leak conductances. Moreover, both Na^+ and K^+ leak conductances contribute to acutely tuning of the resting membrane potential and consequently the frequency of electrical events in these cells. However, the changes in Na^+ leak conductance have a stronger effect on RMP than the changes in K^+ leak conductance. The median value of decay constants for changes in RMP as a function of Na^+ leak conductance is larger by approximately 4.5 folds compared with that of the K^+ leak conductance (11.7 vs 2.4 for GH4 cells, 8.5 vs 2.1 for primary pituitary cells). Additionally, the comparison between the slopes showed that Na^+ leak conductance has a much stronger impact on resting membrane potential than K^+ leak conductance. This is because the reversal potential of Na^+ (+60 mV) is far away from the RMP of pituitary cells (between -55 to -45 mV) which leads to a high depolarising driving force for Na^+. However, the reversal potential of K^+ (-85 mV) is closer to the RMP of pituitary cells, and thus its driving force is weaker than Na^+. This, therefore, endows the Na^+ leak conductance the capability to significantly adjust the RMP and regulate cell excitability. Excitability relies on the resting membrane potential, since action potentials fire once the membrane potential reaches a threshold where voltage-sensitive ion channels open and successively go to inactivation mode. To regenerate action potentials, the voltage-sensitive ion channels must recover from inactivation *via* reaching a negative voltage below the activation threshold and that is the resting membrane potential. Despite the wide heterogeneity observed in the pattern of electrical activity between and within each pituitary cell type, the effect of changes of leak conductances on the

firing frequency, RMP and $[Ca^{2+}]_i$ is consistent and reliable across all recorded cells.

According to the present results, murine primary pituitary cells are more sensitive to changes in leak conductances than GH4 cells. This might be due to the fact that a larger range of cell capacitance in GH4 cells was present compared to that in murine pituitary cells (GH4 cells: median: 5.5 pF, and a range between 4 and 10 pF vs murine pituitary cells: mean: 4.5 pF, with a range between 4 and 6 pF and a standard deviation of 1.7).

Further, the present results showed that the alterations in Na^+ leak conductance lead to changes in the event duration whereas the alterations in K^+ leak conductance have no effect on the event duration. As g_{NS} increases, event duration decreases (for bursts, not spikes). This is a consequence of the decreased inter-burst interval at higher g_{NS} values leading to an enhanced $[Ca^{2+}]_i$ at the beginning of each burst, which in turn terminates bursts quicker *via* activation of slow activated Ca^{2+}- and voltage-gated K^+ channels. By increasing g_K the opposite effect is expected to happen, which means the inter-burst interval is increased leading to a reduced $[Ca^{2+}]_i$ at the beginning of each burst. Hence, it is also expected that the bursts terminate more slowly and thus would have a longer duration. However the burst duration remains unaffected. This may be because when an electrical event reaches its peak amplitude (which normally ranges between -20 to 0 mV), the membrane potential moves further away from the E_K (e.g. equilibrium potential for $K^+ \approx -85$ mV) and thus the K^+ driving force increases. As a result, more hyperpolarising currents are injected into the cells leading to the quick termination of an electrical event. Therefore, the event duration does not change in response to the changes in K^+ leak conductance and there is minimal changes in burst duration. One way to test if g_{NS} or g_K has impact on burst duration would be by blocking BK channels which are responsible for generating burst in pituitary cells (Tabak et al, 2011), and then altering g_{NS} or g_K to investigate if that changes the duration of electrical events.

Recording leak currents from cells of a small size, which have a high input resistance, is difficult, because the ratio of signal to noise is small. Of note, the input resistance of pituitary cells ranges between 3 to 10 GΩ which is similar to the resistance of a gigaohm seal, and thus small vibrations or movements of the electrode tip

may result in introducing some small currents (e.g. few pico amperes) acting like leak currents. Accordingly, it is not feasible to reliably measure how much of leak conductance change is required in response to stimulatory or inhibitory hypothalamic factors in order to create a significant change in the firing rate and $[Ca^{2+}]_i$ oscillations. I attempted to measure changes in g_{NS} in response to hypothalamic factor TRH by blocking all the voltage gated channels as well as K^+ leak channels (using 1 μM Nimodipine, 1 μM TTX, 10 mM TEA-Cl, 2 mM $CsCl_2$, 12 nM Erg-toxin and 2.5 μM T-type calcium channel blocker TTA-A2) in GH4 cells to isolate Na^+ leak current. However, leak current recording under this condition is very noisy and unstable leading to variable and unreproducible results. This random noise could be due to small and stochastic variations in g_{NS} and g_K. Hence, this precluded measuring very small changes in Na^+ leak current and subsequently g_{NS} in response to TRH reliably. Using dynamic clamp, I was able to change the leak conductance precisely by any amount and investigate how that will impact the physiology of the pituitary cells in real time. My observations clearly demonstrated that pituitary cells are extremely sensitive to very small alterations in the leak conductances and very minute changes of these conductances is sufficient to trigger substantial response in cells physiology.

Kucka et al. (2010) demonstrated the effects of partial and complete replacement of bath Na^+ with N-methyl-D-glucamine ($NMDG^+$) on pituitary cell excitability. Indeed, the membrane potential was hyperpolarised and subsequently impacted the pattern of electrical activity in all types of anterior endocrine pituitary cells. They reported that, complete replacement of bath Na^+ with $NMDG^+$ hyperpolarised the membrane potential close to the reversal potential of potassium (-85 mV) and totally prevented the firing activity and the associated Ca^{2+} influx from occurring. However, a steady increase in bath Na^+ concentration depolarised the cell membrane gradually and had a concentration-dependent effect on the hyperpolarisation level (Kucka et al, 2010). My results are consistent with the findings of Kucka et al. (2010) in showing that alterations in the conductance of background Na^+ channels can greatly alter the excitability of pituitary cells.

Several studies have reported that stimulatory hypothalamic neurohormones such

as CRH (Liang et al, 2011; Zemkova et al, 2016) and GHRH (Kato et al, 1988) enhance Na^+ leak conductance leading to an increase in voltage-gated-calcium-current and consequently pituitary cell excitability. Moreover, Kucka and colleagues (2010) reported that forskolin induced c-AMP efflux reduces significantly upon removal of extracellular Na^+ (Kucka et al, 2010). This suggests a crucial role for Na^+ leak conductance in elevating the resting membrane potential in response to stimulatory hypothalamic neurohormones, which leads to increasing the firing frequency and subsequently increasing Ca^{2+} influx, and $[Ca^{2+}]_i$ in turn mediates c-AMP production (Halls and Cooper, 2011). This further implies that the absence of Na^+ leak conductance maintains the resting membrane potential at hyperpolarised level away from the firing threshold leading to substantial reduction of Ca^{2+} influx. Since intracellular Ca^{2+} is one of the most important second messengers, this could lead to the interruption of a plethora of cellular mechanisms such as basal hormone secretion or refilling of the cytosolic Ca^{2+} stores. On the other hand, it was shown that inhibitory hypothalamic neurohormones such as somatostatin partially supress the Na^+ leak current in a cAMP/protein-kinase-A-dependent manner (Kato and Sakuma, 1997).

Although, it has been reported that stimulatory hypothalamic factors such as CRH and arginine vasopressin (AVP) may increase the resting membrane potential in murine corticotrophs by suppressing the background K^+ conductance such as TREK-1 (a Tandem of P-domains in a Weakly Inward rectifying K^+ channel related 1 like conductance), the levels of CRH and AVP used were supraphysiological (e.g. 100 nM, Lee et al, 2011; Lee et al, 2015).

Moreover, it is shown that inhibitory hypothalamic neurohormones such as somatostatin and dopamine reduce the cell input resistance and increase the G-protein coupled background K^+ conductance in somatotrophs and lactotrophs respectively, which results in rapid membrane hyperpolarisation and decline in voltage-gated-calcium-current (Sims et al, 1991; Einhorn et al, 1991). Of note, the somatostatin and dopamine concentration used in these experiments are not in physiological range (e.g. 4 μM and 100 nM respectively). The previous studies however, could not measure the amount of alterations in leak conductances required for the observed

physiological change in pituitary cells. This is due to the very small size and high input resistance of these cells making it difficult to reliably quantify the variations in the Na^+ leak conductance, and distinguish it from artificial noise. Using dynamic clamp, I could mimic the impact of stimulatory and inhibitory hypothalamic neurohormones on leak conductance by varying g_{NS} or g_K and evaluate how much change is required to substantially increase or decrease the cell excitability and Ca^{2+} influx. Consistent with previous experiments, my results highlight that both Na^+ and K^+ leak conductances likely play a key modulatory role in the up- and down-regulation of electrical activity and $[Ca^{2+}]_i$ in endocrine pituitary cells. Further, maintaining a balance between inward and outward positive currents can provide a pivotal mechanism for acutely adjusting the resting membrane potential.

key conclusion

Given that the very small alterations in Na^+ leak conductance is sufficient to significantly modulate the membrane potential in pituitary cells, Na^+ leak channel likely acts as an efficient target for hypothalamic factors to govern the pattern of electrical activity and eventually the pattern of hormone secretion in endocrine anterior pituitary cells. Despite the crucial role of Na^+ leak channels in pituitary cells, the molecular identity of this channel is not yet known. The next chapter will explore the molecular identity of the Na^+ leak channel and its biophysical properties in a mixed population of endocrine anterior pituitary cells.

Chapter 4

Molecular identity of the major sodium leak channel in endocrine anterior pituitary cells

4.1 Introduction

In vitro and under basal conditions, the majority of anterior endocrine pituitary cells, as well as derived cell lines, generate action potentials spontaneously which results in a rhythmic Ca^{2+} entry through voltage-gated calcium channels (Stojilkovic, 2012). The subsequent spontaneous $[Ca^{2+}]_i$ oscillations act as a second messenger and serves various physiological purposes in pituitary cells, such as triggering hormone secretion, maintaining calcium levels in the intracellular calcium stores, and regulating gene expression (reviewed in Mollard and Schlegel, 1996; Kwiecien and Hammond, 1998). Furthermore, hypothalamic stimulatory and inhibitory neurohormones can amplify or suppress this spontaneous firing, respectively. Spontaneous firing in pituitary cells such as somatotrophs and lactotrophs enables long-lasting $[Ca^{2+}]_i$ transients and thus continuous periods of hormone secretion, which stop in response to inhibitory hypothalamic neurohormones. In contrast, this spontaneous firing in cells such as gonadotrophs maintains the intracellular calcium stores in a readily-responsive state. Therefore, in response to stimulatory hypothalamic neurohormones, the intracellular stores release Ca^{2+} in pulses of high amplitude and short duration. This consequently triggers hormone secretion peaks of high amplitude and short duration (Kwiecien and Hammond, 1998; Fletcher et al, 2018). Silencing the spontaneous electrical activity in pituitary cells immediately abolishes the $[Ca^{2+}]_i$ oscillations and basal hormone secretion.

The ability to produce action potentials spontaneously is partly due to the depolarised resting membrane potential (oscillating between -65 to -50 mV), which is positive relative to the K^+ equilibrium potential. Replacing the extracellular Na^+ with large impermeable cations such as $NMDG^+$ immediately hyperpolarises the membrane potential close to the K^+ equilibrium potential ($\approx$ -85 mV), silences the firing activity and abolishes the $[Ca^{2+}]_i$ transients in all pituitary cells (Simasko, 1994; Sankaranarayan & Simasko, 1996; Kwiecien et al, 1998; Tsaneva-Atanasova et al, 2007; Kucka et al, 2010, 2012; Tomic et al, 2011; Liang et al, 2011; Zemkova et al, 2016; Kayano et al, 2019). This reflects the presence of a constitutively active inward depolarising current in pituitary cells that sets the membrane potential near to the firing threshold. Pharmacological investigation of this cationic leak current indicates that it is a TTX-insensitive, voltage-independent and constitutively active Na^+ conductance (reviewed in Fletcher et al, 2018).

While there are numerous studies about the molecular identity and biophysical properties of voltage-gated ion channels involved in depolarisation and repolarization of action potentials in pituitary cells (Stojilkovic et al, 2010), the molecular identity of the resting sodium conductance remains unknown. Although blocking HCN channels (hyperpolarisation- and nucleotide-activated Na^+ current) reduces the inward Na^+ current and consequently decreases the firing frequency in pituitary cells, it does not abolish the spontaneous firing in the same way that extracellular Na^+ removal does (Kretschmannova et al, 2012; Kucka et al 2012). Furthermore, the $[Ca^{2+}]_i$ transients are rescued by forskolin in the presence of 1 mM Cs^+, an HCN channel blocker (Tomić et al, 2011). Also, riluzole, a blocker of persistent Na^+ current generated by Na_vs does not abolish the spontaneous firing and $[Ca^{2+}]_i$ transients in pituitary cells (Tomić et al, 2011).

Overall, there is not any knock out or knock down study confirming the molecular identity of the Na^+ leak channel (or background Na^+ channel) in pituitary cells. A recent study has shown that the Na^+ leak channel NALCN is the main contributor to the background Na^+ conductance in somatolactotroph GH3 cells (Impheng et al, 2021), raising the possibility that this channel could play the same role in primary pituitary cells.

NALCN (Na^+ leak channel/nonselective) encodes for a TTX-insensitive and extracellular Gd^{3+}- and Ca^{2+}-sensitive sodium leak conductance in neurons (Cochet-Bissuel et al, 2014). Several studies have pinpointed NALCN as the major Na^+ leak conductance essential for the spontaneous generation of action potentials in hippocampal neurons (Lu et al, 2007), GABAergic and dopaminergic neurons of the midbrain (Lutas et al, 2016; Philippart and Khaliq, 2018) and neurons of the suprachiasmatic nucleus (SCN) of the hypothalamus (Flourakis et al, 2015). Further, NALCN in ventral respiratory neurons of the brain stem facilitates rhythmic and CO_2 stimulated breathing, and responsiveness to neuropeptides (Lu et al, 2007; Shi et al, 2016; Yeh et al, 2017). The pharmacological profile of the NALCN channel is similar to that of resting sodium conductance in pituitary cells: TTX-insensitive, Gd^{3+}-and $NMDG^+$ sensitive. Swayne et al, (2009) reported a high level of NALCN expression in the pituitary gland, and transcriptomic data indicates that every anterior pituitary cell type significantly expresses NALCN and its known regulatory subunits such as UNC_{79}, UNC_{80} and FAM155A at levels higher than every other known cationic leak channel such as the TRPC family, HCN, TRPM family etc. (Paul Le Tissier, Jacques Drouin and Patrice Mollard, personal communication).

Taken together these data suggest that NALCN is a promising candidate to conduct a major background Na^+ conductance in pituitary cells. In the current study, the presence of the NALCN in murine pituitary cells was confirmed at both the RNA level using q-RT-PCR, and at the protein level using fluorescence immunohistochemistry with an antibody directed against the extracellular domain of the NALCN. Then, a lentiviral-mediated knockdown strategy coupled with electrophysiological recordings and calcium imaging was set up on primary pituitary cells in order to evaluate the contribution of NALCN to the background Na^+ conductance. As previous researchers reported that NALCN conductance alters across the circadian cycle (Flourakis et al, 2015) the electrophysiological and calcium imaging experiments were performed between 12:00 and 19:00 with the aim of minimising circadian effects.

4.2 Results

4.2.1 Comparative expression of all known non-selective cationic channels in pituitary cells

Using quantitative RT-PCR analysis, previous studies have reported the expression of mRNA transcripts for non-selective cationic conductances including TRPC family members (TRPC1 >> TRPC6 > TRPC4 > TRPC5 > TRPC3) as well as HCN family members (HCN2 ≈ HCN3 > HCN1 ≈ HCN4) in pituitary cells (Kucka et al, 2012; Kretschmannova et al, 2012; Tomic et al, 2011). However, thus far there have been no studies reporting the expression level of mRNA transcripts for other known non-selective cationic channels (NSCCs) in pituitary cells. Therefore, to produce a candidate list of NSCCs, the author asked Dr Paul Le Tissier, Jacques Drouin and Patrice Mollard to provide information regarding the expression level of all known NSCCs in pituitary cells (Figures 4.1, 4.2, 4.3 *via* personal communication). The microarray datasets were used to measure the expression level of NSCCs in mouse anterior pituitary cells. The techniques for measuring gene expression are further explained by Budry et al, 2012. These data illustrate that there are NSCCs other than those from TRPC and HCN families expressed in pituitary cells, and that NALCN and its axillary subunits UNC_{79}, UNC_{80} and FAM155A have the highest expression level among all the other NSCCs, followed by TRPML1 and TRPC1. This highlights NALCN as a promising candidate for mediating the major inward depolarising leak current in pituitary cells.

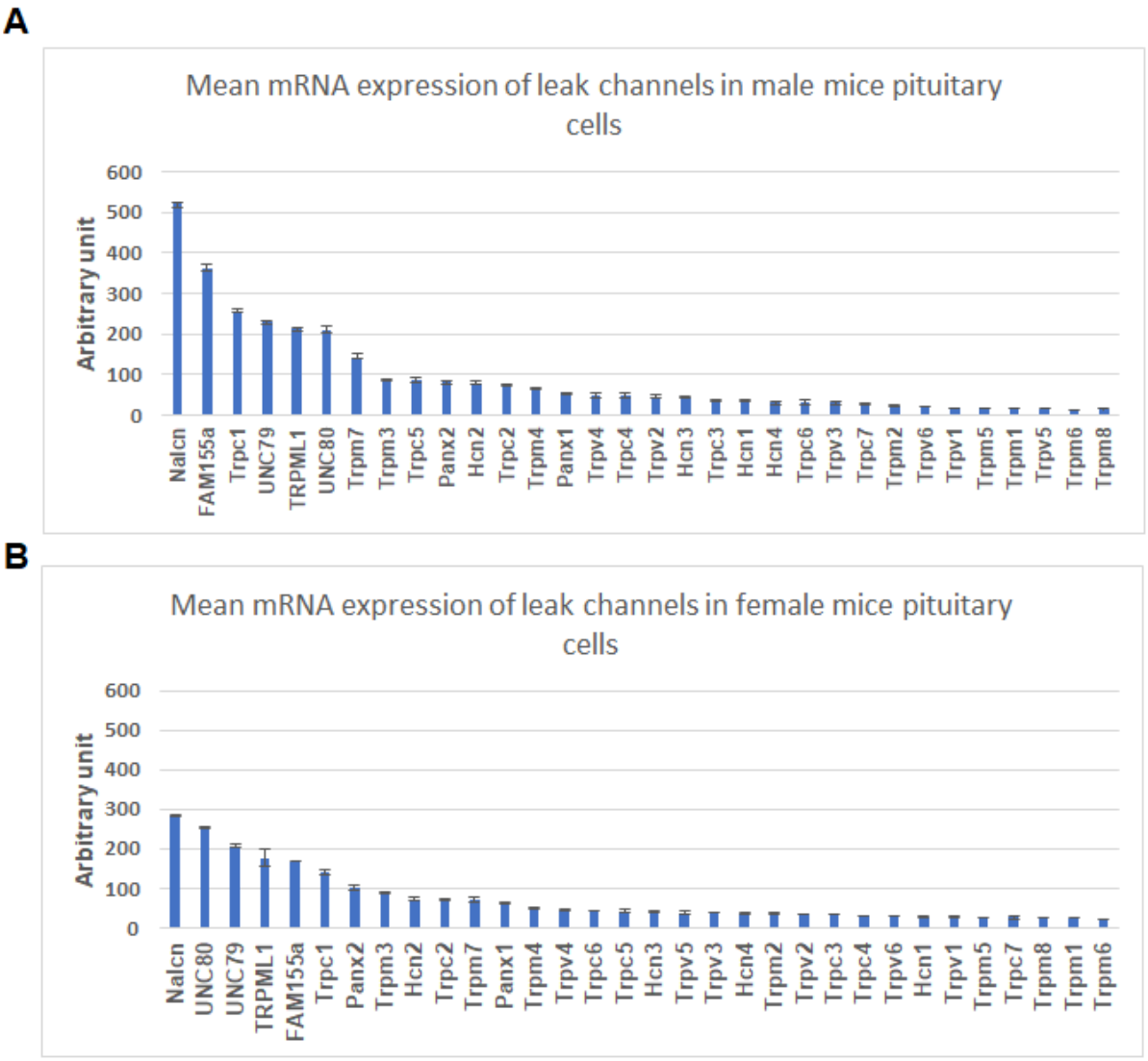

Figure 4.1: The mRNA level of all known NSCCs in a mix population of anterior pituitary cells in both male and female mice.
The data in each graph is the mean of 3 samples each of which is pools of cells from at least 10 mice anterior pituitaries. The microarray datasets were used to measure the expression level of NSCCs in mouse anterior pituitary cells by Le Tissier and colleagues. The values below 20 indicate no significant expression. The error bars represent standard deviation. The X axis indicates the names of the nonselective cationic conductances. The Y axis represents an arbitrary unit. NALCN (Sodium Leak Channel, Non-Selective), UNC_{79}, UNC_{80} and FAM155A are the auxillary subunits of NALCN channel.TRPML (mammalian mucolipin transient receptor potential channel subfamily), TRPC (a family of transient receptor potential cation channels), TRPM (a family of transient receptor potential ion channels, M standing for melastatin), Panx (Pannexins are glycoproteins that form functional single membrane channels), TRPV (Transient receptor potential vanilloid subtype, a family of transient receptor potential cation channels), HCN (Hyperpolarization-activated cyclic nucleotide–gated channels). Unpublished data kindly provided by Dr Paul Le Tissier (University of Edinburgh, UK).

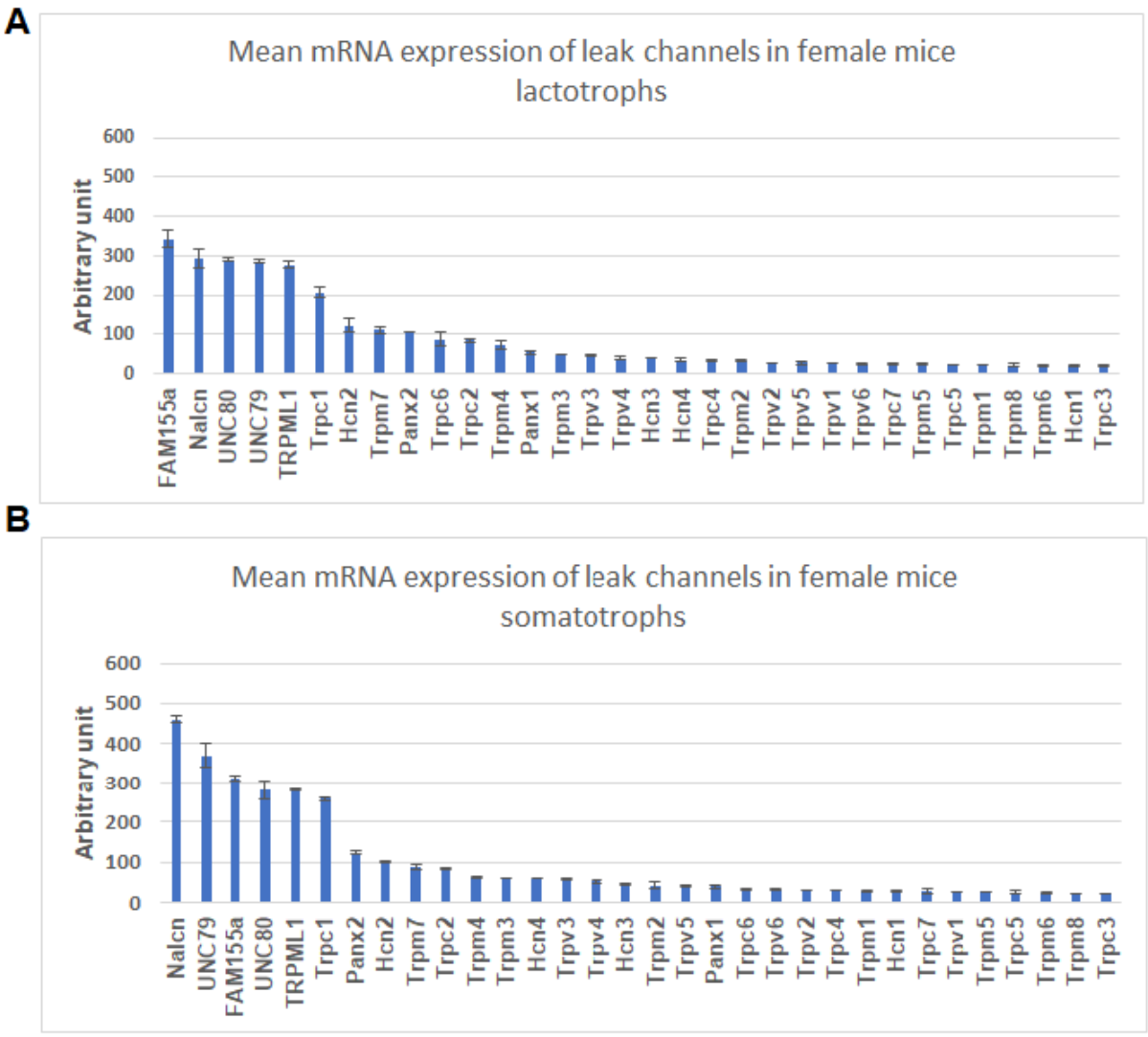

Figure 4.2: The mRNA level of all known NSCCs in subpopulations of anterior pituitary cells in female mice.
The data in each graph is the mean of 3 samples each of which is pools of cells from at least 10 mice anterior pituitaries. The microarray datasets were used to measure the expression level of NSCCs in mouse anterior pituitary cells by Le Tissier and colleagues. The values below 20 indicate no significant expression. The error bars represent standard deviation. The X axis indicates the names of the nonselective cationic conductances. The Y axis represents an arbitrary unit. Unpublished data kindly provided by Dr Paul Le Tissier (University of Edinburgh, UK).

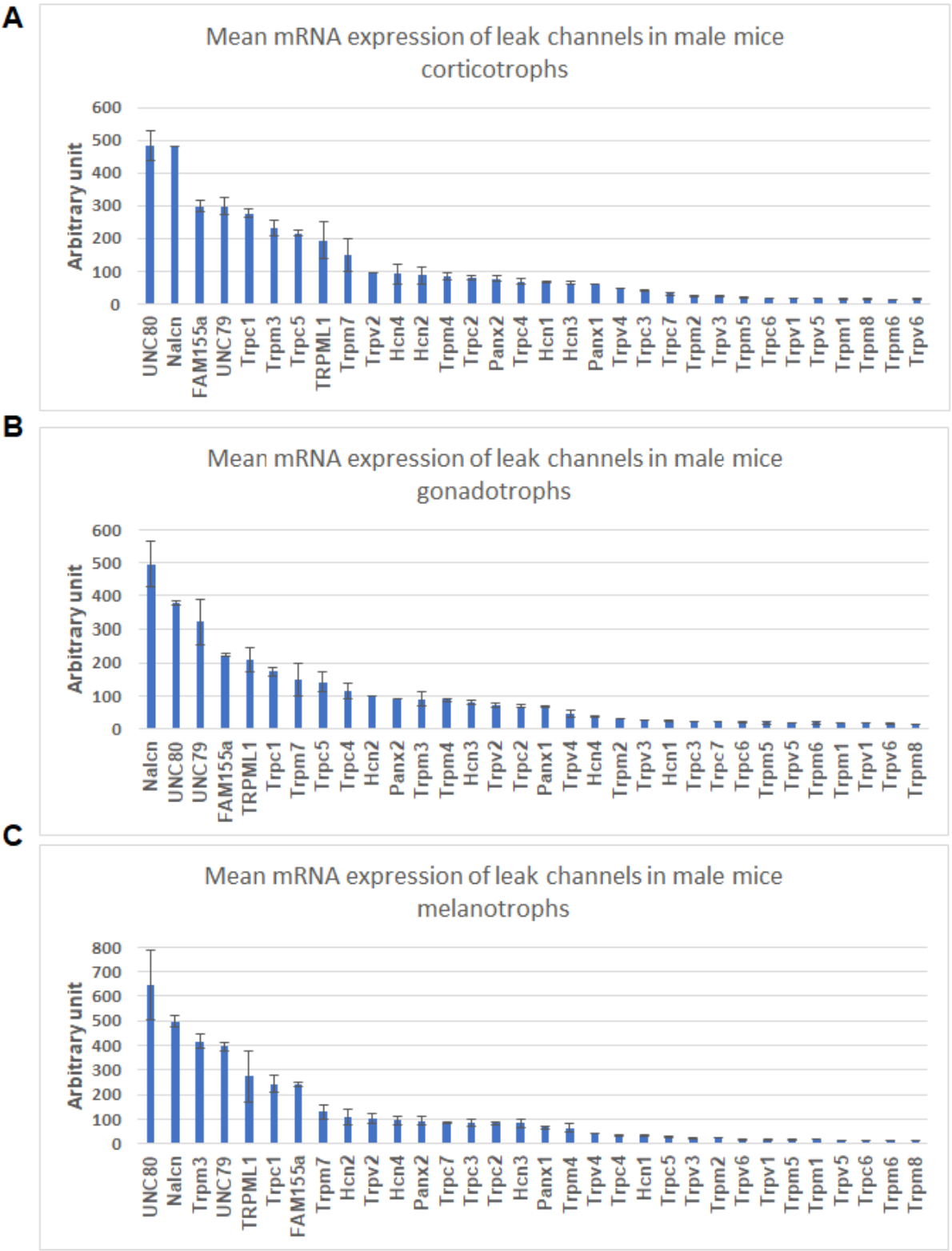

Figure 4.3: The mRNA level of all known NSCCs in subpopulations of anterior pituitary cells in male mice.
The data in each graph is the mean of 3 samples each of which is pools of cells from at least 10 mice anterior pituitaries. The microarray datasets were used to measure the expression level of NSCCs in mouse anterior pituitary cells by Le Tissier and colleagues. The values below 20 indicate no significant expression. The error bars represent standard deviation. The X axis indicates the names of the nonselective cationic conductances. The Y axis represents an arbitrary unit. Unpublished data kindly provided by Dr Paul Le Tissier (University of Edinburgh, UK).

4.2.2 Anterior pituitary gland and its derived cell line GH4 cells express NALCN

Consistent with a previous report (Swayne et al, 2009, supplementary data), my quantitative RT-PCR revealed that the *Nalcn* gene is expressed in mouse anterior pituitary gland (n=4) at levels higher than an unrelated region of mouse brain (amygdala) tissue ($p < 0.05$, Figure 4.4). The presence of NALCN channel protein in murine endocrine anterior pituitary cells was indicated using fluorescence immunohistochemistry *via* a specific NALCN antibody (Anti-NALCN/VGCNL1, #ASC-022, Alomone lab). As shown in Figure 4.5A-G, the majority of the anterior pituitary cells were stained with the NALCN antibody. However, no staining was observed when the primary NALCN antibody was omitted (control, Figure 4.5H). Additionally, the staining of lactosomatoroph GH4 cells with the NALCN antibody showed organized puncta on each GH4 cell membrane confirming the presence of the ion channel in the pituitary derived cell line GH4 cells too (Figure 4.5I-L). The large intracellular accumulations of NALCN signal is detected in GH4 cells suggesting partial permeabilization during washing steps due to the low amounts of Triton present in the washing solution (PBST). These two spots may be presumably the intracellular localisation of NALCN antibody in organelles such as endoplasmic reticulum and Golgi apparatus. In figure 4.5J, TOTO is not localized to the nucleus. TOTO is a cell-impermeant, high-affinity nucleic acid stain that binds to both RNA and DNA. Thus it may be possible that the RNAs were spread over different locations in the cells during fixation process.

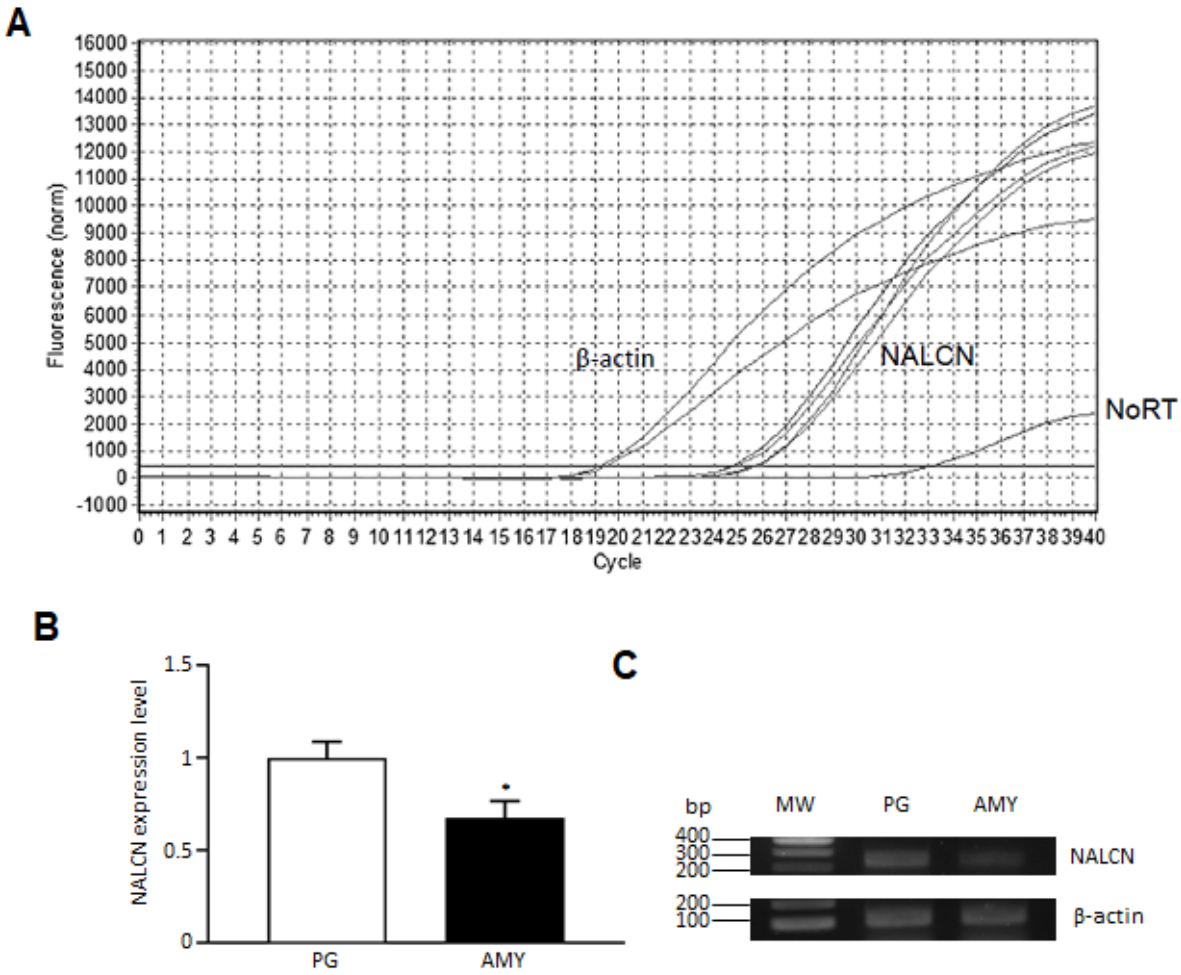

Figure 4.4: NALCN expression in pituitary gland at mRNA level.
A) Representative traces of amplification of the NALCN and positive control beta-actin, and negative control (NoRT) where the extracted RNA did not go through reverse transcription. The first two traces of NALCN from left are from anterior pituitary, and the second two traces are from amygdala. The Y axis indicates the fluorescence intensity. The X axis indicates the number of cycles. **B)** Quantitative RT-PCR revealed that the *Nalcn* gene is expressed in mouse anterior pituitary glands (PG) at levels higher than an unrelated mouse brain tissue amygdala (AMY, $p < 0.05$). **C)** The photograph of an agarose gel electrophoresis of the qRT-PCR reaction products of *Nalcn* and housekeeping *β-actin* genes.

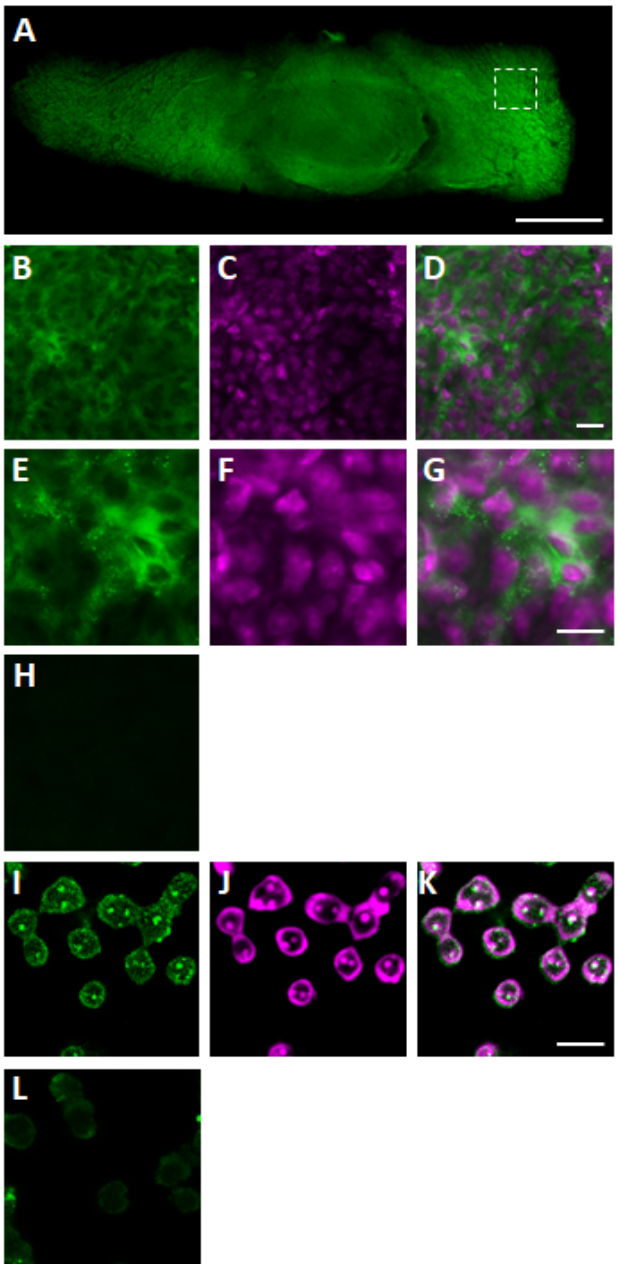

Figure 4.5: NALCN expression in pituitary gland and GH4 cells at protein level.

A-H) Immunohistochemistry staining revealed the presence of NALCN protein in mouse pituitary glands. NALCN is shown in green. TOTO-3 (shown in magenta) was used to visualise cellular nucleic acids (RNA and DNA). **A)** The transverse section of a pituitary gland under 10X magnification excited with 488 nm to monitor NALCN. **B)** NALCN visualisation in a smaller window of anterior pituitary gland. **C)** RNA and DNA visualisation in a smaller window. **D)** Merged images. B, C and D are under 20X magnification. E, F, G are under higher digital magnification. **I)** Immunocytochemistry analysis demonstrated a high level of NALCN protein located in the membrane of GH4 cells in the form of organised puncta. The two large intracellular accumulations of NALCN signal in GH4 cells can be presumably the intracellular localisation of NALCN antibody in protein synthesising and modifying organelles such as endoplasmic reticulum and Golgi apparatus. **J)** RNA and DNA visualisation in GH4 cells using TOTO-3. **K)** Merged images. **H** and **L)** The negative control experiments where the primary anti NALCN antibody was omitted. A slight amount of green light observed in panel L could be either auto fluorescence or non-specific binding of the secondary antibody. The scale bars are 500 μm in panel A, and 20 μm in panels D, G and K respectively.

4.2.3 NALCN regulates spontaneous firing of primary pituitary cells

Given that Gd^{3+} and flufenamic acid (FFA) used by Kucka et al, (2012) on anterior endocrine pituitary cells ceased the spontaneous firing and thus proving the presence of a functional non-selective cation conductance, it is noteworthy that Gd^{3+} and FFA are not specific blockers to a particular NSCC (nonselective cationic conductance). Thus, NSCCs other than NALCN may contribute to the effects of FFA and Gd^{3+} on membrane potential and $[Ca^{2+}]_i$ transients. To resolve the issue of using nonspecific pharmacological blockers, I used a genetic manipulation approach to directly investigate NALCN's role in the regulation of spontaneous firing in anterior pituitary cells. I set up a lentiviral-mediated knockdown strategy to decrease the NALCN expression level and then evaluated the resulting changes in electrophysiological properties of anterior endocrine pituitary cells. I used a pGIPZ plasmid (provided by Dr. Arnaud Monteil, IGF, Montpellier, France) in which a short-hairpin RNA sequence targeting NALCN-encoding mRNA, as well as the turbo-GFP, are expressed under the control of a CMV (cytomegalovirus) promoter. Since primary pituitary cells from adult mice are terminally differentiated and are generally not receptive to transient transfection *in vitro* with high efficiency, I used the plasmid to produce HIV-1 based lentivirus particles (see Materials and Methods section 2.3 for details) and transduced dissociated anterior pituitary cells from adult mice using this viral construct. The turbo-GFP fluorescent (indicating NALCN knock down) cells started to appear 3 days post-transduction. The transduction efficiency was between 30% to 45% between preparations (the type of transduced pituitary cells was not determined). The brightest GFP-positive cells regardless of the cell size were targeted for perforated patch-clamp recordings. Untreated pituitary cells, as well as cells transduced with a scrambled (SCR) sh-RNA-GFP-containing lentivirus, were used as controls.

As expected, most untreated control and SCR control cells exhibited spontaneous electrical activity (Figure 4.6A,B,D,F), as previously reported (reviewed by Fletcher et al, 2018). In contrast, 90% (28 of 31) of cells were found to be silent in the NALCN knockdown (NALCN KD) group (Figure 4.6C,D,F), compared to just 17% (5 of 30)

in SCR control and 19% (6 of 31) in untreated control (Figure 4.6D,F). In addition, NALCN KD cells exhibited a significantly more negative resting membrane potential (RMP) compared to both SCR and untreated control cells (NALCN KD RMP: -63.6 ± 8.5 mV (mean ± SD), n=31; SCR control: -45.2 mV ± 5.8 mV, n=30; untreated control: -47.5 mV ± 7.8, n=31, $p < 0.001$, one-way ANOVA with post hoc Bonferroni correction; Figure 4.6E). Of note, the remaining active cells in the NALCN KD group (3 of 31) exhibited a lower firing frequency than both SCR and untreated control cells (NALCN KD: 0.1 ± 0.02 Hz, n=3 vs SCR control: 0.5 ± 0.4 Hz, n=25 and untreated control: 0.7 ± 0.6 Hz, n=28, $p < 0.001$, one-way ANOVA with post hoc Bonferroni correction; Figure 4.6F). There was no difference between the SCR control and untreated control cells either for the firing frequency (untreated cells: 0.7 ± 0.6 Hz, n=25; SCR cells: 0.5 ± 0.4 Hz, n=25, $p > 0.1$, *t*-test; Figure 4.6F) or for the RMP value (untreated cells: -47.6 ± 7.6 mV, n=31; SCR cells: -45.2 mV ± 5.8 mV, n=30 $p > 0.1$, *t*-test; Figure 4.6E). Thus, the viral transduction *per se* did not affect the firing activity and RMP of pituitary cells. The data were collected across six experimental sessions.

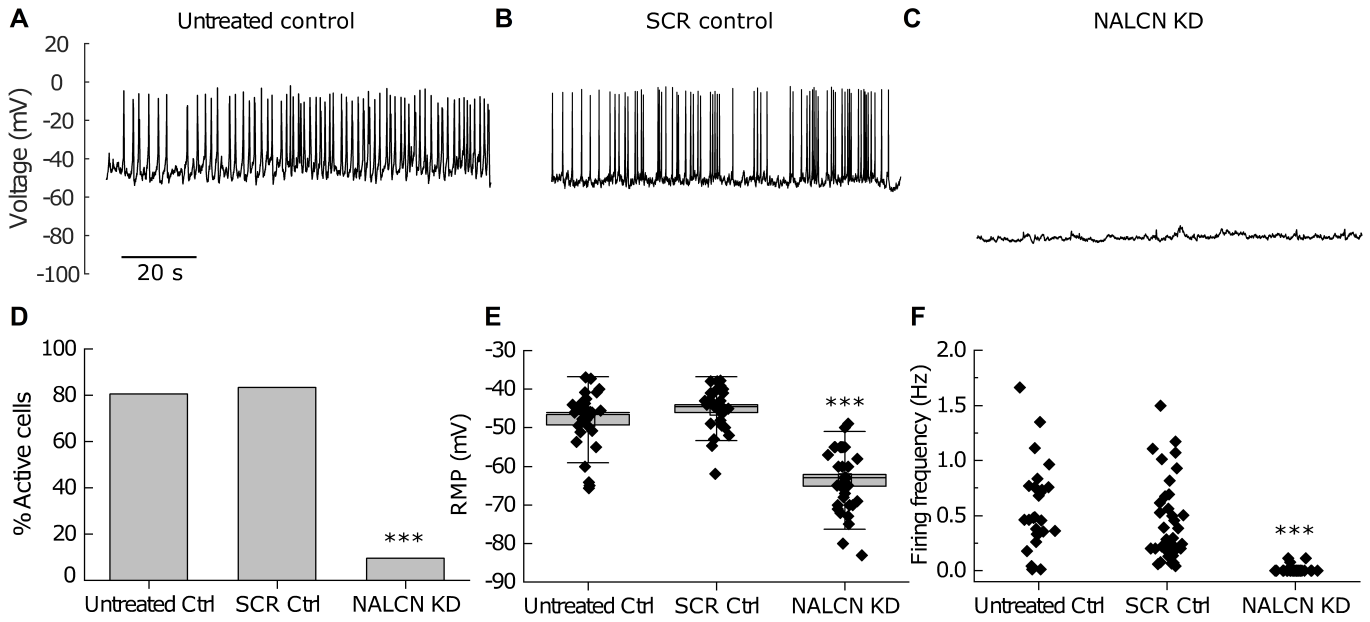

Figure 4.6: NALCN KD silences electrical activity of primary murine pituitary cells.

Representative traces of spontaneous firing activity from **A)** an untreated and **B)** a SCR control pituitary cell. **C)** Representative trace of electrical activity in a NALCN KD pituitary cell. **D)** Percentages of active and silent cells in untreated control, SCR control and NALCN KD pituitary cells. **E)** Resting membrane potential of untreated control, SCR control and NALCN KD pituitary cells (data presented as mean ± SD, untreated control: -47.6 ± 7.6 mV, n=31 vs SCR control: -45 mV ± 5.8 mV, n=30, $p > 0.1$; NALCN KD: -63.6 ± 8.5 mV, n=31 vs SCR and untreated control: $p < 0.001$, one-way ANOVA with Bonferroni correction), the box represents the standard error, the whiskers represent standard deviation (SD) and the black line at the centre of each box represents the mean. **F)** Distribution of firing frequency (number of action potentials /second) between untreated and SCR controls and NALCN KD cells over a course of 600 seconds (data presented as mean ± SD, NALCN KD: 0.1 ± 0.02 Hz, n= 3 vs SCR control: 0.5 ± 0.4 Hz, n= 25 and vs untreated control: 0.7 ± 0.6 Hz, n= 25, $p < 0.001$; SCR control vs untreated control: $p > 0.1$, one-way ANOVA with Bonferroni correction). Only 3 out of 31 NALCN KD cells exhibited firing activity, which occurred at a low frequency. In each graph, triple asterisks ($***$) represents $p < 0.001$.

Small conductance injection restores firing in NALCN KD cells

I next examined whether conductance injection to silent NALCN KD cells could restore spontaneous firing activity in these cells. Indeed, silent NALCN KD cells became active and gained their normal firing activity upon increasing background Na^+ conductance (or non-selective cationic conductance) using dynamic clamp (Figure 4.7A). The minimum added conductance to bring the NALCN KD cells to fire ranged from 0.02 to 0.12 nS (median 0.05 nS, n=28, Figure 4.7B).

Taken together, this first set of results indicates that NALCN is a key player in pituitary cell excitability, by modulating the RMP and subsequently the electrical and Ca^{2+} activity of primary pituitary cells. The amount of NALCN conductance lost by the cells after NALCN KD appears to be on the order of 0.05 nS on average.

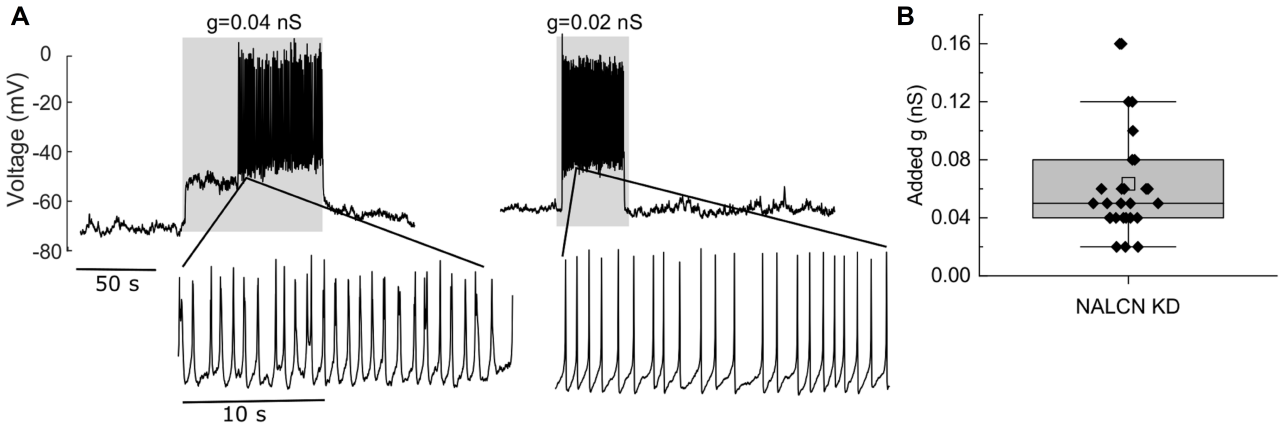

Figure 4.7: Addition of Na^+ leak conductance restores firing activity in silent NALCN KD pituitary cells.
A) Two representative voltage traces of silent NALCN KD pituitary cells. Firing activity was restored once the Na^+ leak conductance (g) was increased by a very minute amount such as 0.02 (right panel) or 0.04 nS (left panel). The cells immediately returned to a silent and hyperpolarised state after removal of the added conductance. **B)** The distribution of added conductance (g) values required for restoring the firing activity in NALCN KD pituitary cells. Median: 0.05 nS, n=28, Box: inter-quartile, Whiskers: range excluding outliers, Central line: median

4.2.4 NALCN contributes to an inward leak current in primary pituitary cells

To further determine the contribution of the NALCN-mediated inward leak current on the sodium background conductance of primary pituitary cells, I performed perforated voltage-clamp recordings and held the cells at -80 mV (the equilibrium potential for K^+) to avoid any contamination from K^+ channels. The holding current at -80 mV was found to be significantly larger in the SCR control cells compared to the NALCN KD group (Figure 4.8A-C, SCR control: -0.72 ± 0.2 pA/pF, n=15; NALCN KD: -0.19 ± 0.13 pA/pF, n=16; p< 0.001, *t*-test). In addition, substitution of extracellular Na^+ with the impermeant cation $NMDG^+$ revealed the existence of a background Na^+ conductance in SCR control cells that was strongly reduced in NALCN KD cells (Figure 4.8D, SCR control: 0.045 ± 0.02 nS, n = 16; NALCN KD: 0.015 ± 0.01 nS , n = 15; $p < 0.001$, Mann Whitney test). These findings show that NALCN contributes to most of the inward leak cconductance in primary pituitary cells. Moreover, I can obtain a rough estimate of the contribution of NALCN channels to the background Na^+ conductance by noting that the difference in background Na^+ conductance between the SCR control and NALCN KD group is 0.045–0.015 = 0.03 nS. This is probably an underestimate since the NALCN KD might not have removed all the channels (knockdown is not a knockout), but it confirms the finding obtained in the previous chapter: a change in background Na^+ conductance of just 0.03 nS can have a profound effect on the electrical activity of endocrine anterior pituitary cells.

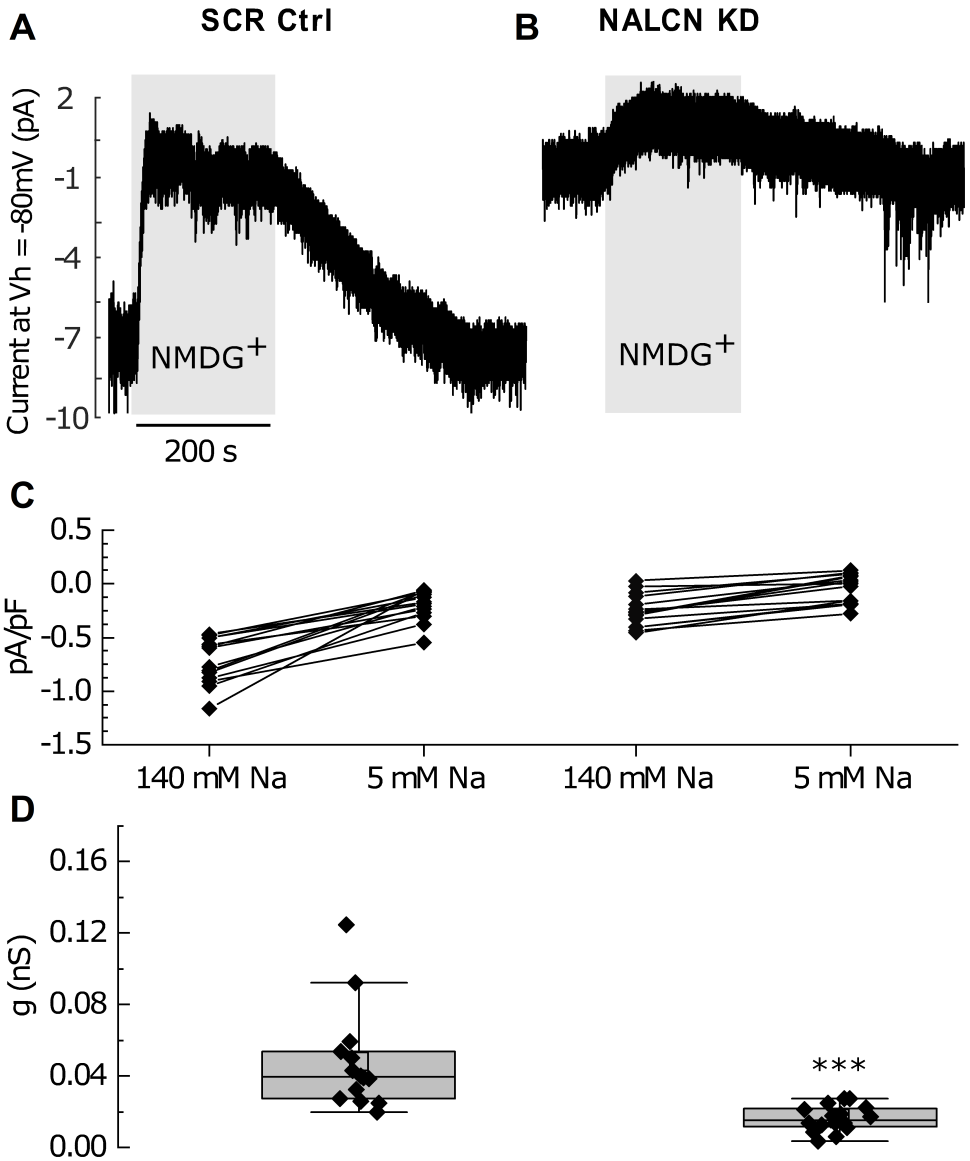

Figure 4.8: NALCN contributes to the inward Na^+ leak current in anterior pituitary.
A) Representative trace of an inward Na^+ leak current (Vh=-80 mV) in a SCR control pituitary cell as revealed by the substitution of extracellular Na^+ with $NMDG^+$. **B)** Representative trace of an inward leak current in a NALCN KD pituitary cell as revealed by the substitution of extracellular Na^+ with $NMDG^+$. **C)** The density of the inward Na^+ leak current in NALCN KD cells was significantly reduced (data presented as mean ± SD, SCR control: -0.72 ± 0.2 pA/pF (-5.2 ± 1.9 pA), n=15; NALCN KD: -0.19 ± 0.13 pA/pF (-1.5 ± 0.9 pA), n=16; $p < 0.001$, t-test). **D)** The background Na^+ conductance was more strongly reduced by Na^+ removal in control cells than in NALCN KD cells (data represented as Median ± interquartile, SCR control: 0.045 ± 0.02 nS, n = 16; NALCN KD: 0.015 ± 0.01 nS , n = 15; $p < 0.001$, Mann Whitney test). Triple asterisks ($***$) represents $p < 0.001$.

4.2.5 NALCN is required for spontaneous intracellular Ca^{2+} oscillations in primary pituitary cells

Previous studies have shown that the pattern of spontaneous firing determines the amplitude and duration of intracellular Ca^{2+} oscillations in anterior pituitary cells (Stojilkovic et al, 2005, Stojilkovic et al, 2012). Thus, I next tested whether NALCN KD affects spontaneous (unstimulated basal conditions) intracellular Ca^{2+} transients in primary anterior pituitary cells. Consistent with a previous report (Tomić et al, 2011), approximately 57% (51 of 90) of SCR control pituitary cells exhibited spontaneous intracellular Ca^{2+} transients (Figure 4.9A). In contrast, approximately 89% (32 of 36) of NALCN KD pituitary cells were quiescent and did not generate any intracellular Ca^{2+} oscillations (Figure 4.9B); approximately 11% (4 of 36) of these displayed relatively low-amplitude intracellular Ca^{2+} transients. To quantitatively compare the size of the intracellular Ca^{2+} fluctuations between the SCR control and NALCN KD cells, the standard deviation of the Ca^{2+} trace for each single cell was calculated over 600 seconds prior to the response to an increased extracellular K^+; comparing the standard deviation between the two groups revealed a statistically-significant difference (Figure 4.9C, SCR control: Median=0.04, n=90; NALCN KD: Median=0.015, n=36; $p<0.001$, Mann Whitney test). The final peak in each graph in Figure 4.9, represents the extracellular K^+ (15 mM) induced depolarisation and consequently a rise in $[Ca^{2+}]_i$, which is used as a control for the viability of cells. This set of experiments indicates that NALCN plays a role in regulating intracellular Ca^{2+} oscillations of primary pituitary cells.

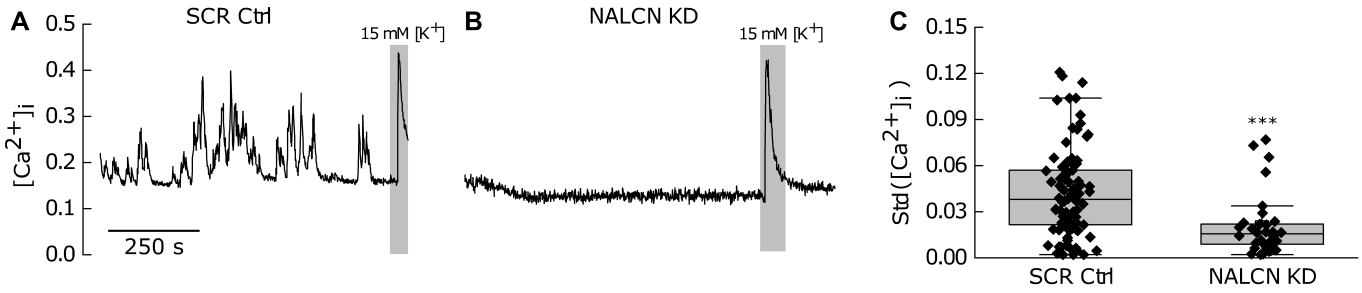

Figure 4.9: NALCN KD impacts on intracellular Ca^{2+} transients.
A) A representative trace of intracellular Ca^{2+} oscillations in an SCR control pituitary cell. The final peak in each graph represents the extracellular K^+ (15 mM) induced depolarisation and consequently a rise in $[Ca^{2+}]_i$. **B)** A representative of an intracellular Ca^{2+} trace in a NALCN KD pituitary cell. **C)** The standard deviation of each $[Ca^{2+}]_i$ trace was calculated and statistical analysis revealed a significant alteration of $[Ca^{2+}]_i$ oscillations between the two groups (SCR control: Median= 0.04, n = 90; NALCN KD: Median= 0.015, n = 36; $p < 0.001$, Mann Whitney test). Box: inter-quartile, Whiskers: range excluding outliers, Central line: median. Triple asterisks $(***)$ represents $p < 0.001$.

4.2.6 NALCN mediates a low extracellular Ca^{2+}-induced depolarisation in primary pituitary cells

In primary anterior pituitary cells, lowering or removing extracellular Ca^{2+} causes membrane depolarisation accompanied with silencing of spontaneous firing activity without elevating $[Ca^{2+}]_i$ (Stojilkovic, 2006; Sankaranarayanan and Simasko, 1996; Kwiecien et al, 1998; Tsaneva-Atanasova et al, 2007). Chu et al, (2003) reported that the removal of extracellular Ca^{2+} in hippocampal neurons activates slow and sustained inward leak currents through the NSCC. Later, Lu and colleagues found that low extracellular Ca^{2+} activates the UNC_{79}-UNC_{80}-NALCN complex to regulate neuronal excitability (Lu et al, 2010). Thus, I next explored the possibility that NALCN could be responsible for the low extracellular Ca^{2+}-induced depolarisation of primary pituitary cells. To test this hypothesis, the inward leak current was measured at a holding potential of -80 mV before and after reducing extracellular Ca^{2+} from 2 mM to 0.1 mM. Consistent with previous studies in neurons, removal of extracellular Ca^{2+} significantly increased the inward leak current in SCR control pituitary cells over a time-course of 20 to 200 seconds (-0.8 ± 0.6 pA/pF to -1.5 ± 0.5 pA/pF (-5.6 ± 2.5 pA to -9.8 ± 4 pA), n=15, p<0.001, Kruskal-Wallis, Figure 4.10A,C). Subsequent replacement of extracellular Na^+ with $NMDG^+$ reduced the holding inward leak current (-1.5 ± 0.5 pA/pF to -0.3 ± 0.2 pA/pF (-9.8 ± 4 pA to -1.9 ± 0.8 pA), n=15, $p < 0.001$; Kruskal-Wallis, Figure 4.10A,C), indicating that the extracellular Ca^{2+}-induced depolarisation is Na^+ mediated. In contrast, lowering the extracellular Ca^{2+} in NALCN KD pituitary cells resulted in a small rise in the inward leak current, which is statistically significant (-0.37 ± 0.35 pA/pF to -0.5 ± 0.25 pA/pF (-1.7 ± 0.8 pA to -2.3 ± 0.8 pA), n=13, $p < 0.05$, one-way ANOVA, Figure 4.10B,C). Substitution of extracellular Na^+ with $NMDG^+$ in NALCN KD cells still reduced the inward leak current (-0.5 ± 0.25 pA/pF to -0.2 ± 0.25 pA/pF (-2.3 ± 0.8 pA to -0.5 ± 0.7 pA), n=13, $p < 0.01$, one-way ANOVA, Figure 4.10C). This current could be the seal conductance, or indicating that there are other NSCCs contributing to the leftover inward leak currents which are still not sufficient to maintain the RMP at depolarized levels to sustain spontaneous firing in pituitary cells. It should also be noted that some residual NALCN may still be

expressed in the NALCN KD cells since knocking down NALCN will not necessary result in a 100% knock out. In this experiment, Ca^{2+} was not replaced with Mg^{2+} since Chua et al, 2020 demonstrated that NALCN can be also blocked by Mg^{2+}.

The overall rise (delta) in the inward leak current after reducing extracellular Ca^{2+} in control pituitary cells was significantly higher than that in NALCN KD pituitary cells (SCR Control: -0.6 ± 0.6 pA/pF (-4.5 pA ± 2.8) n=15; NALCN KD: -0.13 ± 0.1 pA/pF (-0.7 pA ± 0.3), n=13, $p < 0.001$, Mann Whitney test, Figure 4.10D). My results show that, similarly to what has been observed in neurons, NALCN current is reduced by extracellular Ca^{2+} and is involved in the Ca^{2+}-induced depolarisation in primary pituitary cells.

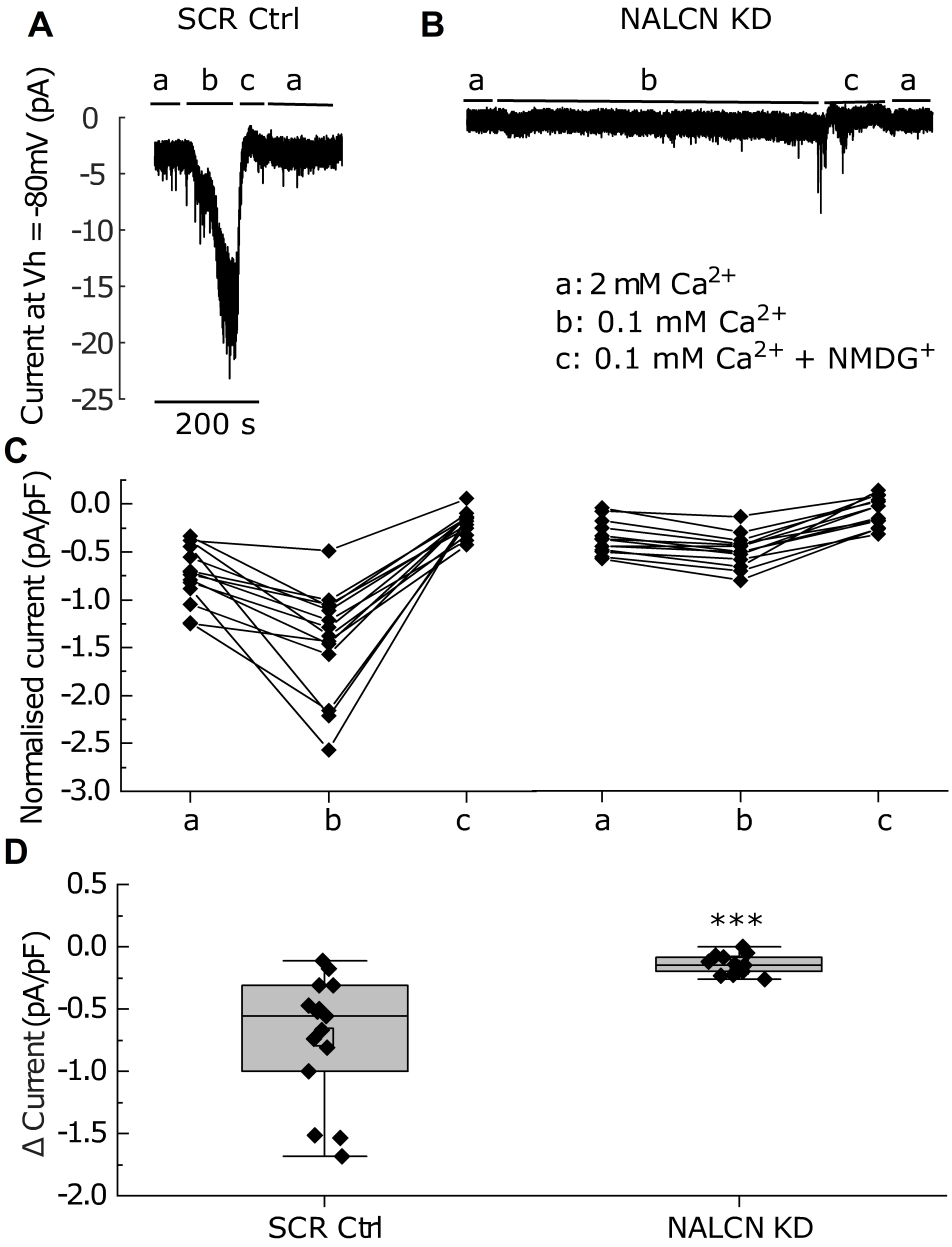

Figure 4.10: NALCN is sensitive to changes in extracellular Ca^{2+} level. **A)** A representative trace of inward leak current in a SCR control pituitary cell; removal of extracellular Ca^{2+} significantly increased the inward leak current over a time-course of 20 seconds to 200 seconds (date presented as Median ± interquartile, panel **C**: -0.8 ± 0.6 pA/pF to -1.5 ± 0.5 pA/pF, n = 15, $p < 0.001$, Kruskal-Wallis). Subsequent replacement of extracellular Na^+ with $NMDG^+$ reduced the holding inward leak current (panel **C**: -1.5 ± 0.5 pA/pF to -0.3 ± 0.2 pA/pF, n = 15, $p < 0.001$, Kruskal-Wallis). **B)** Representative trace of an inward leak current in a NALCN KD pituitary cell; lowering the extracellular Ca^{2+} resulted in a small rise in the inward leak current (data presented as mean ± SD, panel **C**: -0.37 ± 0.35 pA/pF to -0.5 ± 0.25 pA/pF, n = 13, $p < 0.05$, one-way ANOVA) even after an extended period of time (10 minutes). Subsequent replacement of extracellular Na^+ with $NMDG^+$ still reduced the inward leak current (panel **C**: -0.5 ± 0.25 pA/pF to -0.2 ± 0.25 pA/pF, n = 13, $p < 0.01$, one-way ANOVA). **D)** The overall rise (delta) in the inward leak current after reducing extracellular Ca^{2+} in control pituitary cells was significantly larger than that in NALCN KD pituitary cells (Median ± interquartile in SCR Control: -0.6 ± 0.6 pA/pF, n = 13, NALCN KD: -0.13 ± 0.1 pA/pF, n = 13, $p < 0.001$, Mann Whitney test). Box: inter-quartile, Whiskers: range excluding outliers, Central line: median.

4.3 Discussion

4.3.1 NALCN expression in pituitary gland

NALCN expression at mRNA level

Swayne and colleagues have previously shown that pituitary gland expresses NALCN at mRNA level (Swayne et al, 2009). Using quantitative RT-PCR, I could reproduce the finding that pituitary gland expresses NALCN mRNA at levels higher than a region of the brain amygdala. The negative control (NoRT) is a PCR well that only contains primers, master mix and the extracted RNA from pituitary gland, which did not go through reverse transcription procedure. This is to detect if there is any significant contamination with DNA strands. Since PCR is an extremely sensitive technique, it may still pick up minor signals from very small contaminations (e.g. exogenous DNA) and thus produces some minor amplifications that can be detected in the negative control. However, the difference in amplification between the negative control and the test samples is significant implying that the results are valid. Ideally, an additional negative control would be a tissue that does not express NALCN such as liver (Swayne et al, 2009).

NALCN expression at protein level

Using fluorescence immunohistochemistry I could confirm the presence of NALCN protein in pituitary gland and its clonal cell line GH4 cells. The NALCN antibody was found to be localised on the pituitary cell membrane in the form of organised puncta.

The NALCN antibody used in the experiment binds to the extracellular epitopes of NALCN protein. However, two large intracellular accumulations of NALCN signal were detected in GH4 cells implying partial permeabilization during washing steps due to the low amounts of Triton present in the washing solution (PBST). These two spots may be presumably the intracellular localisation of NALCN antibody in protein synthesizing and modifying organelles such as endoplasmic reticulum and Golgi apparatus.

The negative controls used in the experiment were pituitary gland slices and GH4 cells treated with only the secondary antibody where no primary NALCN antibody

was present. An ideal negative control would be either pituitary slices treated with NALCN antigen combined with NALCN antibody or the use of a tissue that does not express NALCN such as liver.

4.3.2 NALCN regulates the electrical activity of primary pituitary cells

All endocrine anterior pituitary cells produce intrinsically-regulated spontaneous firing which is essential for maintaining their normal physiology (e.g. basal hormone secretion, gene expression, and maintaining intracellular Ca^{2+} stores) (Kwiecien and Hammond, 1998; Stojilkovic et al, 2010; Fletcher et al, 2018). However, the molecular mechanism that sustains this spontaneous firing is not fully understood (Fletcher et al, 2018). "Non-selective cationic current (NSCC)" or "background Na^+ leak current" has been a general term attributed to the depolarising inward leak current underlying spontaneous firing in pituitary cells (Stojilkovic et al, 2010; Fletcher et al, 2018). Pharmacological studies have revealed that the NSCC is unequivocally a Na^+-dependent and TTX-resistant depolarising current whose molecular identity remained unknown (Simasko, 1994; Sankaranarayanan and Simasko, 1996; Kucka et al, 2010; Liang et al, 2011; Tomic et al, 2011; Zemkova et al, 2016). Some studies have suggested that TRPC channels could contribute to the background Na^+ conductance described in pituitary cells as well as related cell lines such as the somatolactotroph GH3 cell line (Tomic et al, 2011; Kucka et al, 2012; Kayano et al, 2019). However, these studies were based on RNA expression profiles as well as on the use of non-selective pharmacological compounds; it is not known whether these compounds affect NALCN conductance. Also, RNA expression profiling *per se* does not prove the protein translation and trafficking to the cell membrane. For instance, TRPML channels RNA are highly expressed in some neuronal populations (Lutas et al, 2016), but are not found in the cell membrane (Cheng et al, 2010), and thus are likely not involved in regulating membrane potential (Cheng et al, 2010). In addition, no genetic modification (e.g. modification of the NALCN expression level) was performed to demonstrate their contribution. A recent study revealed that the Na^+ leak channel NALCN is a major contributor to the background Na^+ conductance in GH3 cells (Impheng et al, 2021). Whether this finding may be extended to

primary pituitary cells remains to be established.

To address this issue, I used a combination of genetic and electrophysiology techniques to knock down NALCN channels in cultured mouse pituitary cells and study their electrophysiological properties. I discovered that: (1) the NALCN channel encodes for a Na^+ leak conductance to sustain the intrinsically-regulated spontaneous firing in endocrine pituitary cells; (2) NALCN current is the main contributor to the depolarising inward leak current in pituitary cells, without which the cells remain silent and hyperpolarised; (3) the NALCN channel is crucial for maintaining spontaneous intracellular Ca^{2+} transients in these cells; and (4) as in neurons, NALCN activity is sensitive to the extracellular Ca^{2+} level in pituitary cells. Taken together, these results support a critical role for NALCN in maintaining both the spontaneous firing and the subsequent intracellular Ca^{2+} transients in primary pituitary cells. Thus, my results imply that NALCN may play an important role in regulating pituitary hormone secretion. The use of transgenic mouse models bearing *Nalcn* knock out in specific subpopulations of anterior pituitary cells will be required to investigate this further.

Physiologically, leak conductances play a key role in regulating the resting membrane potential in excitable cells as well as maintaining the firing activity in spontaneously active cells such as anterior pituitary cells (Stojilkovic et al, 2010) and numerous types of neurons (Häusser et al, 2004; Bean, 2007). Many neurons in the brain produce action potentials endogenously even when the animal is at rest or when synaptic transmission is blocked (Häusser et al, 2004). This spontaneous firing, initially discovered in invertebrates (Alving, 1968, Getting, 1989), emerges from particular combinations of intrinsic membrane currents (Llinas, 1988), and is crucial for normal neuronal circuit function (Häusser et al, 2004). Previously, researchers have speculated that other NSCCs such as the persistent sodium current (resulting from window current of voltage-gated sodium channel), transient receptor potential canonical channels (TRPC) and hyperpolarisation-activated ion channels (HCN) may be the NSCC underlying spontaneous firing in pituitary cells (Tomic et al, 2011; Kucka et al, 2012; Kretschmannova et al, 2012) and in neurons (Ren, 2011). In neurons however, it has been demonstrated that NALCN is the major cationic

leak conductance which regulates neuronal excitability (Lu et al, 2007; Philippart & Khaliq, 2018; Lutas et al, 2016; Flourakis et al, 2015).

In the invertebrates *D. melanogaster*, *C. elegans* and L. stagnalis, NALCN homologs are essential for maintaining basic functions such as circadian rhythms, motor activity and respiratory function (Nash et al, 2002; Lear et al, 2005; Yeh et al, 2008; Gao et al, 2015; Lu and Feng, 2011). In mice, the general knock out of NALCN produces neonates that die within 24 hours of birth due to disruption in the rhythmic firing of ventral respiratory neurons of the brain stem, resulting in frequent apnoea and hypoxia (Lu et al, 2007). Moreover, cultured hippocampal neurons from NALCN KO mice display remarkably hyperpolarised membrane voltages by approximately 10 mV (Lu et al, 2007), which may potentially lead to memory deficits in the animal. Flourakis and colleagues reported that NALCN is necessary for circadian firing patterns in neurons of the superchiasmatic nucleus, and drives the circadian rhythm in both mice and flies (Flourakis et al, 2015). Additionally, it has been shown that mice with conditional (only in the forebrain) NALCN KO die after 21 days (Flourakis et al, 2015). Collectively, these discoveries demonstrate that the NALCN channel is a key ion channel for maintaining normal physiology of the organism by regulating the resting membrane potential as well as spontaneous firing in excitable cells.

Given that pituitary cells share many common electrophysiological features with neurons (Stojilkovic et al, 2010), NALCN was a plausible candidate to consider for driving the spontaneous firing observed in pituitary cells. My discoveries in pituitary cells are consistent with findings that NALCN is a key player in controlling cell excitability, and that it does so by regulating the resting membrane potential and subsequently spontaneous firing. I found that NALCN KD pituitary cells are significantly hyperpolarised (by about 15 mV) compared to control pituitary cells. Moreover, 90% of NALCN KD pituitary cells were entirely silent and did not generate any action potentials. Interestingly, restoring the non-selective cationic conductance in NALCN KD pituitary cells using dynamic clamp, rescued the firing activity, while discontinuing current injection returned all cells to the silent state: the previous hyperpolarised potentials. This confirms the results of the previous

chapter that only very small amounts of Na^+ leak conductance can have a drastic effect on pituitary cell excitability. On the other hand, in the majority of silent primary pituitary cells (control), discontinuing the injection of positive currents did not return them to silent but made them sustain the normal firing. One may hypothesise that submicromolar concentrations of Ca^{2+} can activate the Ca^{2+}/calmodulin complex, which in turn activates adenylyl cyclase and results in the activation of cAMP-dependent kinases (Halls and Cooper, 2011) and consequent phosphorylation of L-type voltage-gated calcium channels (Vela et al, 2007). This therefore, could sustain the firing activity even after the removal of the positive current injection. In this case, by injecting positive currents into silent pituitary cells, the cytosolic Ca^{2+} increased at submicromolar levels, which may lead to activation of cAMP-dependent kinases and eventually the phosphorylation of downstream ion channels. This could sustain the firing activity for a while even after the removal of positive currents. This deduction is supported by Vela et al, (2007), who showed that membrane depolarisation, which results in Ca^{2+} entry in pituitary cells, activates numerous kinases involved in a plethora of intracellular pathways, including modifying ion channel activity. However, in NALCN KD pituitary cells, removal of the injected positive current did not sustain the firing activity and returned the cells to silent. This may be because the resting membrane potential is too hyperpolarised for the voltage-dependent Ca^{2+} channels to reach their activation threshold. Thus, phosphorylation of these Ca^{2+} channels upon the injection of positive current and activation of protein kinase A may not be sufficient *per se* to maintain firing activity, and may need cationic background currents to bring the RMP close to the activation threshold.

It has been demonstrated that spontaneous firing in pituitary cells primarily regulates cytosolic Ca^{2+} homeostasis to either induce basal hormone secretion or maintain intracellular Ca^{2+} stores at a responsive state; that is, a state at which the cell's activity can be easily modulated either negatively or positively (Kwiecien and Hammond, 1998). Therefore, spontaneous firing is necessary for the normal secretory function of pituitary cells. My results indicate that, in contrast to control pituitary cells, NALCN KD cells entirely lose their spontaneous $[Ca^{2+}]_i$ transients

and exhibit a flat $[Ca^{2+}]_i$.

4.3.3 NALCN activity is modulated by extracellular Ca^{2+} in primary pituitary cells

Under both physiological and pathological circumstances, extracellular Ca^{2+} concentration can drop markedly in various brain regions (Ren, 2011) and in serum (Ferry et al, 1997). This variation in serum Ca^{2+} appears to regulate adrenocorticotropic hormone (ACTH) secretion from anterior pituitary cells. Indeed, it has been shown that variations in serum Ca^{2+} within the physiological range are associated with changes in ACTH secretion (Isaac et al, 1984; Fuleihan et al, 1996). At the cellular level, a reduction in extracellular Ca^{2+} concentration results in membrane depolarisation of cultured rat lactotrophs and somatotrophs (Sankaranarayanan and Simasko, 1996; Tsaneva-Atanasova et al, 2007). Conversely, an increase in extracellular Ca^{2+}, or Mg^{2+}, from 2 to 10 mM with a concomitant blockade of calcium channels results in a hyperpolarisation of the membrane potential of cultured rat somatotrophs (Tsaneva-Atanasova et al, 2007). It has been suggested that the underlying mechanism of low extracellular Ca^{2+}-induced membrane depolarisation could involve either the inhibition of Ca^{2+}-activated potassium channels and/or the increase of a background Na^+ conductance (Sankaranarayanan and Simasko, 1996; Tsaneva-Atanasova et al, 2007). Of note, the observed increase in the inward leak current upon the reduction of extracellular Ca^{2+} level cannot be due to changes in osmolarity of the extracellular solution. This is because the osmolarity was adjusted to the control solution by adding sucrose. NALCN has been found to be sensitive to the blockade by extracellular Ca^{2+} in primary neurons, HEK-293 cells, NG108-15 cells and GH3 cells (Lu et al, 2010; Bouasse et al, 2019; Lee et al, 2019; Chua et al, 2020; Impheng et al, 2021). Furthermore, my results clearly show that NALCN is sensitive to the blockade by extracellular Ca^{2+} in primary pituitary cells, and mediates the low extracellular Ca^{2+}-induced membrane depolarisation. Two different mechanisms have been proposed to underlie NALCN blockade by extracellular Ca^{2+}. This blockade could occur through the Ca^{2+}-sensing receptor (CaSR) through a Gq-protein dependent pathway that ultimately induces NALCN phosphorylation by PKC (Lu et al, 2010; Lee et al, 2019). Alternatively, a recent study showed

that this blockade could occur through a direct binding of Ca^{2+} to the NALCN pore (Chua et al, 2020). It remains to be determined which mechanism is involved in NALCN modulation by extracellular Ca^{2+} in primary pituitary cells. Of note, Zemkova and colleagues have reported that lowering $[Ca^{2+}]_o$ has no effect on the membrane potential of corticotrophs (Zemkova et al, 2016), despite Le Tissier and colleagues finding that these cells do express the NALCN-coding mRNA (personal communication). One possible explanation for this is that extracellular Ca^{2+} was lowered for only a short period of time (20 seconds) in the Zemkova et al (2016) study, which may not be enough time to allow the membrane potential to depolarise. According to my experiments, the membrane potential in the majority of primary pituitary cells depolarises after 20 seconds to a minute following the reduction of extracellular Ca^{2+}, and then gradually increases over the course of the next few minutes until it reaches a steady state.

4.3.4 NALCN activity can potentially be negatively modulated by the D2 dopamine receptor in primary pituitary cells

In addition to CaSR, NALCN has been found to be negatively and positively regulated by other G-protein dependent and independent signalling pathways (Lu et al, 2009; Swayne et al, 2009; Philippart & Khaliq, 2018). Among these GPCRs, the D2-dopamine receptor negatively modulates NALCN channels in dopaminergic neurons of the midbrain (Philippart & Khaliq, 2018). This receptor is expressed in lactotrophs and melanotrophs where it is involved in the negative regulation of hormone secretion by dopamine (Fletcher et al, 2018). Whether NALCN inhibition is a part of the downstream mechanism involved in the dopaminergic negative modulation of pituitary cell excitability remains to be explored. Further, whether other GPCRs modulate NALCN in pituitary cells remains to be investigated. Indeed, several studies have shown that this resting sodium conductance is not only a passive leak conductance, but is also essential for facilitating the electrical activity and Ca^{2+} influx in response to hypothalamic signals (reviewed in Fletcher et al, 2018). For instance, several groups have shown that removing extracellular Na^+ supresses both growth hormone releasing hormone (GHRH)-induced Ca^{2+} influx (Lussier et

al, 1991; Naumov et al, 1994) and GHRH-induced growth hormone secretion from rat pituitary cells *in vitro* (Kato et al, 1988). Moreover, it has been shown that TTX has no effect on either GHRH-induced GH secretion or GHRH-induced Ca^{2+} influx (Kato et al, 1988). Interestingly, Kato and colleagues have shown that, in the absence of extracellular Na^+, changing the membrane equilibrium potential by increasing the extracellular K^+ to 15 or 30 mM completely rescues GHRH-induced GH secretion (Kato et al, 1988). Liang and colleagues later reported that the removal of extracellular Na^+ substantially delays the stimulatory response to CRH (corticotrophin-releasing hormone) by approximately 13 minutes in murine primary pituitary cells (Liang et al, 2011). Moreover, Tomić et al, (2011) found that the removal of bath Na^+ abolishes spontaneous $[Ca^{2+}]_i$ oscillations and that even forskolin (an adenylyl cyclase and protein kinase A activator) was unable to rescue $[Ca^{2+}]_i$ transients in primary rat pituitary cells. This suggests that excitatory hypothalamic factors trigger c-AMP activation of Na^+ leak conductance (potentially NALCN) to depolarise the resting membrane potential and increase Ca^{2+} influx *via* voltage-gated Ca^{2+} channels.

Key conclusion

The comparison between background inward current in control cells and NALCN KD cells has shown that the NALCN conductance is about 0.05 nS on average. This is a tiny conductance, and this means that possibly very few NALCN channels are expressed (and active) in a given cell. This would explain why the recordings of the background inward currents are so noisy, and thus why the electrical activity is so noisy in pituitary cells. Finally, this is in agreement with the results presented in the previous chapters, that a very small leak conductance can have a profound effect on the electrical activity of pituitary cells. This suggest that any hypothalamic neurohormone that targets these channels can have a strong effect on electrical activity and hence hormone release.

Chapter 5

Conclusions and Future Work

It is well established that endocrine pituitary cells and their clonal cell lines generate action potentials spontaneously, and that both basal and receptor-controlled hormone secretion in these cells are regulated by the cell's electrical activity (Stojilkovic et al, 2010). Hence, elucidating the mechanisms underlying hormone secretion involves characterization of ionic conductances which govern pituitary cell excitability. For pituitary cells to be excitable and produce action potentials (or electrical events), there should be an interplay between numerous types of ion channels located across cell membrane (Fletcher et al, 2018). Amongst the various types of ion channels, background leak channels have a key role in fine tuning the resting membrane potential and consequently cell excitability. Since pituitary cells have a relatively high input resistance, their leak channels only need to conduct several picoamperes of current to adjust the membrane potential or substantially influence electrical activity; this makes it difficult to precisely and reliably measure the contribution of leak conductances to shaping the pattern of electrical activity in endocrine pituitary cells. The dynamic clamp technique helps to overcome this difficulty by enabling us to alter the leak conductances (or any other biophysical properties of ion channels) by exact amounts, and observe how this manipulation affects the pattern of electrical activity and $[Ca^{2+}]_i$ in live pituitary cells in real time. My findings demonstrate that very minute alterations in the conductance of either Na^+ or K^+ leak channels result in significant changes in the pattern of electrical activity and $[Ca^{2+}]_i$ in pituitary cells. More specifically, increasing the conductance of Na^+ leak channels by only 0.02 or 0.04 nS increases the excitability and $[Ca^{2+}]_i$ of pituitary cells significantly. In contrast, increasing the conductance of K^+ leak channels by 0.02 or 0.04 nS re-

duces the excitability and $[Ca^{2+}]_i$ of pituitary cells markedly. These results signify that endocrine anterior pituitary cells are extremely sensitive to even the smallest of changes in Na^+ and K^+ leak conductances. This contrasts with what is seen in other cell types that have lower input resistance (e.g. pyramidal neurons, neurons of substantia nigra etc.), where much greater changes in leak conductance (magnitudes of hundreds of nS or even μS) are required to tune cell excitability (Lu et al, 2007; Philippart and Khaliq, 2018).

Although, both Na^+ and K^+ leak conductances contribute to acutely tuning the resting membrane potential (RMP), and consequently the frequency of electrical events and $[Ca^{2+}]_i$ in these cells, the changes in Na^+ leak conductance have a stronger impact on RMP than the changes in K^+ leak conductance. This is because of the higher driving force of Na^+ near the RMP. Moreover, I discovered that alterations in Na^+ leak conductance lead to changes in event duration, whereas alterations in K^+ leak conductance have no effect on event duration. Only very minute alterations in leak conductance are sufficient to significantly modulate the membrane potential in pituitary cells, raising the possibility that leak channels could act as an efficient target for hypothalamic factors to regulate the pattern of electrical activity, and eventually hormone secretion in, endocrine anterior pituitary cells. However, despite the crucial role of Na^+ leak channels in pituitary cells, the molecular identity of this channel remained unknown. Although there have been studies speculating as to the molecular identity of nonselective cationic leak channels in pituitary cells (e.g. TRPC or HCN channels), these studies were based on RNA expression profiling and the use of nonspecific pharmacological compounds (Kucka et al, 2012; Kretschmannova et al, 2012). For the first time, I used genetic modification (knockdown) to significantly reduce the expression level of the recently-discovered sodium leak channel, non-selective (NALCN) in primary murine pituitary cells *in vitro* using lentiviral transduction. I discovered that strongly-fluorescent pituitary cells (indicating a high degree of NALCN knockdown) are entirely silent with substantially hyperpolarised resting membrane potential and non-oscillatory cytosolic Ca^{2+} level. Interestingly, increasing the Na^+ leak conductance by 0.02, 0.04 or 0.08 nS (using dynamic clamp) rescued the normal spontaneous generation of action potentials in

NALCN knockdown pituitary cells. However, the membrane potential immediately returned to the previous hyperpolarised level upon the removal of the added Na^+ leak current. Moreover, while replacing extracellular Na^+ with $NMDG^+$ resulted in a significant reduction in the inward leak current in control primary pituitary cells, it had no significant impact on the inward leak current in NALCN KD pituitary cells. Furthermore, reducing the extracellular Ca^{2+} level significantly increased the inward leak current and cell excitability in control primary pituitary cells whereas it had no significant effect on the inward leak current in NALCN KD pituitary cells.

Overall, my findings demonstrate that: (1) NALCN forms the long-sought Na^+ leak channel to acutely tune RMP and sustain the intrinsically-regulated spontaneous firing in endocrine pituitary cells; (2) NALCN current is the main contributor to the depolarising inward leak current in pituitary cells, without which the cells remain silent and hyperpolarised; (3) the NALCN channel is crucial for maintaining spontaneous intracellular Ca^{2+} oscillations in these cells; and (4) as in neurons, NALCN activity is sensitive to the extracellular Ca^{2+} level in pituitary cells. Taken together, these results support a critical role for NALCN in both maintaining the spontaneous firing and subsequently the intracellular Ca^{2+} transients in primary pituitary cells. These results also, strongly support a key role for NALCN in regulating basal hormone secretion. Figure 5.1 illustrates the key findings of this thesis.

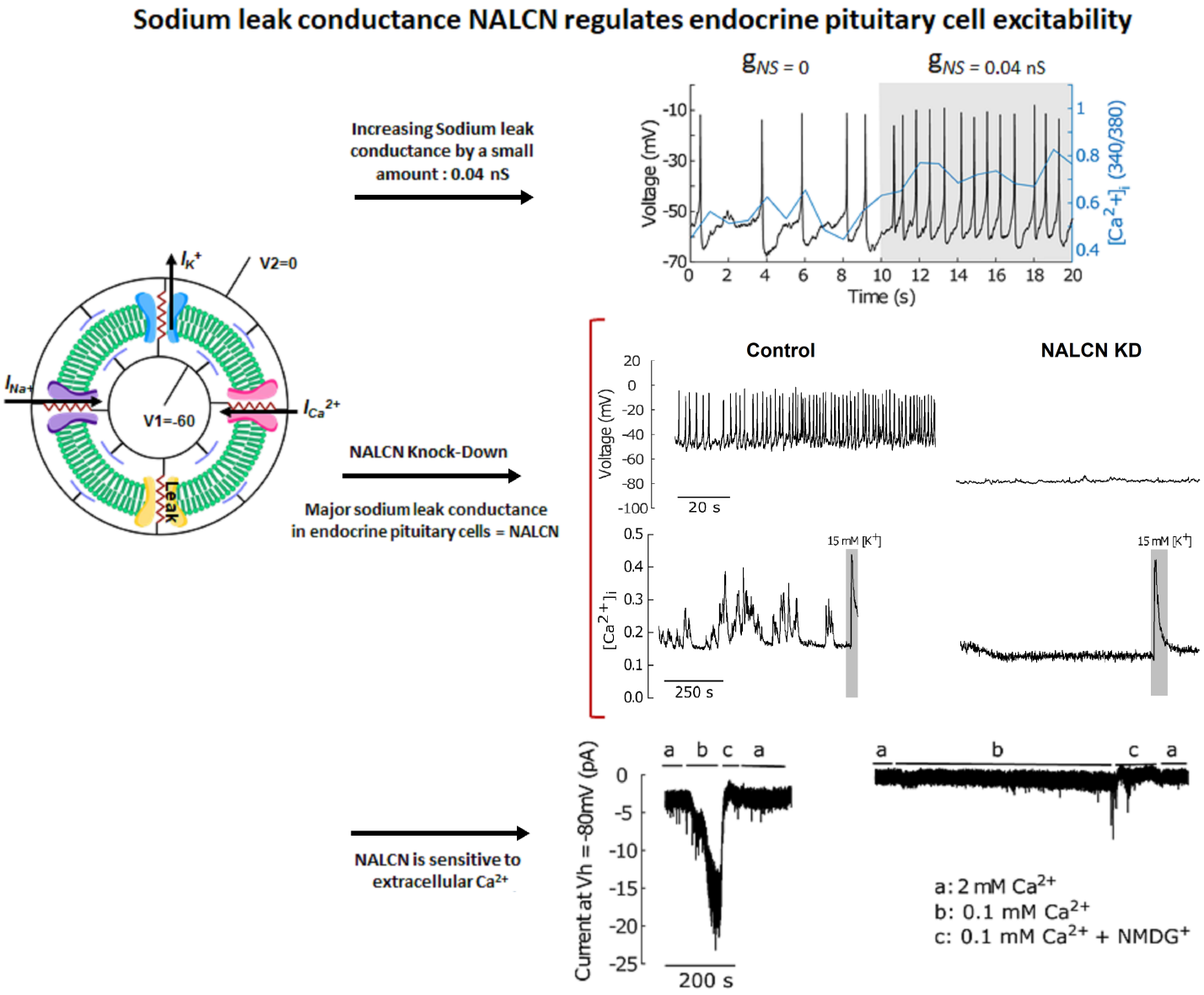

Figure 5.1: Sodium leak conductance NALCN regulates endocrine pituitary cell excitability.
A small variation in sodium leak conductance results in significant changes in endocrine pituitary cell excitability and cytosolic calcium level. The knock-down of NALCN, the major sodium leak conductance expressed in endocrine pituitary cells, silences electrical and $[Ca^{2+}]_i$ activity of these cells. NALCN is sensitive to extracellular Ca^{2+} level.

My results show that, as has been observed in neurons, NALCN is likely to be a fundamental key player in the control of endocrine pituitary cell excitability. However, further investigations will be required to establish the physiological relevance of my findings. Since Na^+ leak conductance is not only a passive leak conductance but is also essential for facilitating electrical activity and Ca^{2+} influx in response to hypothalamic signals, further investigations could focus on evaluating hypothalamic modulation of NALCN *via* G-protein coupled receptors (GPCRs) in pituitary cells. Additionally, *in vivo* studies making use of transgenic mouse models bearing a knockout for *Nalcn* in specific subpopulations of anterior pituitary cells would be valuable in understanding the role NALCN plays in regulating the level of anterior pituitary hormones in the general blood circulation. My immunohistochemistry experiments, and the transcriptomic data (Paul Le Tissier, University of Edinburgh), have demonstrated NALCN expression throughout the anterior pituitary gland and thus presumably in a variety of cell types such as corticotrophs, melanotrophs, lactotrophs, somatotrophs, and thyrotrophs. A natural next step, therefore, would be to investigate the relative contribution of NALCN to the Na^+ leak conductance in different cell types of the anterior pituitary gland. Several studies have shown that peripheral tissues as well as endocrine pituitary cells possess intrinsic circadian oscillators (e.g. *Per1*, *Per2*, *Cry1*, *Cry2*, *Bmal1/Clock* genes etc.) that can function independently of the suprachiasmatic nucleus of the hypothalamus (Yoo et al, 2004, Hughes et al, 2007, O'Neill and Reddy, 2011, Wunderer et al, 2013). Moreover, hormone secretion from anterior pituitary cells displays a clear circadian rhythm *in vivo* (Esquifino et al, 2004, Egli et al, 2010, Park et al, 2013). It is also a well-known phenomenon that the frequency of electrical activity is tightly associated with the amount of hormone secretion in anterior pituitary cells (Stojilkovic et al, 2010). However, there is a substantial knowledge gap in understanding how the intracellular molecular circadian clock modulates the electrophysiology of endocrine pituitary cells. Flourakis et al. (2015) reported that the level of activity of Na^+ leak channels (NALCN) in cells of the hypothalamic suprachiasmatic nucleus (SCN) differs throughout the circadian day and that its activity follows a circadian pattern to control daily changes in the membrane excitability of SCN neurons. More specif-

ically, the conductance of Na^+ leak channels is higher during the day when SCN neurons generate higher firing frequency, but lower during the night when SCN neurons produce lower firing frequency. It is tempting to speculate that the excitability of endocrine pituitary cells may follow a circadian rhythm, and that these circadian changes in membrane excitability may be partly governed by alterations in the conductance of Na^+ leak channels. Further investigation is required to evaluate *in vitro* at the single cell level whether the intrinsic electrical activity of anterior pituitary cells follows a circadian rhythm, and the role that Na^+ leak channels may or may not play in this.

The period1 (*Per1*) gene is a crucial component of the molecular clock in circadian biology; its expression in the anterior pituitary gland of nocturnal rodents peaks during the day and is low at night (Bur et al, 2010, Wunderer et al, 2013). The expression pattern of *Per1* can be utilized as an indicator of the circadian phase (time marker) of clock-containing endocrine pituitary cells. Thus, using genetically engineered mouse models (such as Venus reporter for *Per1*; described by Cheng et al, 2009) that report the real time promoter activity of the *Per1* gene will be required (Cheng et al, 2009). Using this mouse model, the circadian rhythmicity in the reporter activity of *Per1* gene could be monitored over the course of several days. During this period, the frequency of electrical events from *Per1*-positive and *Per1*-negative primary pituitary cells could be measured over the course of a day and at night to determine the relationship between the core clock and the frequency of electrical activity. The same experiments would then need to be performed in NALCN knockdown pituitary cells to evaluate the role of NALCN in regulating the circadian excitability of pituitary cells.

Since the Na^+ leak channel has a critical role in tuning the membrane potential and consequently the excitability of pituitary cells, future studies looking into this ion channel's activity at different times of the circadian day would be valuable. This could be achieved by replacing extracellular Na^+ with $NMDG^+$ at different time points across a day. In principle, if the Na^+ leak channel is more active, then the replacement of extracellular Na^+ should result in an increased hyperpolarisation of the membrane potential, whereas if the Na^+ leak channel is less active and

has lower conductance, the replacement of extracellular Na^+ should result in less hyperpolarisation.

At the molecular level, single cell RNA-sequencing could be performed to measure the expression level of NALCN mRNA, as well as its regulatory components UNC_{79}, UNC_{80} and Nlf-1 (NALCN localisation factor-1), and its activator src family kinase (Flourakis et al, 2015) at different time points of the circadian day in endocrine pituitary cells. Flourakis and colleagues have shown that the rate of change in the level of NALCN, UNC_{79}, UNC_{80} and src family kinase mRNAs is constant and does not display a circadian rhythm in fly clock neurons or murine SCN (Flourakis et al, 2015). Instead, it is NLF-1 (NALCN localisation factor-1) that has been observed to display a circadian rhythm in its expression. In fact, NLF-1 acts as a chaperone to stabilise NALCN in the membrane (Xie et al, 2013). The rhythmic expression of NLF-1 has been detected in the DN1p clock neurons of fruit fly or drosophila, even in constant darkness (Flourakis et al, 2015), indicating the conserved role of NLF-1 in the circadian regulation of NALCN activity. It remains to be seen whether circadian clock genes regulate membrane excitability *via* NALCN in pituitary cells, and whether FAM155A (mammalian orthologue of NLF-1) expression follows a circadian rhythm to control NALCN activity across the circadian cycle, and consequently regulating the circadian excitability of endocrine pituitary cells.

Limitations of the present study

In the present study, adult mice were chosen randomly regardless of their sex. However, it is worth noting that the composition of ion channels is slightly different between male and female corticotrophs, and as a result their response to hypothalamic factors (CRH/AVP) is also variable (Duncan et al, 2016). Although the fundamental function of NALCN which is regulating RMP may not differ between male and female pituitary cells, the expression level of NALCN may differ between them. In females, this expression level, as well as the expression levels of other ion channels and receptors, may also change according to the oestrous cycle. As a consequence, the magnitude of their response to changes in leak conductance by hypothalamic factors or drugs may also be different, which in turn would influence dose-response

or exposure-response relationships. Therefore, a study in which male and female mice are categorised and evaluated separately would be valuable.

Increased firing activity (hyperactivity) in the neurons of substantia nigra pars reticulata, which results in motor dysfunction, has been observed by ageing in Parkinson's disease (Wichmann et al, 1999). It has been shown that disruption of the repetitive firing by ablating substantia nigra pars reticulata neurons improves the symptoms of this disease (Wichmann et al, 2001). One hypothesis is that the over expression or gain of function of NALCN can happen by ageing or mutation, resulting in the hyperactivity in these neurons (Lutas et al, 2016). In the present study, adult mice aged between two and six months were selected. However, in light of the studies discussed above, it is possible that NALCN expression or function and its response to various stimuli may alter in ageing in anterior pituitary cells too.

Although NALCN KD silences the firing activity in 90% of the recorded pituitary cells, it does not hyperpolarize the RMP to the K^+ reversal potential (-85 mV). This could be because the knockdown is not a knockout *per se*, and therefore some NALCN channel is still left contributing to the remaining inward leak current. Another possibility could be that other highly-expressed nonselective/Na^+ leak channels such as TRPC1 (Kucka et al, 2012) are contributing to the leftover inward leak current which depolarises the RMP above the K^+ reversal potential. Studying TRPC1 knockout in anterior pituitary cells could help to better understand the nonselective cationic conductance machinery in these cells. My results suggest that this contribution of TRPC1 channels is minor, since in NALCN KD cells the remaining background inward current is a fraction of its control value (Figure 3, Chapter 4). In addition, the seal conductance must also contribute to this background current. I am conscious, however, that this small inward current is the net sum of currents flowing through both inward and outward conductances (due to leak, or to voltage-dependent channels open around RMP). In the end, the RMP is determined by the balance between these different currents. What I have shown is that without the NALCN channels this balance is altered, and the cells cannot compensate for this change in inward conductance within the time frame of my experiments.

Bibliography

Abruzzi, K., Rodriguez, J., Menet, J., Desrochers, J., Zadina, A., Luo, W., Tkachev, S. and Rosbash, M., 2011. Drosophila CLOCK target gene characterization: implications for circadian tissue-specific gene expression. Genes & Development, 25, 2374-2386.

Akkina, R.K., Walton, R.M., Chen, M.L., Li, Q.X., Planelles, V., Chen, I.S., 1996. High-efficiency gene transfer into CD34+ cells with a human immunodeficiency virus type 1-based retroviral vector pseudotyped with vesicular stomatitis virus envelope glycoprotein G. J. Virol. 70, 2581–2585.

Alving, B.O., 1968. Spontaneous Activity in Isolated Somata of Aplysia Pacemaker Neurons. J. Gen. Physiol. 51, 29–45.

Anderson, L., Jeftinija, S. and Scanes, C., 2004. Growth Hormone Secretion: Molecular and Cellular Mechanisms and In Vivo Approaches. Experimental Biology and Medicine, 229, 291-302.

Baker, P. and Reuter, H., 1975. Calcium Movement In Excitable Cells. Oxford, New York, Toronto, Sydney, Braunschweig: Pergamon Press.

Gerfen, C.R., Crawley, J.N., Skolnick, P., 2003. Current Protocols in Neuroscience. Chapter 4:Unit 4.21.

Barinaga, M., Yamonoto, G., Rivier, C., Vale, W., Evans, R. and Rosenfeld, M., 1983. Transcriptional regulation of growth hormone gene expression

by growth hormone-releasing factor. Nature, 306, 84-85.

Barros, F., del Camino, Donato, Luis A. Pardo, Teresa Palomero, Teresa Giráldez, Pilar de la Peña and D. del Camino, 1997. Demonstration of an inwardly rectifying K^+ current component modulated by thyrotropin-releasing hormone and caffeine in GH 3 rat anterior pituitary cells. Pflügers Archiv. Eur. J. Physiol. 435, 119–129.

Bean, B.P., 2007. The action potential in mammalian central neurons. Nat. Rev. Neurosci. 8, 451–465.

Belchetz, P., Plant, T., Nakai, Y., Keogh, E. and Knobil, E., 1978. Hypophysial responses to continuous and intermittent delivery of hypopthalamic gonadotropin-releasing hormone. Science, 202, 631-633.

Benz, R. and Läuger, P., 1976. Kinetic analysis of carrier-mediated ion transport by the charge-pulse technique. The Journal of Membrane Biology, 27, 171-191.

Bernstein, J., 1902. Untersuchungen zur Thermodynamik der bioelektrischen Ströme: Erster Theil. Pflüg. Arch. Für Gesammte Physiol. Menschen Thiere 92, 521–562.

Berry, C., Hannenhalli, S., Leipzig, J., Bushman, F.D., 2006. Selection of Target Sites for Mobile DNA Integration in the Human Genome. PLoS Comput. Biol. 2, e157.

Bilezikjian, L. and Vale, W., 1983. Stimulation of Adenosine 3',5'-Monophosphate Production by Growth Hormone-Releasing Factor and Its Inhibition by Somatostatin in Anterior Pituitary Cells in Vitro. Endocrinology, 113, 1726-1731.

Birnboim, H. and Doly, J., 1979. A rapid alkaline extraction procedure for screening recombinant plasmid DNA. Nucleic Acids Research, 7, 1513-1523.

Blake, W., KÆrn, M., Cantor, C. and Collins, J., 2003. Noise in eukaryotic gene expression. Nature, 422, 633-637.

Bonnefont, X., Mollard, P., 2003. Electrical activity in endocrine pituitary cells in situ: A support for a multiple-function coding. FEBS Lett. 548, 49–52.

Bonnefont, X., Fiekers, J., Creff, A. and Mollard, P., 2000. Rhythmic Bursts of Calcium Transients in Acute Anterior Pituitary Slices. Endocrinology, 141, 868-875.

Bouasse, M., Impheng, H., Servant, Z., Lory, P., Monteil, A., 2019. Functional expression of CLIFAHDD and IHPRF pathogenic variants of the NALCN channel in neuronal cells reveals both gain- and loss-of-function properties. Sci. Rep. 9, 11791.

Brown, E.M., MacLeod, R.J., 2001. Extracellular Calcium Sensing and Extracellular Calcium Signaling. Physiol. Rev. 81, 239–297.

Buckler, K. J., Williams, B. A. & Honore, E., 2000. An oxygen-, acid- and anaesthetic-sensitive TASK-like background potassium channel in rat arterial chemoreceptor cells. J. Physiol. (Lond.) 525, 135–142.

Budry, L., Balsalobre, A., Gauthier, Y., Khetchoumian, K., L'Honore, A., Vallette, S., Brue, T., Figarella-Branger, D., Meij, B., Drouin, J., 2012. The selector gene Pax7 dictates alternate pituitary cell fates through its pioneer action on chromatin remodeling. Genes Dev. 26, 2299–2310.

Bur, I.M., Zouaoui, S., Fontanaud, P., Coutry, N., Molino, F., Martin, A.O., Mollard, P., Bonnefont, X., 2010. The Comparison between Circadian Oscillators in Mouse Liver and Pituitary Gland Reveals Different Integration of Feeding and Light Schedules. PLoS ONE 5, e15316.

Burgo, A., Carmignoto, G., Pizzo, P., Pozzan, T., Fasolato, C., 2003. Paradoxical Ca^{2+} Rises induced by Low External Ca^{2+} in Rat Hippocampal Neurones. J. Physiol. 549, 537–552.

Charles, A.C., Piros, E.T., Evans, C.J., Hales, T.G., 1999. L-type Ca^{2+} Channels and K^{+} Channels Specifically Modulate the Frequency and Amplitude of Spontaneous Ca^{2+} Oscillations and Have Distinct Roles in Prolactin Release in GH 3 Cells. J. Biol. Chem. 274, 7508–7515.

Cheng, H.-Y.M., Alvarez-Saavedra, M., Dziema, H., Choi, Y.S., Li, A., Obrietan, K., 2009. Segregation of expression of mPeriod gene homologs in neurons and glia: possible divergent roles of mPeriod1 and mPeriod2 in the brain. Hum. Mol. Genet. 18, 3110–3124.

Cheng, X., Shen, D., Samie, M., Xu, H., 2010. Mucolipins: Intracellular TRPML1-3 channels. FEBS Lett. 584, 2013–2021.

Chu, X. P., Zhu, X. M., Wei, W. L., Li, G. H., Simon, R. P., MacDonald, J. F., and Xiong, Z. G., 2003. Acidosis decreases low Ca (2+)-induced neuronal excitation by inhibiting the activity of calcium-sensing cation channels in cultured mouse hippocampal neurons. J Physiol 550, 385-399.

Chua, H.C., Wulf, M., Weidling, C., Rasmussen, L.P., Pless, S.A., 2020. The NALCN channel complex is voltage sensitive and directly modulated by extracellular calcium. Sci. Adv. 6, eaaz3154.

Clapham, D.E., 2007. Calcium Signaling. Cell 131, 1047–1058.

Clarke, I., 2019. Control of GnRH secretion. Bioscientifica Proceedings. 9, 1-8.

Clarke I. J., 2002. Two decades of measuring GnRH secretion. Reprod. Suppl. 59, 1–13

Clark, R., Carlsson, L. and Robinson, I., 1988. Growth hormone (GH) secretion in the conscious rat: negative feedback of GH on its own release. Journal of Endocrinology 119, 201-209.

Cochet-Bissuel, M., Lory, P. and Monteil, A., 2014. The sodium leak channel, NALCN, in health and disease. Frontiers in Cellular Neuroscience, 8, 132.

Cole, K.S., Curtis, H.J., 1941. Membrane potential of the squid giant axon during current flow. J. Gen. Physiol. 24, 551–563.

Cooper, D.M., Mons, N., Karpen, J.W.:, 1995. Adenylyl cyclases and the interaction between calcium and cAMP signalling. Nature 374, 421-424.

Cordell, A. R., 1995. Milestones in the development of cardioplegia. Ann Thorac Surg 60, 793-796.

Corrette, B. J., Bauer, C. K. & Schwarz, J. R., 1996. An inactivating inward-rectifying K current present in cells from the pituitary of lactating rats. Journal of Membrane Biology 150, 185–195.

Cronin, J., Zhang, X. and Reiser, J., 2005. Altering the Tropism of Lentiviral

Vectors through Pseudotyping. Current Gene Therapy, 5, 387-398.

Deng, Q., Riquelme, D., Trinh, L., Low, M., Tomić, M., Stojilkovic, S. and Aguilera, G., 2015. Rapid Glucocorticoid Feedback Inhibition of ACTH Secretion Involves Ligand-Dependent Membrane Association of Glucocorticoid Receptors. Endocrinology, 156, 3215-3227.

Deutsch, C., 2003. The Birth of a Channel. Neuron, 40, 265-276.

Douglas, W., 1968. Stimulus-secretion coupling: the concept and clues from chromaffin and other cells. British Journal of Pharmacology, 34, 451-474.

Doyle, D.A., 1998. The Structure of the Potassium Channel: Molecular Basis of K^+ Conduction and Selectivity. Science 280, 69–77.

Dubinsky, J. M. & Oxford, G. S., 1984. Ionic currents in two strains of rat anterior pituitary tumor cells. Journal of General Physiology 83, 309-339.

Dufy, B., Vincent, J., Fleury, H., Du Pasquier, P., Gourdji, D. and Tixier-Vidal, A. 1979. Membrane effects of thyrotropin-releasing hormone and estrogen shown by intracellular recording from pituitary cells. Science, 204, 509-511.

Duncan, P.J., Tabak, J., Ruth, P., Bertram, R., Shipston, M.J., 2016. Glucocorticoids Inhibit CRH/AVP-Evoked Bursting Activity of Male Murine Anterior Pituitary Corticotrophs. Endocrinology 157, 3108–3121.

Egli, M., Leeners, B. and Kruger, T. 2010. Prolactin secretion patterns: basic mechanisms and clinical implications for reproduction. Reproduction, 5, 643-654.

Einhorn, L., Gregerson, K., Oxford, G., 1991. D2 dopamine receptor acti-

vation of potassium channels in identified rat lactotrophs: whole-cell and single-channel recording. J. Neurosci. 11, 3727–3737.

Emanuel, R., Adler, G., Kifor, O., Quinn, S., Fuller, F., Krapcho, K. and Brown, E., 1996. Calcium-sensing receptor expression and regulation by extracellular calcium in the AtT-20 pituitary cell line. Molecular Endocrinology, 10, 555-565.

Esquifino, A., Chacón, F., Jimenez, V., Reyes Toso, C. and Cardinali, D. 2004. 24-hour changes in circulating prolactin, follicle-stimulating hormone, luteinizing hormone and testosterone in male rats subjected to social isolation. Journal of Circadian Rhythms, 2, 1.

Farley, D., Iqball, S., Smith, J., Miskin, J., Kingsman, S. and Mitrophanous, K., 2007. Factors that influence VSV-G pseudotyping and transduction efficiency of lentiviral vectors—in vitro andin vivo implications. The Journal of Gene Medicine, 9, 345-356.

Ferry, S., Chatel, B., Dodd, R., Lair, C., Gully, D., Maffrand, J. and Ruat, M., 1997. Effects of Divalent Cations and of a Calcimimetic on Adrenocorticotropic Hormone Release in Pituitary Tumor Cells. Biochemical and Biophysical Research Communications, 238, 866-873.

Fletcher, P.A., Sherman, A., Stojilkovic, S.S., 2018. Common and diverse elements of ion channels and receptors underlying electrical activity in endocrine pituitary cells. Mol. Cell. Endocrinol. 463, 23–36.

Flourakis, M., Kula-Eversole, E., Hutchison, A.L., Han, T.H., Aranda, K., Moose, D.L., White, K.P., Dinner, A.R., Lear, B.C., Ren, D., Diekman, C.O., Raman, I.M., Allada, R., 2015. A Conserved Bicycle Model for Circadian Clock Control of Membrane Excitability. Cell, 162, 836–848.

Formenti, A., De Simoni, A., Arrigoni, E., and Martina, M., 2001. Changes in extracellular Ca^{2+} can affect the pattern of discharge in rat thalamic neurons. J Physiol. 535, 33-45.

Frankenhaeuser, B., 1957. The effect of calcium on the myelinated nerve fibre. J. Physiol. 137, 245–260.

Frankenhaeuser, B., and Hodgkin, A. L., 1955. The effect of calcium on the sodium permeability of a giant nerve fibre. J Physiol. 128, 40-41P.

Frankenhaeuser, B., Hodgkin, A.L., 1957. The action of calcium on the electrical properties of squid axons. J. Physiol. 137, 218–244.

Fuleihan, G.E., Brown, E.M., Gleason, R., Scott, J., Adler, G.K., 1996. Calcium modulation of adrenocorticotropin levels in women–a clinical research center study. J. Clin. Endocrinol. Metab. 81, 932–936. Gadsby, D., 2007. Ion pumps made crystal clear. Nature, 450, 957-959.

Gao, S., Xie, L., Kawano, T., Po, M.D., Pirri, J.K., Guan, S., Alkema, M.J., Zhen, M., 2015. The NCA sodium leak channel is required for persistent motor circuit activity that sustains locomotion. Nat. Commun. 6, 6323.

Getting PA., 1989. Emerging principles governing the operation of neural networks. Annu Rev Neurosci 12: 185-204.

Ghezzi, A., Liebeskind, B., Thompson, A., Atkinson, N. and Zakon, H., 2014. Ancient association between cation leak channels and Mid1 proteins is conserved in fungi and animals. Frontiers in Molecular Neuroscience, 7.

Goldbeter A.1996. Biochemical oscillations and cellular rhythms: the molecular

basis of periodic and chaotic behaviour Cambridge, UK: Cambridge University Press.

Goldstein, S.A.N., Bockenhauer, D., O'Kelly, I., Zilberberg, N., 2001. Potassium leak channels and the KCNK family of two-p-domain subunits. Nat. Rev. Neurosci. 2, 175–184.

Grynkiewicz, G., Poenie, M., and Tsien, R. Y. 1985. J. Biol Chem. 260: 3440–3450.

Guerineau, N., Corcuff, J., Tabarin, A. and Mollard, P., 1991. Spontaneous and Corticotropin-Releasing Factor-Induced Cytosolic Calcium Transients in Corticotrophs. Endocrinology, 129, 409-420.

Guérineau, N.C., Bonnefont, X., Stoeckel, L., Mollard, P., 1998. Synchronized Spontaneous Ca^{2+} Transients in Acute Anterior Pituitary Slices. J. Biol. Chem. 273, 10389–10395.

Guillemin, R. and Rosenberg, B. 1955. Humoral hypothalamic control of anterior pituitary: a study with combined tissue cultures. Endocrinology, 57, 599-607.

Guillemin, R. 1967. The Adenohypophysis and its Hypothalamic Control. Annual Review of Physiology, 29, 313-348.

Hablitz, J. J., Heinemann, U., and Lux, H. D. 1986. Step reductions in extracellular Ca^{2+} activate a transient inward current in chick dorsal root ganglion cells. Biophys J 50,753-757.

Hagiwara, S., Ohmori, H., 1983. Studies of single calcium channel currents in rat clonal pituitary cells. J. Physiol. 336, 649–661.

Halls, M.L., Cooper, D.M.F., 2011. Regulation by Ca^{2+}-Signalling Pathways of Adenylyl Cyclases. Cold Spring Harb. Perspect. Biol. 3, a004143–a004143.

Hauser, S., Kasper, D., Fauci, A., Longo, D., Jameson, J. and Loscalzo, J., 2013. Harrison's Manual of Medicine, 18th Edition. McGraw-Hill.

Hausser, M., 2004. The Beat Goes On: Spontaneous Firing in Mammalian Neuronal Microcircuits. J. Neurosci. 24, 9215–9219.

Heinemann, S.H., Terlau, H., Stühmer, W., Imoto, K., Numa, S., 1992. Calcium channel characteristics conferred on the sodium channel by single mutations. Nature 356, 441–443.

Henley DE, Leendertz JA, Russell GM,Wood SA, Taheri S, Woltersdorf WW, Lightman SL., 2009. Development of an automated blood sampling system for use in humans. J Med Eng Technol. 33, 199-208.

Hille, B., 2001. Ion Channels Of Excitable Membranes. Sunderland, Mass. Sinauer.

Hodgkin, A. L. (1937a). Evidence for electrical transmission in nerve: Part I. J Physiol 90, 183-210.

Hodgkin, A. L. (1937b). Evidence for electrical transmission in nerve: Part II. J Physiol 90, 211-232.

Hodgkin, A.L., Huxley, A.F., 1952. A quantitative description of membrane current and its application to conduction and excitation in nerve. J. Physiol. 117, 500–544.

Hodgkin, A.L., Katz, B., 1949. The effect of sodium ions on the electrical activity of the giant axon of the squid. J. Physiol. 108, 37–77.

Holl, R., Thorner, M. and Leong, D., 1988. Intracellular Calcium Concentration and Growth Hormone Secretion in Individual Somatotropes: Effects of Growth Hormone-Releasing Factor and Somatostatin*. Endocrinology, 122, 2927-2932.

Hughes, M., DeHaro, L., Pulivarthy, S., Gu, J., Hayes, K., Panda, S. and Hogenesch, J. 2007. High-resolution Time Course Analysis of Gene Expression from Pituitary. Cold Spring Harbor Symposia on Quantitative Biology, 72, 381-386.

Iida, T., Stojilković, S., Izumi, S. and Catt, K., 1991. Spontaneous and Agonist-Induced Calcium Oscillations in Pituitary Gonadotrophs. Molecular Endocrinology, 5, 949-958.

Impheng, H., Lemmers, C., Bouasse, M., Legros, C., Pakaprot, N., Guérineau, N.C., Lory, P., Monteil, A., 2021. The sodium leak channel NALCN regulates cell excitability of pituitary endocrine cells. FASEB J. 35.

Isaac, R., Raymond, J.-P., Rainfray, M., Ardaillou, R., 1984. Effects of an acute calcium load on plasma ACTH, cortisol, aldosterone and renin activity in man. Acta Endocrinol. (Copenh.) 105, 251–257.

Jospin, M., Watanabe, S., Joshi, D., Young, S., Hamming, K., Thacker, C., Snutch, T., Jorgensen, E. and Schuske, K., 2007. UNC-80 and the NCA Ion Channels Contribute to Endocytosis Defects in Synaptojanin Mutants. Current Biology, 17, 1595-1600.

Kato, M., Hattori, M.A., Suzuki, M., 1988. Inhibition by extracellular

Na+ replacement of GRF-induced GH secretion from rat pituitary cells. Am. J. Physiol.-Endocrinol. Metab. 254, 476–481.

Kato, M., Sakuma, Y., 1997. Regulation by Growth Hormone-Releasing Hormone and Somatostatin of a Na+ Current in the Primary Cultured Rat Somatotroph*. Endocrinology 138, 5096–5100.

Kayano, T., Sasaki, Y., Kitamura, N., Harayama, N., Moriya, T., Dayanithi, G., Verkhratsky, A., Shibuya, I., 2019. Persistent Na+ influx drives L-type channel resting Ca^{2+} entry in rat melanotrophs. Cell Calcium, 79, 11–19.

Khaliq, Z.M., Bean, B.P., 2010. Pacemaking in Dopaminergic Ventral Tegmental Area Neurons: Depolarizing Drive from Background and Voltage-Dependent Sodium Conductances. J. Neurosci. 30, 7401–7413.

Kidokoro, Y., 1975. Spontaneous calcium action potentials in a clonal pituitary cell line and their relationship to prolactin secretion. Nature, 258, 741-742.

Koch, S., Bodi, I., Schwartz, A. and Varadi, G., 2000. Architecture of Ca^{2+}Channel Pore-lining Segments Revealed by Covalent Modification of Substituted Cysteines. Journal of Biological Chemistry, 275, 34493-34500.

Köroğlu, Ç., Seven, M., Tolun, A., 2013. Recessive truncating NALCN mutation in infantile neuroaxonal dystrophy with facial dysmorphism. J. Med. Genet. 50, 515–520.

Kretschmannova, K., Kucka, M., Gonzalez-Iglesias, A.E., Stojilkovic, S.S., 2012. The Expression and Role of hyperpolarisation-Activated and Cyclic Nucleotide-Gated Channels in Endocrine Anterior Pituitary Cells. Mol. Endocrinol. 26, 153–164.

Kschonsak, M., Chua, H.C., Noland, C.L., Weidling, C., Clairfeuille, T., Bahlke, O.Ø., Ameen, A.O., Li, Z.R., Arthur, C.P., Ciferri, C., Pless, S.A., Payandeh, J., 2020. Structure of the human sodium leak channel NALCN. Nature 587, 313–318.

Kucka, M., Kretschmannova, K., Murano, T., Wu, C.-P., Zemkova, H., Ambudkar, S.V., Stojilkovic, S.S., 2010. Dependence of Multidrug Resistance Protein-Mediated Cyclic Nucleotide Efflux on the Background Sodium Conductance. Mol. Pharmacol. 77, 270–279.

Kucka, M., Kretschmannova, K., Stojilkovic, S., Zemkova, H. and Tomić, M., 2012. Dependence of Spontaneous Electrical Activity and Basal Prolactin Release on Nonselective Cation Channels in Pituitary Lactotrophs. Physiol Res, 61, 267-275.

Kuryshev, Y., Childs, G. and Ritchie, A., 1995. Three high threshold calcium channel subtypes in rat corticotropes. Endocrinology, 136, 3916-3924.

Kwiecien, R., Hammond, C., 1998. Differential Management of Ca^{2+} Oscillations by Anterior Pituitary Cells: A Comparative Overview. Neuroendocrinology 68, 135–151.

Laprade R, Ciani S, Eisenman G, Szabo G., 1975. The kinetics of carrier-mediated ion permeation in lipid bilayers and its theoretical interpreatation. Membranes, 3,127-214.

Lear, B., Darrah, E., Aldrich, B., Gebre, S., Scott, R., Nash, H. and Allada, R., 2013. UNC79 and UNC80, Putative Auxiliary Subunits of the NARROW ABDOMEN Ion Channel, Are Indispensable for Robust Circadian Locomotor Rhythms in Drosophila. PLoS ONE, 8, e78147.

Lear, B.C., Lin, J.-M., Keath, J.R., McGill, J.J., Raman, I.M., Allada, R., 2005. The Ion Channel Narrow Abdomen Is Critical for Neural Output of the Drosophila Circadian Pacemaker. Neuron, 48, 965–976.

Lee, J.-H., Cribbs, L.L., Perez-Reyes, E., 1999. Cloning of a novel four repeat protein related to voltage-gated sodium and calcium channels. FEBS Lett. 445, 231–236.

Lee, A.K., Smart, J.L., Rubinstein, M., Low, M.J., Tse, A., 2011. Reciprocal Regulation of TREK-1 Channels by Arachidonic Acid and CRH in Mouse Corticotropes. Endocrinology 152, 1901–1910.

Lee, A.K., Tse, F.W., Tse, A., 2015. Arginine Vasopressin Potentiates the Stimulatory Action of CRH on Pituitary Corticotropes via a Protein Kinase C–Dependent Reduction of the Background TREK-1 Current. Endocrinology 156, 3661–3672.

Lee, S.-Y., Vuong, T.A., Wen, X., Jeong, H.-J., So, H.-K., Kwon, I., Kang, J.-S., Cho, H., 2019. Methylation determines the extracellular calcium sensitivity of the leak channel NALCN in hippocampal dentate granule cells. Exp. Mol. Med. 51, 1–14.

Lehninger, A., Nelson, D. and Cox, M., 2013. Lehninger Principles Of Biochemistry. New York: W.H. Freeman.

Leng, G., and Brown, D., 1997. The Origins and Significance of Pulsatility in Hormone Secretion from the Pituitary. Journal of Neuroendocrinology, 9, 493-513.

Lesage, F., 2003. Pharmacology of neuronal background potassium chan-

nels. Neuropharmacology, 44, 1-7.

Lewis, D., Goodman, M., ST. John, P. and Barker, J., 1988. Calcium Currents and Fura-2 Signals in Fluorescence-Activated Cell Sorted Lactotrophs and Somatotrophs of Rat Anterior Pituitary. Endocrinology, 123, 611-621.

Liang, Z., Chen, L., McClafferty, H., Lukowski, R., MacGregor, D., King, J.T., Rizzi, S., Sausbier, M., McCobb, D.P., Knaus, H., Ruth, P., Shipston, M.J., 2011. Control of hypothalamic–pituitary–adrenal stress axis activity by the intermediate conductance calcium-activated potassium channel, SK4. J. Physiol. 589, 5965–5986.

Lledo, P., Israel, J. and Vincent, J., 1991. Chronic stimulation of D2 dopamine receptors specifically inhibits calcium but not potassium currents in rat lactotrophs. Brain Research, 558, 231-238.

Llinas RR., 1988. The intrinsic electrophysiological properties of mammalian neurons: insights into central nervous system function. Science, 242, 1654-1664.

Li, S.L., Cougnon, N., Bresson-Bépoldin, L., Zhao, S.J., Schlegel, W., 1996. c-fos mRNA and FOS protein expression is induced by Ca^{2+} influx in GH3B6 pituitary cells. J. Mol. Endocrinol, 3, 229–238.

Li SL Godson C, Roche E, Zhao SJ, Prentld M, Schlegel W: 1994. Induction of c-los in pituitary cells by thyrotrophin-releasing hormone and phorbol 12-myristate 13-acetate depends upon Ca^{2+} influx. J Mol Endocrinol. 13, 303-312.

Lightman, S., Wiles, C., Atkinson, H., Henley, D., Russell, G., Leendertz, J., McKenna, M., Spiga, F., Wood, S. and Conway-Campbell, B., 2008. The

significance of glucocorticoid pulsatility. European Journal of Pharmacology, 583, 255-262.

Lu, T. and Feng, Z., 2012. NALCN: A Regulator of Pacemaker Activity. Molecular Neurobiology, 45, 415-423.

Lu, B., Su, Y., Das, S., Liu, J., Xia, J., Ren, D., 2007. The Neuronal Channel NALCN Contributes Resting Sodium Permeability and Is Required for Normal Respiratory Rhythm. Cell 129, 371–383.

Lu, B., Su, Y., Das, S., Wang, H., Wang, Y., Liu, J., Ren, D., 2009. Peptide neurotransmitters activate a cation channel complex of NALCN and UNC-80. Nature 457, 741–744.

Lu, B., Zhang, Q., Wang, H., Wang, Y., Nakayama, M., Ren, D., 2010. Extracellular Calcium Controls Background Current and Neuronal Excitability via an UNC79-UNC80-NALCN Cation Channel Complex. Neuron 68, 488–499.

Lussier, B.T., French, M.B., Moor, B.C., Kraicer, J., 1991. Free Intracellular Ca^{2+} Concentration and Growth Hormone (GH) Release from Purified Rat Somatotrophs, III. Mechanism of Action of GH-Releasing Factor and Somatostatin*. Endocrinology 128, 592–603.

Lutas, A., Lahmann, C., Soumillon, M., Yellen, G., 2016. The leak channel NALCN controls tonic firing and glycolytic sensitivity of substantia nigra pars reticulata neurons. eLife, 5, e15271.

Milescu, L.S., Yamanishi, T., Ptak, K., Mogri, M.Z., Smith, J.C., 2008. Real-Time Kinetic Modeling of Voltage-Gated Ion Channels Using Dynamic Clamp. Biophys. J. 95, 66–87.

Miranda P, de la Peña P, Gómez-Varela D, Barros F., 2003. Role of BK potassium channels shaping action potentials and the associated $[Ca^{2+}]_i$ oscillations in GH(3) rat anterior pituitary cells. Neuroendocrinology 77:162–176

Mollard, P. and Schlegel, W., 1996. Why are endocrine pituitary cells excitable?. Trends in Endocrinology & Metabolism, 7, 361-365.

Moore, B., 1911. In Memory of Sidney Ringer [1835-1910]: Some account of the Fundamental Discoveries of the Great Pioneer of the Bio-Chemistry of Crystallo-colloids in Living Cells. Biochem J 5, i b3-xix.

Musumeci, G., Castorina, S., Castrogiovanni, P., Loreto, C., Leonardi, R., Aiello, F., Magro, G. and Imbesi, R., 2015. A journey through the pituitary gland: Development, structure and function, with emphasis on embryo-foetal and later development. Acta Histochemica, 117, 355-366.

Naor, Z., Leifer, A. and Catt, K., 1980. Calcium-Dependent Actions of Gonadotropin-Releasing Hormone on Pituitary Guanosine 3',5'-Monophosphate Production and Gonadotropin Release. Endocrinology, 107, 1438-1445.

Naumov, A.P., Herrington, J., Hille, B., 1994. Actions of growth-hormone-releasing hormone on rat pituitary cells: intracellular calcium and ionic currents. Pflugers Arch. Eur. J. Physiol. 427, 414–421.

Nash, H.A., Scott, R.L., Lear, B.C., Allada, R., 2002. An Unusual Cation Channel Mediates Photic Control of Locomotion in Drosophila. Curr. Biol. 12, 2152–2158.

Neher, E., and Sakmann, B., 1976. Single-channel currents recorded from membrane of denervated frog muscle fibres. Nature 260, 799-802.

Nernst, W., 2015. Experimental and Theoretical Applications of Thermodynamics to Chemistry - Scholar's Choice Edition. Creative Media Partners, LLC.

Nicholls, J. and Kuffler, S., 2012. From Neuron To Brain. 5th ed. Oxford University Press.

O'Connell, A.D., Morton, M.J., Hunter, M., 2002. Two-pore domain K^+ channels—molecular sensors. Biochim. Biophys. Acta BBA - Biomembr. 1566, 152–161.

O'Neill, J. and Reddy, A. 2011. Circadian clocks in human red blood cells. Nature, 469, 498-503.

Ou, M., Zhao, W., Liu, J., Liang, P., Huang, H., Yu, H., Zhu, T., Zhou, C., 2020. The General Anesthetic Isoflurane Bilaterally Modulates Neuronal Excitability. iScience, 23, 100760.

Park, S., Walker, J., Johnson, N., Zhao, Z., Lightman, S. and Spiga, F. 2013. Constant light disrupts the circadian rhythm of steroidogenic proteins in the rat adrenal gland. Molecular and Cellular Endocrinology, 371, 114-123.

Parsons TD, Coorssen JR, Horstmann H, Almers W., 1995. Docked granules, the exocytic burst, and the need for ATP hydrolysis in endocrine cells. Neuron 15, 1085-1096.

Philippart, F., Khaliq, Z.M., 2018. Gi/o protein-coupled receptors in dopamine neurons inhibit the sodium leak channel NALCN. eLife, 7, e40984.

Plotsky, P., Vale, W., 1985. Patterns of growth hormone-releasing factor and somatostatin secretion into the hypophysial-portal circulation of the rat.

Science 230, 461–463.

Raman, I.M., Bean, B.P., 1997. Resurgent Sodium Current and Action Potential Formation in Dissociated Cerebellar Purkinje Neurons. J. Neurosci. 17, 4517–4526.

Raman, I.M., Gustafson, A.E., Padgett, D., 2000. Ionic Currents and Spontaneous Firing in Neurons Isolated from the Cerebellar Nuclei. J. Neurosci. 20, 9004–9016.

Reinl, Erin L., 2016. A Study on the Role and Regulation of the Na+-Leak Channel, Non-Selective (NALCN) in Myometrial Function.

Ren, D., 2011. Sodium Leak Channels in Neuronal Excitability and Rhythmic Behaviors. Neuron 72, 899–911.

Richards, D.M., Walker, J.J., Tabak, J., 2020. Ion channel noise shapes the electrical activity of endocrine cells. PLOS Comput. Biol. 16, e1007769.

Russo, M.J., Mugnaini, E., Martina, M., 2007. Intrinsic properties and mechanisms of spontaneous firing in mouse cerebellar unipolar brush cells: Intrinsic firing in unipolar brush cells. J. Physiol. 581, 709–724.

Saffran, M., Schally, A.V., Benfey, B.G., 1955. Stimulation of the release of corticotropin from the adenohypophysis by a neurohypophysial factor 1. Endocrinology 57, 439–444.

Salmon, P. and Trono, D., 2010. Production and Titration of Lentiviral Vectors. Current Protocols in Neuroscience, 37, 4.21.1-4.21.24.

Sankaranarayanan, S., Simasko, S.M., 1996. A role for a background sodium

current in spontaneous action potentials and secretion from rat lactotrophs. Am. J. Physiol.-Cell Physiol. 271, C1927–C1934.

Schlegel, W., Winiger, B., Mollard, P., Vacher, P., Wuarin, F., Zahnd, G., Wollheim, C. and Dufy, B., 1987. Oscillations of cytosolic Ca^{2+} in pituitary cells due to action potentials. Nature, 329, 719-721.

Shen, K.Z., North, R.A., Surprenant, A., 1992. Potassium channels opened by noradrenaline and other transmitters in excised membrane patches of guinea-pig submucosal neurones. J. Physiol. 445, 581–599.

Shi, Y., Abe, C., Holloway, B.B., Shu, S., Kumar, N.N., Weaver, J.L., Sen, J., Perez-Reyes, E., Stornetta, R.L., Guyenet, P.G., Bayliss, D.A., 2016. Nalcn Is a "Leak" Sodium Channel That Regulates Excitability of Brainstem Chemosensory Neurons and Breathing. J. Neurosci. 36, 8174–8187.

Shorten, P.R., Robson, A.B., Mckinnon, A.E., Wall, D.J.N., 2000. CRH-induced Electrical Activity and Calcium Signalling in Pituitary Corticotrophs. J. Theor. Biol. 206, 395–405.

Siegelbaum, S.A., Camardo, J.S., Kandel, E.R., 1982. Serotonin and cyclic AMP close single K^+ channels in Aplysia sensory neurones. Nature 299, 413–417.

Simasko, S.M., 1994. A background sodium conductance is necessary for spontaneous depolarisations in rat pituitary cell line GH3. Am. J. Physiol.-Cell Physiol. 266, C709–C719.

Sims, S.M., Lussier, B.T., Kraicer, J., 1991. Somatostatin activates an inwardly rectifying K^+ conductance in freshly dispersed rat somatotrophs. J. Physiol. 441, 615–637.

Singh, A., Hildebrand, M., Garcia, E. and Snutch, T., 2010. The transient receptor potential channel antagonist SKF96365 is a potent blocker of low-voltage-activated T-type calcium channels. British Journal of Pharmacology, 160, 1464-1475.

Smith, S. M., Bergsman, J. B., Harata, N. C., Scheller, R. H., and Tsien, R. W., 2004. Recordings from single neocortical nerve terminals reveal a nonselective cation channel activated by decreases in extracellular calcium. Neuron, 41, 243-256.

Snutch, T.P., Monteil, A., 2007. The Sodium "Leak" Has Finally Been Plugged. Neuron, 54, 505–507.

Speca, D.J., Chihara, D., Ashique, A.M., Bowers, M.S., Pierce-Shimomura, J.T., Lee, J., Rabbee, N., Speed, T.P., Gularte, R.J., Chitwood, J., Medrano, J.F., Liao, M., Sonner, J.M., Eger, E.I., Peterson, A.S., McIntire, S.L., 2010. Conserved Role of unc-79 in Ethanol Responses in Lightweight Mutant Mice. PLoS Genet. 6, e1001057.

Stanfield, P.R., Nakajima, S., Nakajima, Y., 2002. Constitutively active and G-protein coupled inward rectifier K^+ channels: Kir2.0 and Kir3.0, in: Reviews of Physiology, Biochemistry and Pharmacology, Reviews of Physiology, Biochemistry and Pharmacology. Springer Berlin Heidelberg, Berlin, Heidelberg, 47–179.

Steinbach, H.B., 1940. Sodium and potassium in frog muscle. J. biol. Chem. 133, 695-701.

Steinbach, H. B., 1941. J. cell. comp. Physiol. 17, 57. Steinbach, H.B., Spiegelman, S., 1943. The sodium and potassium balance in squid nerve axoplasm. J. Cell. Comp. Physiol. 22, 187–196.

Stephens, R., Guan, W., Zhorov, B. and Spafford, J., 2015. Selectivity filters and cysteine-rich extracellular loops in voltage-gated sodium, calcium, and NALCN channels. Frontiers in Physiology, 6.

Stojilkovic, S. and Catt, K., 1992. Calcium Oscillations in Anterior Pituitary Cells. Endocrine Reviews, 13, 256-280.

Stojilkovic, S.S., Kretschmannova, K., Tomić, M., Stratakis, C.A., 2012. Dependence of the Excitability of Pituitary Cells on Cyclic Nucleotides: Cyclic nucleotides and excitability of pituitary cells. J. Neuroendocrinol. 24, 1183–1200.

Stojilkovic, S.S., 2006. Pituitary cell type-specific electrical activity, calcium signalling and secretion. Biol. Res. 39.

Stojilkovic, S.S., Tabak, J., Bertram, R., 2010. Ion Channels and Signalling in the Pituitary Gland. Endocr. Rev. 31, 845–915.

Stojilkovic, S., Zemkova, H. and Van Goor, F., 2005. Biophysical basis of pituitary cell type-specific Ca^{2+} signaling–secretion coupling. Trends in Endocrinology & Metabolism, 16, 152-159.

Swayne, L.A., Mezghrani, A., Varrault, A., Chemin, J., Bertrand, G., Dalle, S., Bourinet, E., Lory, P., Miller, R.J., Nargeot, J., Monteil, A., 2009. The NALCN ion channel is activated by M3 muscarinic receptors in a pancreatic β-cell line. EMBO Rep. 10, 873–880.

Tabak, J., Tomaiuolo, M., Gonzalez-Iglesias, A.E., Milescu, L.S., Bertram, R., 2011. Fast-Activating Voltage- and Calcium-Dependent Potassium (BK) Conductance Promotes Bursting in Pituitary Cells: A Dynamic Clamp Study. J. Neurosci. 31, 16855–16863.

Taraskevich, P. and Douglas, W. (1980). Electrical behaviour in a line of anterior pituitary cells (GH cells) and the influence of the hypothalamic peptide, thyrotrophin releasing factor. Neuroscience, 5, 421-431.

Tasker, J.G., Herman, J.P., 2011. Mechanisms of rapid glucocorticoid feedback inhibition of the hypothalamic–pituitary–adrenal axis. Stress 14, 398–406.

Therien, A. and Blostein, R., 2000. Mechanisms of sodium pump regulation. American Journal of Physiology-Cell Physiology, 279, C541-C566.

Thomas, P., Smith, P.A., 2001. Tetrabutylammonium: a selective blocker of the somatostatin-activated hyperpolarizing current in mouse AtT-20 corticotrophs. Pflugers Arch. Eur. J. Physiol. 441, 816–823.

Thorner, M., Vance, M., Hartman, M., Holl, R., Evans, W., Veldhuis, J., Van Cauter, E., Copinschi, G. and Bowers, C., 1990. Physiological role of somatostatin on growth hormone regulation in humans. Metabolism, 39, 40-42.

Tomić, M., Koshimizu, T., Yuan, D., Andric, S., Zivadinovic, D. and Stojilkovic, S., 1999. Characterization of a Plasma Membrane Calcium Oscillator in Rat Pituitary Somatotrophs. Journal of Biological Chemistry, 274, 35693-35702.

Tomić, M., Kucka, M., Kretschmannova, K., Li, S., Nesterova, M., Stratakis, C.A., Stojilkovic, S.S., 2011. Role of nonselective cation channels in spontaneous and protein kinase A-stimulated calcium signaling in pituitary cells. Am. J. Physiol.-Endocrinol. Metab. 301, E370–E379.

Tsaneva-Atanasova, K., Sherman, A., van Goor, F. and Stojilkovic, S., 2007. Mechanism of Spontaneous and Receptor-Controlled Electrical Activity in Pituitary Somatotrophs: Experiments and Theory. Journal of Neurophysiology,

98, 131-144.

Van Goor, F., Li, Y. and Stojilkovic, S., (2001a). Paradoxical Role of Large-Conductance Calcium-Activated K^+ (BK) Channels in Controlling Action Potential-Driven Ca^{2+}Entry in Anterior Pituitary Cells. The Journal of Neuroscience, 21, 5902-5915.

Van Goor, F., Zivadinovic, D. and Stojilkovic, S., (2001b). Differential Expression of Ionic Channels in Rat Anterior Pituitary Cells. Molecular Endocrinology, 15, 1222-1236.

Vela, J., Pérez-Millán, M.I., Becu-Villalobos, D., Díaz-Torga, G., 2007. Different kinases regulate activation of voltage-dependent calcium channels by depolarisation in GH3 cells. Am. J. Physiol.-Cell Physiol. 293, C951–C959.

Vitale ML, Seward EP, Trifaro JM: 1995. Chromaffin cell cortical actin network dynamics control the size of the release-ready vesicle pool and the initial rate of exocytosis. Neuron 14:353-363.

Wang, G., Ciuffi, A., Leipzig, J., Berry, C. and Bushman, F., 2007. HIV integration site selection: Analysis by massively parallel pyrosequencing reveals association with epigenetic modifications. Genome Research, 17, 1186-1194.

Wang, H. and Ren, D., 2009. UNC80 functions as a scaffold for Src kinases in NALCN channel function. Channels, 3, 161-163.

Wagner, K., Yacono, P., Golan, D. and Tashjian, A., 1993. Mechanism of spontaneous intracellular calcium fluctuations in single GH4C1 rat pituitary cells. Biochemical Journal, 292, 175-182.

Wagner, P. G. & Dekin, M. S., 1997. cAMP modulates an S-type K^+

channel coupled to GABAB receptors in mammalian respiratory neurons. Neuroreport, 8, 1667– 1670.

Wichmann, T., Bergman, H., Starr, P.A., DeLong, M.R., Watts, R.L., Subramanian, T., 1999. Comparison of MPTP-induced changes in spontaneous neuronal discharge in the internal pallidal segment and in the substantia nigra pars reticulata in primates. Exp. Brain Res. 125, 397–409.

Wichmann, T., Kliem, M.A., DeLong, M.R., 2001. Antiparkinsonian and Behavioral Effects of Inactivation of the Substantia Nigra Pars Reticulata in Hemiparkinsonian Primates. Exp. Neurol. 167, 410–424.

Wunderer, F., Kühne, S., Jilg, A., Ackermann, K., Sebesteny, T., Maronde, E., Stehle, J.H., 2013. Clock Gene Expression in the Human Pituitary Gland. Endocrinology, 154, 2046–2057.

Xie, L., Gao, S., Alcaire, S., Aoyagi, K., Wang, Y., Griffin, J., Stagljar, I., Nagamatsu, S. and Zhen, M., 2013. NLF-1 Delivers a Sodium Leak Channel to Regulate Neuronal Excitability and Modulate Rhythmic Locomotion. Neuron, 77, 1069-1082.

Xiong, Z., Lu, W., and MacDonald, J. F., 1997. Extracellular calcium sensed by a novel cation channel in hippocampal neurons. Proc Natl Acad Sci USA 94, 7012-7017.

Xu, R., Zhao, Y., Chen, C., 2002. Growth hormone-releasing peptide-2 reduces inward rectifying K^+ currents via a PKA-cAMP-mediated signalling pathway in ovine somatotropes. J. Physiol. 545, 421–433.

Yaari, Y., Konnerth, A., and Heinemann, U., 1983. Spontaneous epileptiform activity of CA1 hippocampal neurons in low extracellular calcium

solutions. Exp Brain Res. 51,153-156.

Yeh, E., Ng, S., Zhang, M., Bouhours, M., Wang, Y., Wang, M., Hung, W., Aoyagi, K., Melnik-Martinez, K., Li, M., Liu, F., Schafer, W. and Zhen, M., 2008. A Putative Cation Channel, NCA-1, and a Novel Protein, UNC-80, Transmit Neuronal Activity in C. elegans. PLoS Biology, 6, p.e55.

Yeh, S.-Y., Huang, W.-H., Wang, W., Ward, C.S., Chao, E.S., Wu, Z., Tang, B., Tang, J., Sun, J.J., Esther van der Heijden, M., Gray, P.A., Xue, M., Ray, R.S., Ren, D., Zoghbi, H.Y., 2017. Respiratory Network Stability and Modulatory Response to Substance P Require Nalcn. Neuron, 94, 294.

Yoo, S., Yamazaki, S., Lowrey, P., Shimomura, K., Ko, C., Buhr, E., Siepka, S., Hong, H., Oh, W., Yoo, O., Menaker, M. and Takahashi, J. 2004. PERIOD2: LUCIFERASE real-time reporting of circadian dynamics reveals persistent circadian oscillations in mouse peripheral tissues. Proceedings of the National Academy of Sciences, 101, 5339-5346.

Young, E., Abelson, J. and Lightman, S., 2004. Cortisol pulsatility and its role in stress regulation and health. Frontiers in Neuroendocrinology, 25, 69-76.

Young, E., Ribeiro, S. and Ye, W., 2007. Sex differences in ACTH pulsatility following metyrapone blockade in patients with major depression. Psychoneuroendocrinology, 32, 503-507.

Zemkova, H., Tomić, M., Kucka, M., Aguilera, G., Stojilkovic, S.S., 2016. Spontaneous and CRH-Induced Excitability and Calcium Signaling in Mice Corticotrophs Involves Sodium, Calcium, and Cation-Conducting Channels. Endocrinology, 157, 1576–1589.

Zivadinovic, D., Tomić, M., Yuan, D., Stojilkovic, S.S., 2002. Cell-Type Specific Messenger Functions of Extracellular Calcium in the Anterior Pituitary. Endocrinology, 143, 445–455.

Zorec R: 1996. Calcium signaling and secretion in pituitary cells. Trend Endocrinol Metab. 7:384-388.